THESIS FOR THE DEGREE OF DOCTOR OF PHILOSOPHY

Ruthenium-Catalyzed Strategies for the Synthesis of Functional Molecules and Organic Receptors

Ru-Catalyzed Azide-Alkyne Cycloadditions and Hydrogen Transfer Reactions for the Construction of Bio-Based Materials and 1,2,3-Triazole-Derived Functional Scaffolds

Flavia Ferrara

Department of Chemistry and Chemical Engineering

CHALMERS UNIVERSITY OF TECHNOLOGY

Gothenburg, Sweden 2025

Ruthenium-Catalyzed Strategies for the Synthesis of Functional Molecules and Organic Receptors

Ru-Catalyzed Azide-Alkyne Cycloadditions and Hydrogen Transfer Reactions for the Construction of Bio-Based Materials and 1,2,3-Triazole-Derived Functional Scaffolds
FLAVIA FERRARA
ISBN 978-91-8103-323-6

Doktorsavhandlingar vid Chalmers tekniska högskola
Ny serie nr 5780
ISSN 0346-718X

Department of Chemistry and Chemical Engineering
Chalmers University of Technology
SE-412 96 Gothenburg
Sweden
Telephone + 46 (0)31-772 1000

Cover: Credits to Samsung Galaxy AI image generator (One UI version 8.0)

Chalmers Digitaltryck
Gothenburg, Sweden 2025

Ruthenium-Catalyzed Strategies for the Synthesis of Functional Molecules and Organic Receptors

Ru-Catalyzed Azide-Alkyne Cycloadditions and Transfer Hydrogen Reactions for the Construction of Bio-Based Materials and 1,2,3-Triazole-Derived Functional Scaffolds

FLAVIA FERRARA
Department of Chemistry and Chemical Engineering
Chalmers University of Technology

ABSTRACT

This thesis explores the development of ruthenium-catalyzed methodologies for the synthesis of functional molecules with potential applications in green chemistry, catalysis and molecular recognition. The work presented aims at establishing new strategies for the construction of bio-based materials and 1,2,3-triazole-derived functional scaffolds, using ruthenium-catalyzed hydrogen transfer and azide-alkyne cycloaddition reactions (RuAAC).

The first part of this work demonstrates the potential of ruthenium catalysis in biomass valorization through the dimerization of vanillin derivatives into an epoxy divanillin ester (EDVE), a renewable precursor for polymer synthesis that may serve as a sustainable alternative to the reprotoxic bisphenol A molecule. Then, a sequential ruthenium-catalyzed azide–alkyne cycloaddition and hydrogen-borrowing strategy was developed, providing access to novel tricyclic 1,2,3-triazole-fused piperazines, architecturally complex heterocycles with potential catalytic or biological applications. The pyrrolidine-appended triazoles obtained as intermediates in this route were further investigated as organocatalysts in asymmetric aldol reactions employing green reaction conditions, illustrating how structural modifications within the triazole scaffold can influence reactivity and selectivity. Finally, 1,4,5-trisubstituted 1,2,3-triazole-based oligomers were constructed by combining ruthenium-catalyzed azide–alkyne cycloaddition for the modular synthesis of the triazole monomers with subsequent amide coupling to assemble linear and cyclic peptidotriazolamers. These structures were then evaluated for their ion recognition properties.

Altogether, the work presented in this thesis shows how the combination of Ru catalysis and molecular design can deliver new synthetic tools for renewable materials, asymmetric catalysis, and molecular sensing.

Keywords: RuAAC, transfer hydrogenation, hydrogen borrowing, organocatalysis, vanillin, biomass valorization, heterocycles, synthetic receptors, triazoles, sensing

LIST OF PUBLICATIONS

This thesis is based on the following manuscripts:

I. **Ruthenium-catalyzed dimerization of vanillin for the formation of a biobased epoxy thermoset**
Ferrara, F.; Ribca, I.; Prabhu, N.; Mante, J.; Gumbo, M.; Johansson, M.; Ekebergh, A.; Kann, N.; *RSC Sustainability* **2025**, 3, 2366–2376.

II. **Ruthenium-catalyzed synthesis of tricyclic 1,5-fused 1,2,3-triazole piperazines** Said Stalsmeden, A.; Ferrara, F.; Ekebergh, A.; Runemark, A.; Johansson, J. R.; Norrby, P.-O.; Kann, N.; *Org. Biomol. Chem.*, **2025**, 23, 8001 – 8011.

III. **1,4,5-trisubstituted 1,2,3-triazoles appended prolinol derivatives as organocatalysts in aldol reactions**
Ferrara, F.; Roy, A.; Marty, A.; Sundén, H.; Kann, N.;
Preliminary manuscript

IV. **Modular Triazole-Based Receptors for Metal Ion and Halide Ion Detection**
Ferrara, F.; Trivedi, M.; Wang, Y.; Gumbo, M.; Amombo Noa, F.; Abrahamsson, M.; Grøtli, M.; Kann, N.;
Manuscript

Related publication, not included in this thesis:

Recent Developments in the Ruthenium-Catalyzed Azide Alkyne Cycloaddition (RuAAC) Reaction.
Ferrara, F.; Beke-Somfai, T. and Kann, N. *Eur. J. Org. Chem.* **2025**, 23, 8001 – 8011.

CONTRIBUTION REPORT

The author has made the following contributions to the papers:

I. Contributed to optimization of the reaction conditions for the synthesis of the epoxy divanillin ester EDVE, purification of the product, interpretation of the results and contributed to writing of the manuscript.

II. Optimized the ruthenium-catalyzed azide-alkyne cycloaddition reaction conditions, performed screening of different conditions for the hydrogen borrowing step, interpretated the results, performed the RuAAC and hydrogen borrowing reaction on selected substrates.

III. Formulated the research problem, performed or supervised the experimental work, analyzed and interpreted the results and wrote the manuscript.

IV. Partecipated in the formulation of the research problem, performed or supervised the synthetic experimental work, analyzed and interpreted the synthetic part of the results, contributed to the interpretation of the ion detection part and contributed to writing of the manuscript.

LIST OF ABBREVIATIONS

BINAP	2,2'-Bis(diphenylphosphino)-1,1'-binaphthyl
Boc	*tert*-Butoxycarbonyl
BPA	Bisphenol A
Cat	Catalyst
cod	1,5-Cyclooctadiene
Cp*	1,2,3,4,5-Pentamethylcyclopentadienyl
CuAAC	Copper(I)-Catalyzed Azide–Alkyne Cycloaddition
p-Cymene	1-Isopropyl-4-methylbenzene
dba	Dibenzylideneacetone
DCM	Dichloromethane
DIPEA	*N,N*-Diisopropylethylamine
DMAP	4-(Dimethylamino)pyridine
DMF	*N,N*-Dimethylformamide
DMSO	Dimethyl sulfoxide
DPEphos	Bis[(2-diphenylphosphino)phenyl] ether
dr	Diastereomeric ratio
ee	Enantiomeric excess
FTIR	Fourier Transform Infrared Spectroscopy
HATU	*O*-(7-Azabenzotriazol-1-yl)-*N,N,N',N'*-tetramethyluronium hexafluorophosphate

HPLC	High-Performance Liquid Chromatography
HRMS	High-Resolution Mass Spectrometry
*i*Pr	isopropyl
MW	Microwave
NMR	Nuclear Magnetic Resonance
NOESY	Nuclear Overhauser Effect Spectroscopy
rt	Room Temperature
RuAAC	Ruthenium-Catalyzed Azide–Alkyne Cycloaddition
SPAAC	Strain-Promoted Azide–Alkyne Cycloaddition
TBAF	Tetrabutylammonium Fluoride
TBACl	Tetrabutylammonium Chloride
THF	Tetrahydrofuran
TIPS	Triisopropylsilyl
XRD	X-ray Diffraction
UV/Vis	Ultraviolet–Visible Spectroscopy

Table of Contents

1. Introduction

1.1 Organic Synthesis and Catalysis

Known as the *"chemistry of life"*, organic chemistry explores the structure, properties, and reactivity of carbon-containing compounds. Many of these molecules are found in nature and understanding their behavior has been essential for the development of synthetic organic chemistry. Organic synthesis allows the design and construction of complex molecules, which can find applications ranging from pharmaceuticals and agrochemicals to material science and energy. However, achieving efficient, selective, and sustainable synthetic routes has always been an important goal of research in the field of organic chemistry.[1]Notably, the use of catalysis makes organic synthesis more efficient and sustainable.

By definition, a catalyst is a chemical species that actively participates in a reaction by providing an alternative pathway with a lower energy barrier, increasing the reaction rate. Importantly, the catalyst is not consumed during the process but is continuously regenerated at the end of each catalytic cycle, facilitating multiple reaction turnovers.[2]

In particular, metal catalysis plays a fundamental role both in nature and in the development of synthetic methodologies. In biological systems, metalloenzymes use metal centers coordinated by amino acid residues to catalyze essential reactions, with functions ranging from oxidation and reduction to bond activation. For example, the metal complex in photosystem II, a tetranuclear manganese-oxo cluster, drives water oxidation and oxygen formation during photosynthesis.[3] Inspired by these natural systems, metal complexes have become powerful catalysts in organic chemistry, operating either through redox activity, where the metal changes oxidation state to transfer electrons, or through Lewis acidity, in which the metal center activates substrates without changing its oxidation state.[4]

Catalysts can be classified as heterogeneous or homogeneous, depending on their physical state relative to the reaction medium. While heterogeneous catalysts operate in a different phase from the reactants, typically on a solid surface (e.g., hydrogenation of olefins with Pd/C), homogeneous catalysts are dissolved in the same phase as the reactants (acid/base catalysts, enzymes, and many organometallic complexes). In homogeneous catalysis, transition-metal complexes have been essential for the development of modern organic synthesis, but more recently organocatalysts (small, metal-free organic molecules) have emerged as powerful and sustainable alternatives.[5]

1.1.1 Transition Metal Catalysis

Transition metal catalysis has become one of the cornerstones of modern organic synthesis thanks to the ability of metal complexes to alter the reactivity of functional groups and to unlock transformations that are otherwise difficult or impossible to achieve under classical metal-free conditions. Notably, coordination to a transition metal center can change the electronic properties of a substrate, enabling selective bond activation and precise control over chemo-, regio-, and stereoselectivity.[6] This has made transition-metal catalysis a central tool, for instance, in asymmetric synthesis, providing access to enantiomerically pure compounds, which are crucial in drug development.[7]

The major achievements in transition metal catalysis of the last decades have been widely recognized through several Nobel Prizes in Chemistry. In 2001, Knowles, Noyori, and Sharpless were awarded the prize for their pioneering contributions to asymmetric catalysis, which enabled the efficient synthesis of enantiomerically pure compounds essential in pharmaceuticals.[8] In 2005, Chauvin, Grubbs, and Schrock received the prize for the development of olefin metathesis, a powerful and versatile method for C–C bond formation with broad applications in materials science and drug discovery.[9] In 2010, Suzuki, Negishi, and Heck were recognized for their work on palladium-catalyzed cross-coupling reactions, which revolutionized the construction of complex molecular architectures and became indispensable tools in modern organic synthesis.[10] More recently, in 2022, Sharpless (for the second time), Meldal, and Bertozzi received the award for the development of click chemistry and bioorthogonal reactions, providing robust and selective strategies for molecular assembly and bioconjugation under mild conditions.[11] Together, these landmark discoveries fundamentally reshaped synthetic methodologies and continue to influence both academic and industrial research.

As an example, the stereoselective reduction of a *β*-keto ester with a Ru-BINAP catalyst, reported by Noyori, allows the clean and operationally simple synthesis of optically active *β*-hydroxy esters (Scheme 1a).[12] Such compounds are essential building blocks for the pharmaceutical industry and until the development of this methodology it was only possible to access them via biochemical transformations e.g. using baker's yeast (*Saccharomyces cerevisiae*).[13]

Similarly, the establishment of cross-coupling reactions allowed a solid methodology for the formation of carbon–carbon bonds using organometallic reagents. These reactions are widely valued in synthesis for their functional group tolerance, high efficiency, and ability to construct complex molecules from simple building blocks. Scheme 1b shows an example of a Heck coupling between an aryl halide and a vinyl ester.[14]

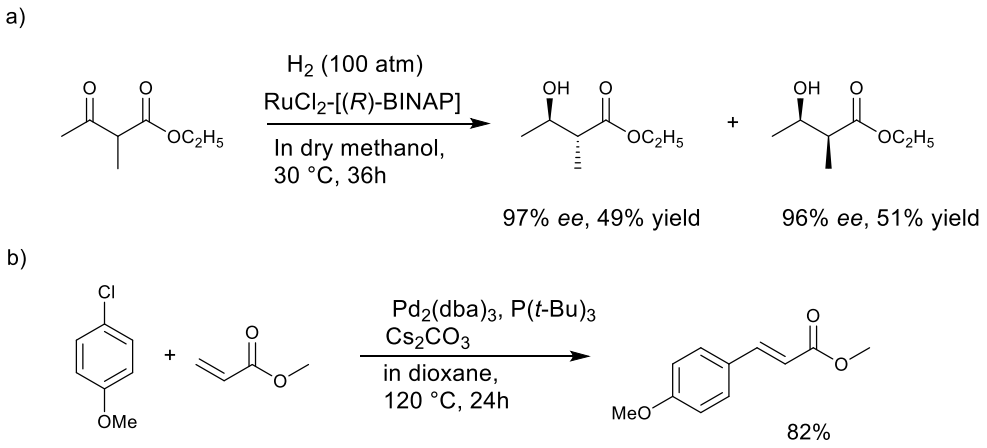

Scheme 1. a) Hydroxylation of a *β*-keto ester with a ruthenium catalyst; b) palladium-catalyzed Heck coupling between an aryl halide and a vinyl ester.

The versatility of transition-metal catalysis can be understood with mechanistic insight. Key processes such as oxidative addition, migratory insertion, transmetallation, and reductive elimination allow metals to mediate bond construction and cleavage selectively. Furthermore, their ability to switch oxidation states and to handle different coordination environments is complemented by the electronic and steric control operated by the ligands, which shape the reactivity and selectivity of the catalytic cycle. Together, these features enable transition metals not only to activate inert bonds but also to orchestrate multistep cascade processes within a single catalytic cycle.[6]

In summary, transition metal catalysis has revolutionized organic synthesis by combining redox flexibility, ligand control, and well-defined mechanisms to achieve highly efficient, selective, and broadly applicable transformations.

1.1.2 Organocatalysis

Asymmetric organic synthesis using small, metal-free organic molecules as catalysts was first reported in 1971 with the proline-catalyzed intramolecular asymmetric aldol reaction of a triketone.[15, 16] After remaining almost unexplored for three decades, this approach, later named organocatalysis, is now considered one of the central strategies in modern catalysis. Organocatalysts allows to carry out a wide range of asymmetric carbon–carbon and carbon–heteroatom bond-forming reactions, including Diels–Alder and 1,3-dipolar cycloadditions, aldol and Mannich reactions, Michael additions, epoxidations, hydride transfers, α-halogenations, and aminations.[17]

Representing a powerful alternative to transition metal catalysts, organocatalysts can mimic some of the roles typically associated with metals, such as Lewis acid/base activation or alternatively act as redox agents.[18] Furthermore, these molecules are generally inexpensive,

stable and environmentally benign, as well as compatible with aerobic and aqueous reaction conditions, which is usually not the case for organometallic catalysts.

The rapid growth and the large impact of the field were recognized by the 2021 Nobel Prize in Chemistry, awarded to Benjamin List and David MacMillan for their pioneering work on asymmetric organocatalysis.[19]

Mechanistically, organocatalysts can promote reactions through distinct modes of activation: covalent activation (e.g. enamine or iminum ion catalysis), non-covalent interactions (e.g., hydrogen bonding, ion pairing), phase-transfer catalysis and activation under confinement, mimicking enzyme-like cavities. These strategies provide well-organized transition states directing a selective enantiomer formation, often in ways reminiscent of enzymatic catalysis.[20]

The majority of organocatalytic reactions involve the use of aminocatalysts, where natural (e.g. aminoacids, peptides) and synthetic nitrogen containing compounds are employed as chiral catalysts. Most of these reactions proceed via a generalized enamine activation (Scheme 2a) or through the formation of iminum ions intermediates (Scheme 2b). Usually, donor molecules are activated with the formation of a nucleophilic enamine, which increases electron density at the reactive site and makes them suitable to react with electrophiles, whereas acceptor molecules are activated by the formation of an electrophilic iminium ion, which can then undergo nucleophilic attack (Scheme 2).[21]

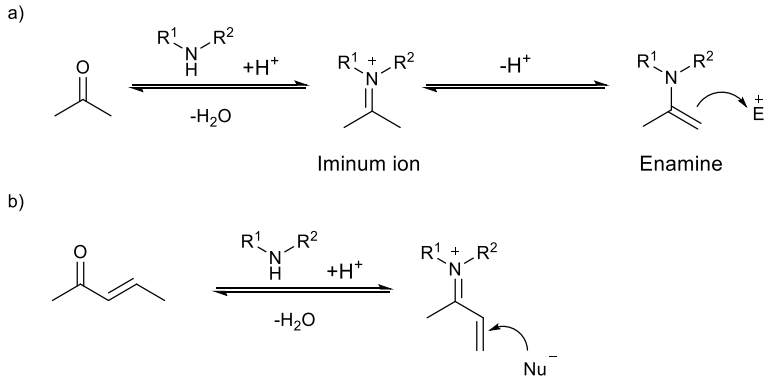

Scheme 2. Type of aminocatalysis. a) nucleophilic (enamine) activation; b) electrophilic (iminum ion) activation.

L-Proline is the most widely used catalyst in enamine-type organocatalysis. The secondary amine functionality increases the pK_a and the nucleophilicity of the molecule, allowing proline to act as a nucleophile with carbonyl compounds and Michael acceptors to form iminum ions or enamines. The bifunctional nature of proline, involving the basic pyrrolidine ring and the Brønsted-acidic carboxyl group, enables not only substrate activation, but also

the stabilization of transition states through hydrogen bonding, often leading to high enantioselectivity (Scheme 3).

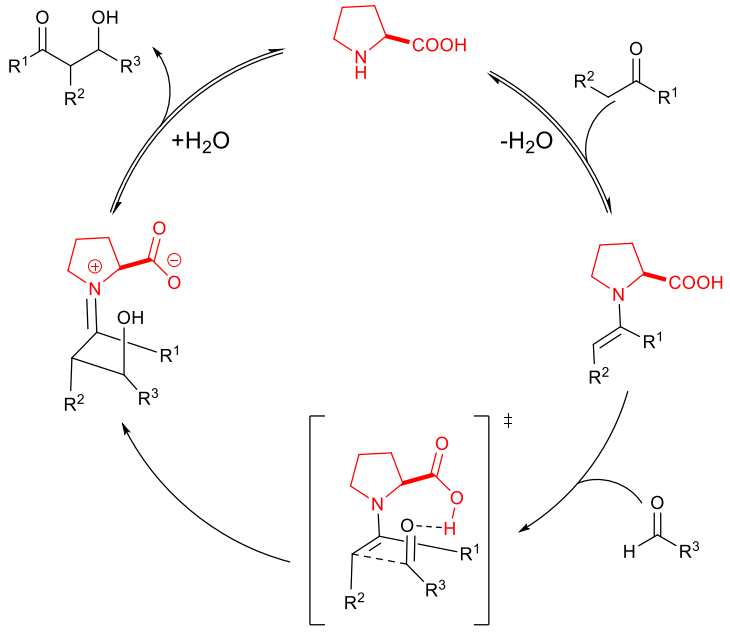

Scheme 3. L-proline promoted enamine catalysis for aldol reaction (figure adapted from reference).[21]

In the study initially carried out by List and co-workers, L-proline was shown to catalyze asymmetric aldol reaction between acetone and a variety of aldehydes in moderate to good yields and enantioselectivities (Scheme 4).[22]

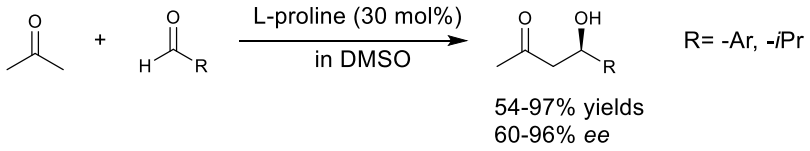

Scheme 4. Asymmetric aldol reaction catalyzed by L-proline

Despite its simplicity compared to enzymatic systems such as class I aldolases, proline catalyzes a remarkable range of reactions,[23] and research efforts are currently aiming at designing and synthesizing analogues in order to broaden the substrate scope, enhance its catalytic efficiency and allow greener reaction conditions for organocatalysis.[24]

As an example, fluorous pyrrolidine sulfonamide has been reported by Wang et al. to catalyze aldol reaction in water, allowing the recovery of the catalyst by simple fluorous solid phase extraction (Scheme 5a).[25]

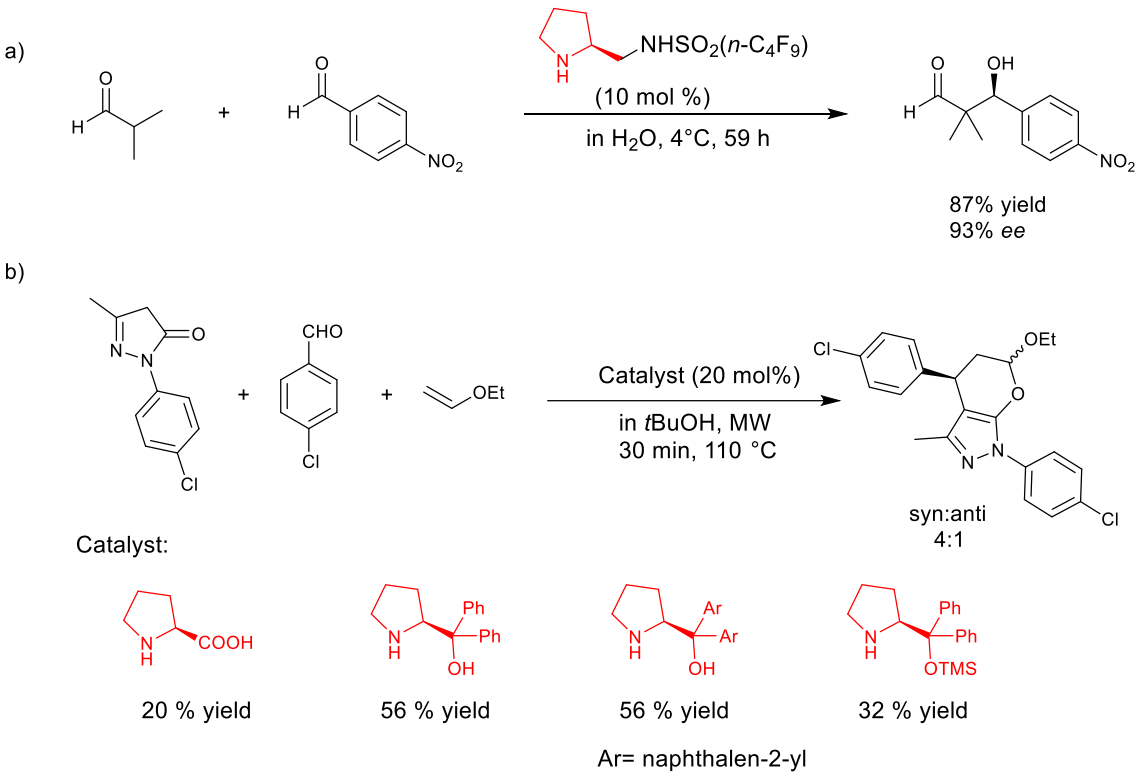

Scheme 5. a) Proline derivative catalysis in water; b) domino reaction catalyzed by proline and its analogues.

Asymmetric domino processes have the potential of forming multiple bonds and stereocenters in a one-pot manner. The possibility of performing such transformations with organocatalysis has stimulated extensive research in this field, with many results achieved recently. As an example, proline and derivatives were found to be suitable catalysts for a cascade reaction involving a Knoevenagel condensation and a hetero Diels-Alder reaction for the synthesis of a pyrazole derivative under microwave irradiation conditions (Scheme 5b).[26]

1.2 Click Chemistry

Inspired by nature's principles, click chemistry is a powerful and versatile strategy that enables the efficient assembly of complex molecules by joining modular units through heteroatom linkages (C–X–C).[27-29] This methodology represents a fundamental strategy characterized by rigorous criteria, ensuring its utility for various applications. To be classified as a click reaction, a chemical transformation should be modular, efficient, easily adaptable and combinable, have broad applicability across diverse chemical contexts, proceed in high yields and should also allow straightforward product isolation.

Reactions that fulfill the click chemistry principles are further sub-classifed into six groups: (i) addition reactions to carbon–carbon multiple bonds, (ii) cycloaddition reactions, (iii)

nucleophilic ring opening reactions, (iv) non-aldol carbonyl chemistry, (v) bond cleavage reactions and (iv) Staudinger ligations.[30]

The 1,3-dipolar cycloaddition reaction between an alkyne and an organic azide allows the access to different types of substituted 1,2,3-triazoles, highly versatile molecules that find many different applications. While their primary use lies in drug discovery,[31-33] they have also found other important applications, such as in supramolecular chemistry[34] or materials science.[35] Over time, various synthetic methods have been developed to improve the efficiency of this reaction. Beginning with thermal cycloaddition, the following section of this thesis details the most relevant techniques used to perform the azide-alkyne cycloaddition.

1.2.1 Azide-Alkyne Cycloaddition Reactions

The Huisgen (3+2) 1,3-dipolar cycloaddition between an azide and alkyne proceeds via a concerted addition of the 1,3-dipole (azide) to the dipolarophile (alkyne) resulting in the formation of two regioisomeric triazole products (Scheme 6).[36, 37]

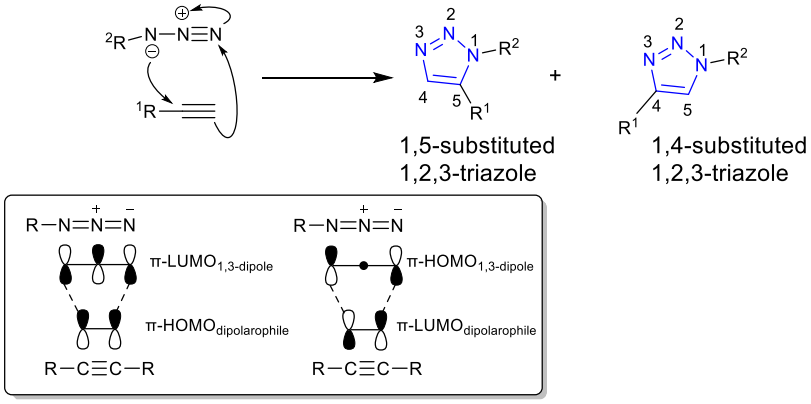

Scheme 6. Concerted mechanism of the 1,3-dipolar azide-alkyne cycloaddition.

The first reported conditions allowing this reaction employed high temperature to push the transformation of the starting materials to product and is known as the Thermal Azide-Alkyne Cycloaddition (TAAC). The orbital interactions that govern this transformation are the ones of the Highest Occupied Molecular Orbital (HOMO) and the Lowest Unoccupied Molecular Orbital (LUMO) of both the 1,3-dipole and dipolarophile (Scheme 6).[38] The reaction typically yields a mixture of 1,4- and 1,5-disubstituted 1,2,3-triazole regioisomers (Scheme 7a).

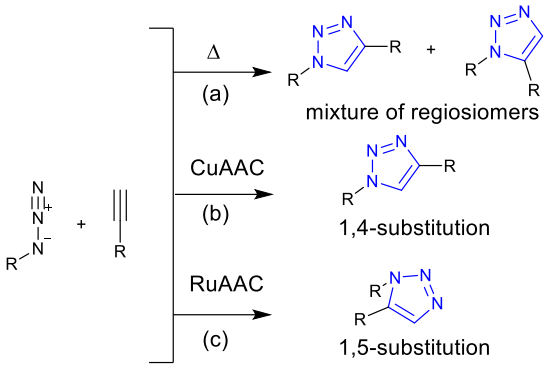

Scheme 7. Formation of 1,2,3 triazoles: (a) Huisgen thermal 1,3-dipolar cycloaddition, (b) copper-catalyzed azide-alkyne cycloaddition (CuAAC), and (c) ruthenium-catalyzed azide-alkyne cycloaddition (RuAAC).

In 2001, achieving regioselectivity towards the 1,4-disubstituted 1,2,3-triazole in this reaction was made possible by the discovery of the Cu(I)-catalyzed azide-alkyne cycloaddition (CuAAC, Scheme 7b). Meldal first reported the reaction in the context of peptide chemistry,[39] while Sharpless independently described it as a general and robust transformation,[40] laying the foundation of modern click chemistry. The reaction mechanism of the CuAAC has been the object of many studies over the years. Initially, Himo and co-workers suggested a mononuclear copper pathway involving the formation of a copper acetylide intermediate, followed by coordination and cycloaddition with the azide.[41] The most recent mechanism proposal for this reaction, reported by Fokin et al., involves two Cu(I) centers acting cooperatively (Scheme 8).[42] It begins with the coordination of two Cu(I) species to the terminal alkyne, which activates it for nucleophilic attack, facilitating the reaction with the azide. Finally, upon formation of the triazole product, the copper catalyst is regenerated.

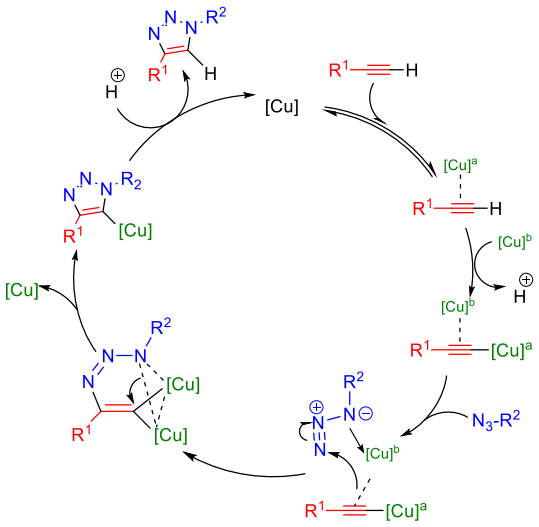

Scheme 8. Mechanism of the copper-catalyzed azide alkyne cycloaddition (CuAAC) (figure adapted from reference).[42]

The CuAAC method rapidly gained widespread recognition due to its mild reaction conditions and broad applicability across multiple fields,[43] in particular for medicinal chemistry and drug discovery.[44] In peptidomimetics, 1,4-disubstituted 1,2,3-triazoles prepared via CuAAC were employed as isosteres for the trans amide bond. As an example, the triazole reported in Figure 1a is used to mimic a β-turn structure, which is a structural motif usually used in peptidomimetics to maintain bioactive conformations.[45] Modification of natural products through CuAAC is also highly valuable, for instance to improve properties such as solubility or bioavailability. Such is the case for the 1,2,3-triazole-modified antitumor alkaloid camptothecin (Figure 1b), which exhibited markedly enhanced water solubility while retaining its biological activity.[46]

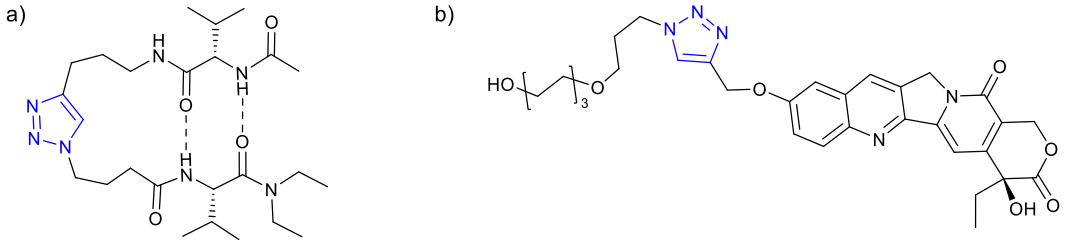

Figure 1. a) β-turn mimetic molecule; b) triazole functionalized camptothecin.

A complementary methodology, allowing access to 1,5-disubstituted-1,2,3 triazoles, was proposed by Fokin and Jia a few years later (in 2005) and involves the use of ruthenium catalysis (RuAAC, Scheme 9).[47] The scope and mechanism of the reaction were elucidated by Weinreb in 2006[48] and by Fokin in 2008[49] respectively.

The mechanism of RuAAC is shown in Scheme 9. Initially, the ruthenium catalyst coordinates both the alkyne and the azide by displacement of two ligands (Step A). Unlike CuAAC, which involves the formation of a copper-acetylide, RuAAC proceeds through a ruthenium-carbene intermediate (Step B). This species then reacts with the azide to form the triazole product (Step C). Finally, liberation of the triazole allows the ruthenium catalyst regeneration, therefore completing the catalytic cycle (Step D).

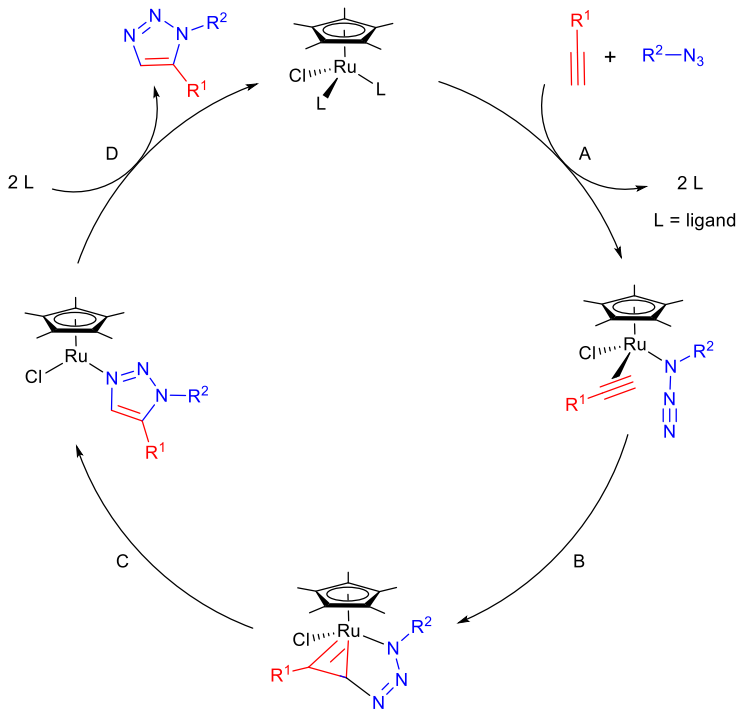

Scheme 9. Mechanism of the ruthenium-catalyzed azide-alkyne cycloaddition (figure adapted from reference).[49]

The regioselectivity and catalytic efficiency of the RuAAC reaction are strongly influenced by the ligands bound to the ruthenium center. Electron-rich Cp*RuCl-based complexes, such as [Cp*RuCl(cod)] and [Cp*RuCl(PPh_3)$_2$], consistently provide excellent activity and selectivity, affording 1,5-disubstituted 1,2,3-triazoles in high yields, whereas catalysts lacking Cp* and Cl ligands generally favor the 1,4-isomer or fail to catalyze the reaction. Unlike CuAAC, internal alkynes can be efficiently employed in the RuAAC reaction, greatly expanding its synthetic utility. In this case, regioselectivity is further governed by directing groups, typically hydrogen-bond donors such as propargyl alcohols or amines on the internal alkyne, which interact with the chloride ligand on the catalyst and guide bond formation between the β-carbon of the alkyne and the terminal nitrogen. In the absence of such substituents, regioselectivity is instead dictated by electronic and steric factors, with the most electronegative and least hindered alkyne carbon preferentially occupying the C-4 position of the triazole product.[50]

Both alkyl and aryl azides are compatible with the RuAAC conditions, and the reaction shows a robust tolerance towards the substituents on the alkyne. Notably, while CuAAC is restricted to the formation of 1,4-disubstituted triazoles, RuAAC uniquely grants access to both 1,5-disubstituted and 1,4,5-trisubstituted 1,2,3-triazoles, highlighting its broader synthetic versatility.

Both the 1,5-disubstituted and 1,4,5-trisubstituted 1,2,3-triazoles prepared with RuAAC have found wide applications across different fields, particularly in medicinal chemistry and peptidomimetics as *cis* amide bond isoteres.[51, 52] For example, 1,5-disubstitued 1,2,3-triazoles have been explored as mimics of disulfide linkages (Figure 2a)[53].

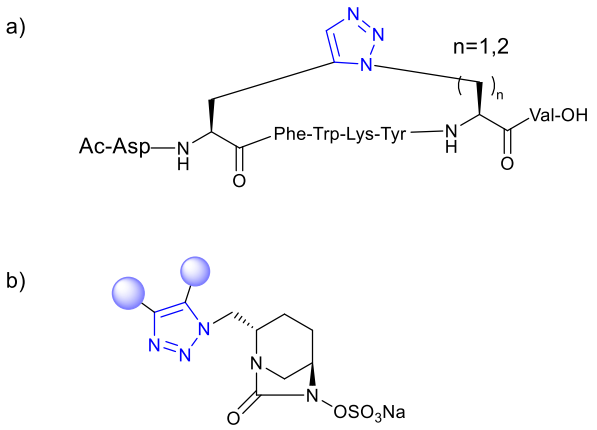

Figure 2. 1,5-Disubstituted 1,2,3- triazole applications a) disulfide bond mimetics; b) Triazole containing DBO-based derivatives.

RuAAC synthesis of β-lactamase inhibitors using diazabicyclooctane (DBO) as a scaffold led to the compound shown in Figure 2b. Such triazole derivatives increase the efficacy when used in combination with an antibiotic. Changing the substitution pattern in two positions on the triazole scaffolds could add the possibility for new interactions, improving the biological activity of these DBO-based derivatives.[54]

Before concluding, it is also important to mention the SPAAC reaction, or Strain-Promoted Azide-Alkyne Cycloaddition, reported by Bertozzi and co-workers. This reaction does not rely on transition metal catalysis for the azide alkyne cycloaddition, having as its driving force instead the release of ring strain energy upon formation of the triazole product (Scheme 10).[55] Starting from a strained cyclic alkyne (cyclooctyne) the reaction proceeds efficiently with azides under mild and biocompatible conditions, making it particularly valuable for applications in chemical biology and for bioconjugation purposes.

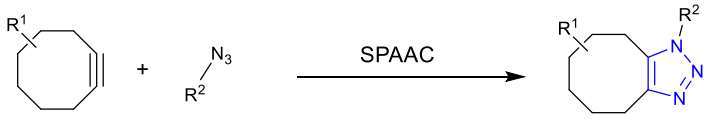

Scheme 10. Schematic representation of the Strain-Promoted Azide Alkyne Cycloaddition (SPAAC).

1.3 Transfer Hydrogenation Reactions

Among hydrogenation methods, transfer hydrogenation is distinguished by the use of a donor molecule to transfer hydrogen to a substrate, rather than using molecular hydrogen (H_2) as the hydrogen source.[56] This approach offers several advantages, including the replacement of hazardous pressurized H_2 gas and the complex experimental set ups required for its use, instead relying on the use of inexpensive and easy-to-handle hydrogen donors, allowing the recyclability of the hydrogen source, and the availability of robust catalysts.[57-59]

Hydrogen transfer reactions are classified by Braude and Linstead into three types: (i) hydrogen migration taking place within one single molecule; (ii) hydrogen disproportionation, involving hydrogen transfer between identical donor and acceptor units; and (iii) transfer hydrogeation (TH), occurring between unlike donor and acceptor units.[60]

1.3.1 Aldehyde Disproportionation

In aldehyde disproportionation reactions, two molecules of the same aldehyde undergo simultaneous oxidation and reduction where one is reduced to the alcohol and the other oxidized to the carboxylic acid or ester.

An early example of aldehyde disproportionation is the Cannizzaro reaction.[61] Dating back to 19th century, this very useful synthetic transformation is among the oldest known processes in synthetic organic chemistry, involving the base-induced disproportionation of aromatic aldehydes into the corresponding alcohols and carboxylic acids (Scheme 11a). It proceeds only with aldehydes lacking α-hydrogens, since the use of strong bases causes the abstraction of the acidic α-proton to form an enolate, leading to aldol products instead.

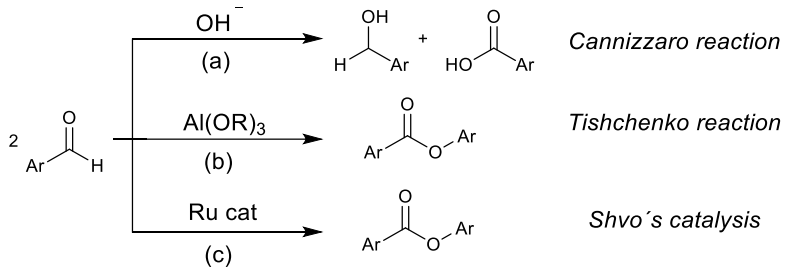

Scheme 11. a) Cannizzaro reaction; b) Tishchenko reaction; c) Tishchenko reaction using Shvo´s catalyst.

The Tishchenko reaction is an interesting variant of the Cannizzaro reaction, where the initial alcohol and acid formed undergo further coupling to give an ester (Scheme 11b). [62] However, this transformation is often challenging for aliphatic aldehydes, as it typically requires harsh conditions such as high temperatures and the use of strong bases like aluminum alkoxides.

The metal catalyzed version of this reaction can be conducted using the Shvo catalyst, thus bypassing the need for strong bases (Scheme 11c). Reported for the first time in 1984,[63] the Shvo catalyst (**I**, Scheme 12) is a cyclopentadienone-ligated diruthenium complex, $[Ru_2(CO)_4(\mu\text{-}H)(C_4Ph_4COHOCC_4Ph_4)]$, which is capable of mediating many hydrogenation processes.[64, 65] It has been widely applied in hydrogen transfer reactions, including in the hydrogenation of carbonyl compounds, transfer hydrogenation of ketones and imines, disproportion of aldehydes to esters, and Oppenauer-type oxidations of alcohols and amines.[66] Upon heating, diruthenium complex **I** dissociates into two catalytically active monoruthenium species: an isolable 18-electron complex **II** and a highly reactive 16-electron species **III**, the latter never being observed directly (Scheme 12). The 18-electron complex functions as a hydrogenation catalyst, while the 16-electron species promotes dehydrogenation. These two active forms are interconvertible, enabling hydrogen-transfer processes.

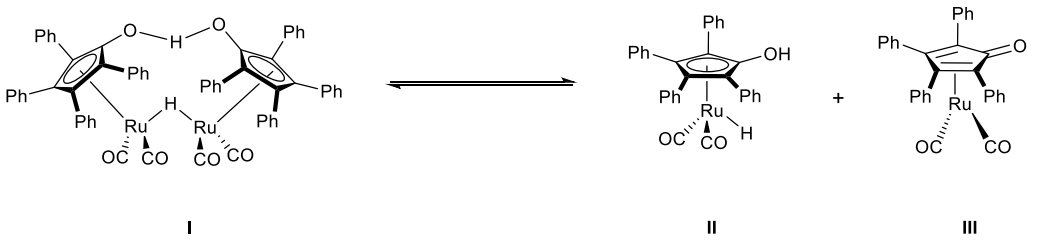

I **II** **III**

Scheme 12. Dissociation of the Shvo catalyst **I** into the active forms **II** and **III**.

The mechanism for the aldehyde disproportionation catalyzed by the active forms of **I** is shown in Scheme 13. Initially, the aldehyde is reduced to the corresponding alcohol by complex **II**, which oxidizes to complex **III**. The formed alcohol then reacts with a second aldehyde molecule to form a hemiacetal intermediate, which is then oxidized to the ester, simultaneously regenerating complex **II**.

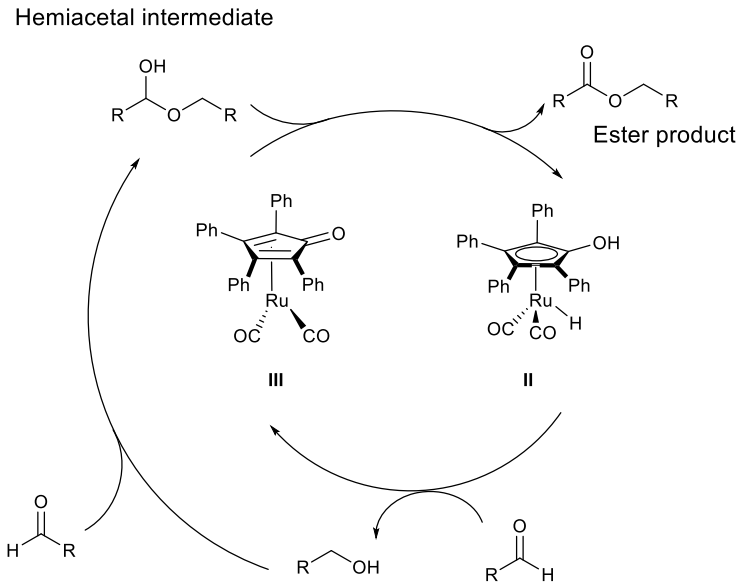

Scheme 13. Mechanistic cycle for the disproportionation of an aldehyde catalyzed by active forms **II** and **III** of the Shvo catalyst.

1.3.2 Hydrogen Borrowing

The hydrogen borrowing (HB) principle, also known as hydrogen autotransfer, is a powerful strategy involving transfer hydrogenation and subsequent transformations to build more complex molecules, while avoiding the direct use of molecular hydrogen and unnecessary isolation steps. This approach is highly valued for its synthetic versatility as well as its economic and environmental advantages.[67] For this transformation, alcohols are usually used as starting materials, together with amines or carbon nucleophiles, to form C-N or C-C bonds.

The general pathway for the *N*-alkylation of amines with alcohol via hydrogen borrowing is shown in Scheme 14. [68]

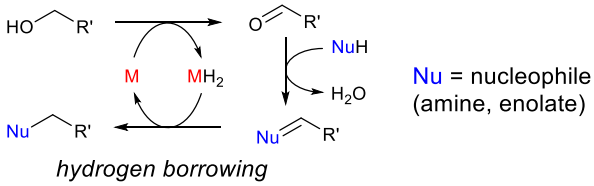

Scheme 14. General transition-metal catalyzed borrowing hydrogen reactions.

The reaction starts with a transition-metal catalyzed dehydrogenation of the alcohol, producing a reactive carbonyl intermediate. This carbonyl compound can undergo diverse subsequent transformations by reacting with carbon or nitrogen nucleophile, such as condensation with an amine to form an imine. The resultant imine is then reduced by [MH_2], which is produced in the initial dehydrogenation phase, thereby restoring the active catalyst

and releasing the reaction product (specifically, an N-alkylated amine), thus concluding the catalytic process. The sequence is similar to reductive amination, except that the aldehyde and hydride reagents are generated *in situ*.

The formation of C–N bonds is a fundamental step in the synthesis of fine chemicals and pharmaceuticals. Among the many approaches available, ranging from classical methods such as amination of halides[69] and reductive amination,[70] to modern catalytic techniques like amine–aryl halide coupling (Buchwald-Hartwig coupling)[71] and hydroamination,[72] hydrogen-borrowing alkylation of amines with alcohols represent a promising alternative.

Examples of transition-metals catalyzing this reaction include [Ru],[73] [Ir],[74] [Pd],[75] [Mn],[76] [Fe],[77] [Co],[78] [Os],[79] [Cu],[80] [Cr],[81] and the development of new methodologies has led to many different experimental conditions compatible with a wide substrate scope.[82]

The application of this metal catalyzed transformation has brought many advantages for the development of industrial synthetic routes to therapeutic compounds.[83] For example, the $[Cp^*IrCl_2]_2$-catalyzed N-heterocyclization of primary amines with diols[84] has proven to be a valuable strategy for preparing an intermediate (Scheme 15) in the synthesis of noranabasamine, an amphibian alkaloid showing therapeutic effect on the nicotinic acetylcholine receptor.[85] The reaction proceeded in high yields for both (*R*)- and (*S*)-phenylethylamine to afford the corresponding diastereomer in excellent selectivity.

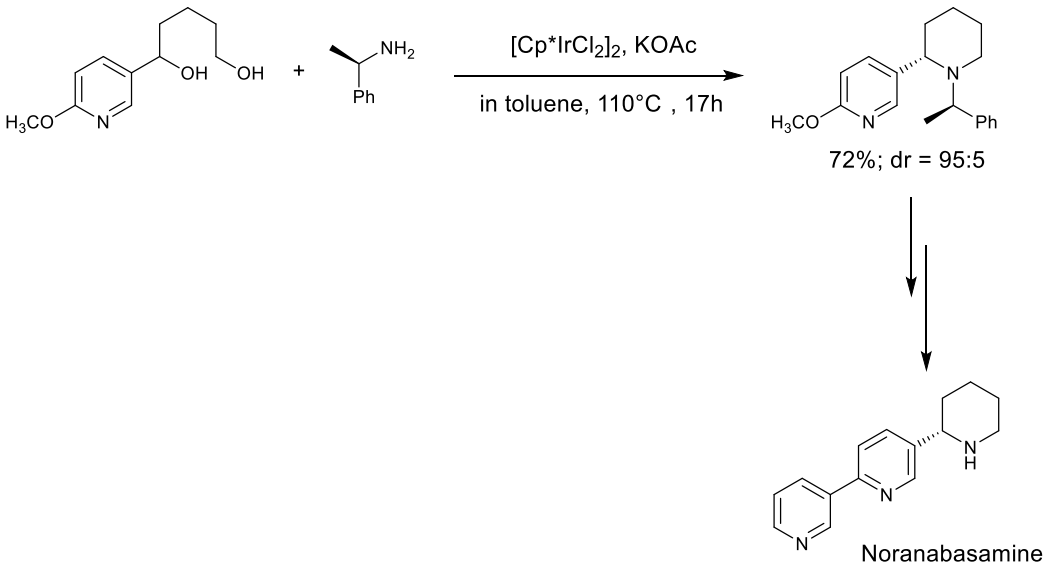

Scheme 15. Synthesis of an intermediate in the route towards noranabasamine.

1.4 Synthetic Receptors for Sensing Applications

Receptors are molecular systems designed to recognize and bind specific targets, playing a central role in mediating interactions at the molecular level. Their design can be tailored toward either biomolecules or ions, enabling selective recognition and functional applications.

Bio-based receptors, like deoxyribonucleic acid (DNA), aptamers, cells, enzymes or antibodies, are the most common types of receptors used for the recognition of biomolecules. For example, utilization of enzymes has proven to guarantee high recognition specificity, thanks to the lock and key mechanism employed in the interaction with the substrate. After the recognition, the enzyme (e.g. alcohol oxidase, glucose oxidase, lactose oxidase) catalyzes a specific biochemical reaction that transforms the analyte in an electroactive, measurable byproduct.[86]

Despite the high degree of specificity and affinity that is provided by using these biomolecules as receptors, they also present some limitations.[87] Biological receptors face environmental sensitivity, affected by factors like temperature, pH, and ionic strength, which potentially compromises stability and detection accuracy. Furthermore, their production, particularly of antibodies, is costly and complex, often requiring methods like animal immunization or cell culture, posing challenges for scalability and reproducibility. This type of biomolecules are also difficult to functionalize. The design of synthetic organic receptors addresses most of these limitations, as these receptors can be synthesized in the lab and bypass the requirement for biological materials.

Depending on the type of interactions that the receptors are meant to establish with the target, we can have different molecular designs. For example, a type of *p*-sulfonatocalix[n] arene has been shown to form complexes with charged amino acid lateral chains of lysine and especially arginine, thanks to electrostatic interactions and π–π interactions between its guanidinium group and the aromatic rings in the cavity (Figure 3). [88]

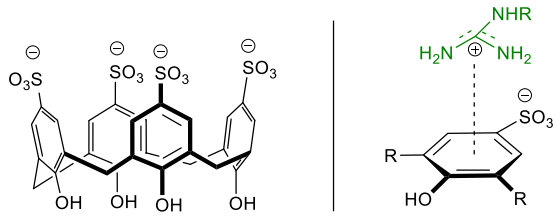

Figure 3. SC4 receptor and its interaction with arginine

Synthetic organic receptors are also widely used in ion sensing.[89] Precise detection and quantification of trace-level contamination by heavy and transition metals is essential for safe environmental and biological health.[90] Commonly monitored ions include Hg^{2+}, Ni^{2+},

Cu^{2+}, Cd^{2+}, Zn^{2+}, Ag^{+}, Pd^{2+}, Pb^{2+}, Fe^{2+}, Cr^{3+}, Pt^{2+}, and Co^{2+}, all of which are widely employed in industry yet pose toxicological risks when present in excess.[91] Similarly, anions are central to physiological processes and industrial applications, but can also act as harmful environmental pollutants. Consequently, research in anion recognition and trapping has expanded rapidly over the past two decades, establishing itself as a robust and dynamic field within molecular sensing.[92]

A nanopore-based sensing system employing a fluorescent peptide (Figure 4a) has been developed for the ultrasensitive and selective detection of Cu^{2+}, achieving femtomolar sensitivity even in complex media such as human urine mimics. The sensor is reversible upon EDTA washing and shows strong potential for translation into lab-on-chip devices for medical diagnostics, particularly in monitoring copper-related disorders.[93]

A series of oligo (phenyl-amidetriazole) foldamers (Figure 4b) were synthesized and shown to adopt helical conformations upon binding halide ions, with their binding behavior strongly influenced by foldamer length, medium, and the nature of the halide. Short foldamers (n=2) with one helical turn bind halides in a 1:1 ratio, while longer foldamers (n=4 or 6) can form 1:2 complexes with chloride and bromide, increasing affinity by adjusting their helical pitch to minimize electrostatic repulsion.[94]

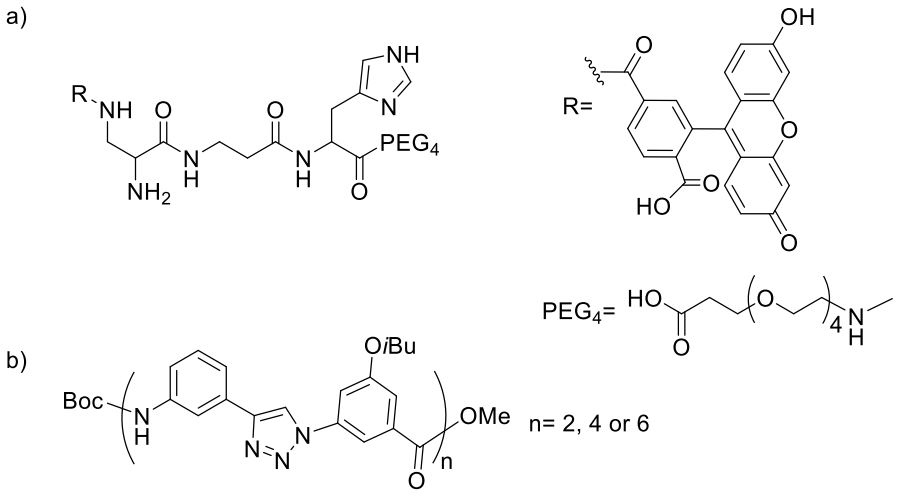

Figure 4. a) Cu^{2+} ion selective peptide; b) oligo(phenyl-amidetriazole) foldamers for detection of halides.

In summary, synthetic receptors can offer powerful strategies for the selective recognition of biomolecules and ions, each with unique advantages and limitations. While bioreceptors provide unmatched specificity, synthetic systems offer enhanced stability, tunability, and broader applicability, as illustrated by examples ranging from calixarene-based molecular recognition to advanced sensors for metal and halide ions. Together, these developments highlight the central role of receptor design in advancing molecular sensing for biomedical, environmental, and industrial applications.

1.5 Aim of the Thesis

This thesis focuses on four main projects that aim to expand the scope of ruthenium-catalyzed synthetic methodologies for the preparation of functional molecules and synthetic receptors.

The first project, described in Chapter 2, explores a ruthenium-catalyzed aldehyde disproportionation for the dimerization of vanillin derivatives. Vanillin, an aromatic compound derived from lignin, represents a renewable and industrially available feedstock. Because bisphenol A (BPA) remains a widely used yet reprotoxic molecule in polymer manufacturing, this study addresses the current need for sustainable alternatives that could replace BPA in future materials. The work investigates whether vanillin-derived aldehydes can undergo efficient Ru-catalyzed disproportionation to form dimers, and whether these dimeric products display the structural and physicochemical characteristics required to mimic BPA's role in polymeric systems.

The second project, presented in Chapter 3, investigates a two-step ruthenium-catalyzed strategy for the synthesis of tricyclic 1,5-fused 1,2,3-triazole piperazines. Despite the growing interest in triazole-containing heterocycles, efficient and general methods for constructing functionalized tricyclic triazole-piperazine scaffolds remain limited. This chapter therefore employs a sequential RuAAC reaction followed by a hydrogen-borrowing cyclization to provide an atom-economical and versatile approach for the preparation of such complex ring systems, broadening the synthetic potential of Ru-catalyzed methodologies.

Chapter 4 examines the application of the prolinol-appended 1,4,5-trisubstituted 1,2,3-triazoles obtained from the previous synthetic route as organocatalysts in aldol reactions. This project seeks to determine whether these triazole-based structures can promote stereoselective transformations in aqueous media, addressing the broader challenge of developing greener and metal-free catalytic systems. By evaluating their catalytic activity and stereochemical influence, the study aims to assess the potential of triazole-functionalized prolinol scaffolds as sustainable organocatalysts.

Finally, Chapter 5 focuses on the design and synthesis of modular 1,4,5-trisubstituted 1,2,3-triazole-based synthetic receptors. These triazoles were constructed as versatile building blocks via RuAAC and subsequently assembled into linear dimers and trimers through amide coupling to yield oligomeric structures designed to mimic peptide backbones. This project addresses the knowledge gap between simple triazole recognition motifs and more complex peptide-inspired receptors by examining how molecular architecture affects their ability to recognize metal ions and/or small biomolecules.

2.Ruthenium-Catalyzed Dimerization of Vanillin for the Formation of a Biobased Epoxy Thermoset Resin

2.1 Background

The urgent need to mitigate climate change and reduce greenhouse gas emissions has prompted industries worldwide to minimize their dependence on fossil resources and shift toward sustainable alternatives.[95] Within this framework, the concepts of circular economy has emerged as a guiding model, aiming to establish a synergy between economic growth, societal well-being, and environmental preservation.

Circular economy is generally defined as an economic model in which the products and the materials they contain are kept at their highest value for as long as possible, in contrast to the traditional linear model of "take–make–dispose".[96] Its central aim is to reutilize and recycle by-products and waste generated during the processing of raw materials, thereby transforming them into new valuable resources (Figure 5).

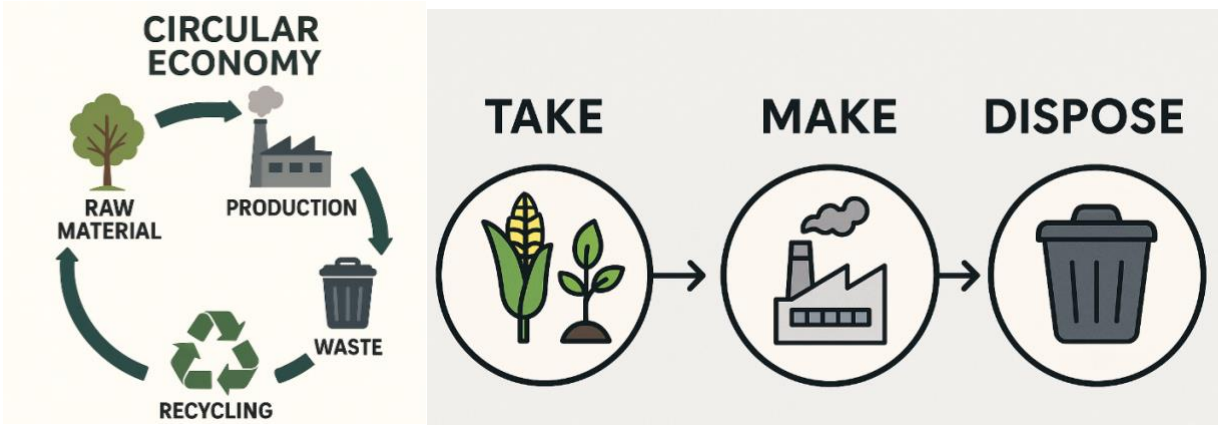

Figure 5. Schematic representation of the circular economy model highlighting resource recovery, reuse, and recycling loops compared to the traditional linear 'take–make–dispose' process.

Among existing solutions, lignocellulosic biomass stands out as a renewable feedstock derived from agricultural residues and forestry by-products. Its valorization through integrated biorefineries offers a pathway to generate biofuels, platform chemicals, bioplastics, resins, and a wide range of other biobased materials, thereby reducing reliance on nonrenewable petrochemicals.[97]

Lignocellulosic waste, which represents a major fraction of agricultural and industrial residues, is mainly composed of three biopolymers: cellulose, hemicellulose, and lignin. Cellulose is a rigid polymer of glucose units, whereas hemicelluloses are branched heteropolysaccharides. On the other hand, lignin is a highly cross-linked polyphenolic

network which acts as a binding agent embedding cellulose and hemicellulose into a rigid structure.[98]

Depolymerization of lignin has drawn particular attention, as it enables access to valuable aromatics such as vanillin (Figure 6), a platform chemical with wide-ranging applications in the synthesis of biomass-derived polymers, fine chemicals, and other high-value materials.[99]

In particular, lignin-derived aromatics have emerged as promising candidates for the development of bisphenol A substitutes. Bisphenol A (BPA, Figure 6), one of the highest-volume chemicals produced worldwide, is mainly used as a monomer for polycarbonates and epoxy resins that find applications in packaging, electronics, coatings, and medical devices. Its widespread use is linked to valuable mechanical and thermal properties, yet BPA is now recognized as an endocrine disruptor with reproductive and developmental toxicity, leading to strict regulations and partial bans in several countries. This has prompted an urgent search for safer, sustainable alternatives.[100]

The potential for vanillin-derived dimers to mimic the diaryl backbone of BPA has inspired numerous efforts to develop methodologies for their synthesis, with several groups exploring vanillin dimerization as a strategy to mimic BPA. Among these, one approach employed the Tishchenko reaction to obtain allylated vanillin dimers with promising polymer applications.[101] However, the Tishchenko reaction requires harsh conditions that are incompatible with sensitive functional groups such as epoxides, thereby limiting its use in epoxy-based resins. To address this challenge, our work proposes a complementary strategy for the synthesis of epoxide-containing polymer precursor molecules (EDVE, Figure 6) through the solvent-free disproportionation of vanillin derivatives catalyzed by Shvo's complex, offering a milder and more sustainable route toward renewable BPA substitutes.

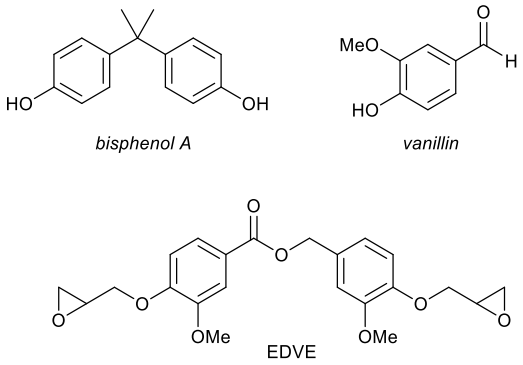

Figure 6. Structures of bisphenol A (BPA), vanillin, and the epoxy divanillin ester (EDVE) developed in this study.

2.2 Synthesis of the Epoxy Divanillin Ester (EDVE)

Since the initial goal of the project was to introduce polymerizable handles (epoxy or allyl groups) onto the vanillin dimer (**2a**), the dimerization of vanillin with itself (**1a**) using Shvo catalyst was at first attempted. Unfortunately, no formation of the desired product was observed, likely due to the coordination of the catalyst with the free hydroxyl groups of vanillin, which interferes with the catalytic cycle (Scheme 16). This outcome led to exploring two alternative approaches: either (i) temporarily protecting the hydroxyl groups prior to dimerization, followed by deprotection and subsequent functionalization, or (ii) introducing the functional group into the vanillin monomer before performing the dimerization step.

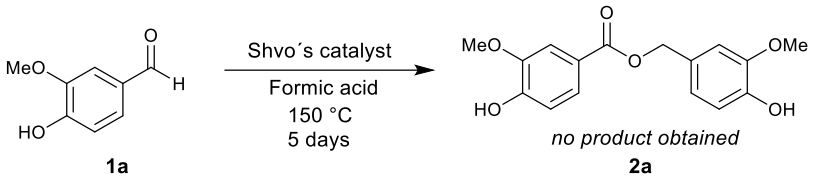

Scheme 16. Attempted dimerization of vanillin via ruthenium catalysis.

In the first strategy, a protection–deprotection sequence was investigated using two different protecting groups. Initially, acetylation of vanillin (**1a**) with acetic anhydride afforded the protected derivative **1b** in 98% yield (Scheme 17a). The subsequent dimerization was successfully promoted by Shvo catalyst (Scheme 17b). Optimizing the conditions by adding a small amount of toluene as solvent and adding the catalyst in two portions (at t = 0 h and t = 18 h) improved the yield, raising it from 50–60% under solvent-free, single-addition conditions to 70% under the modified conditions.

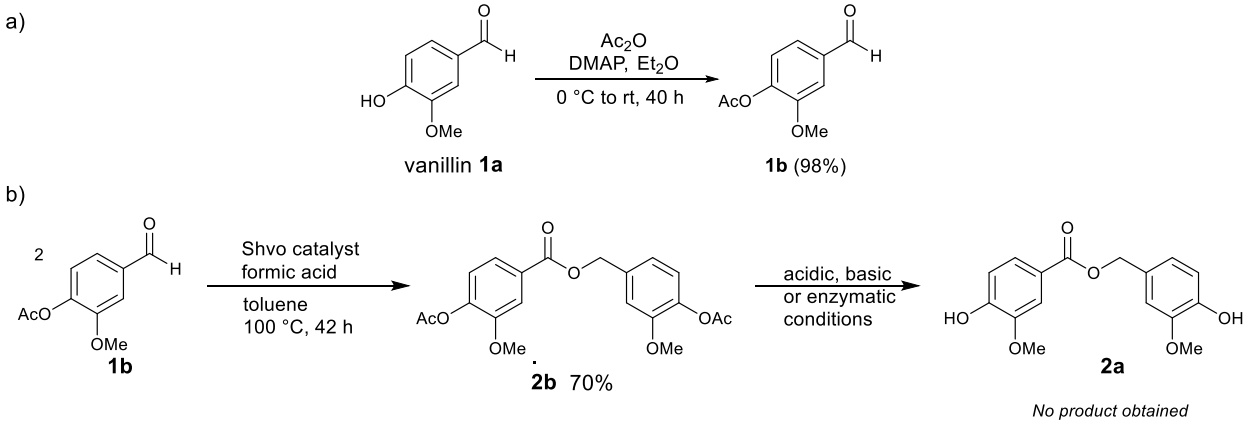

Scheme 17. a) Acetylation of vanillin monomer; b) dimerization and subsequent deprotection of the protected dimer.

The deprotection of the acetate proved challenging since competitive cleavage of the benzyl alcohol is favored upon treatment of substrate **2b** with HCl. Similarly, basic conditions can

promote an elimination reaction, which also results in ester cleavage (Scheme 19b). Porcine lipase was also investigated for the cleavage of the acetate, but unfortunately did not yield any significant results. On the other hand, deprotection of TBS protected vanillin **2c** (obtained after protection and dimerization of **1a**, Scheme 18) proceeded smoothly, affording compound **2a** in 49% yield.

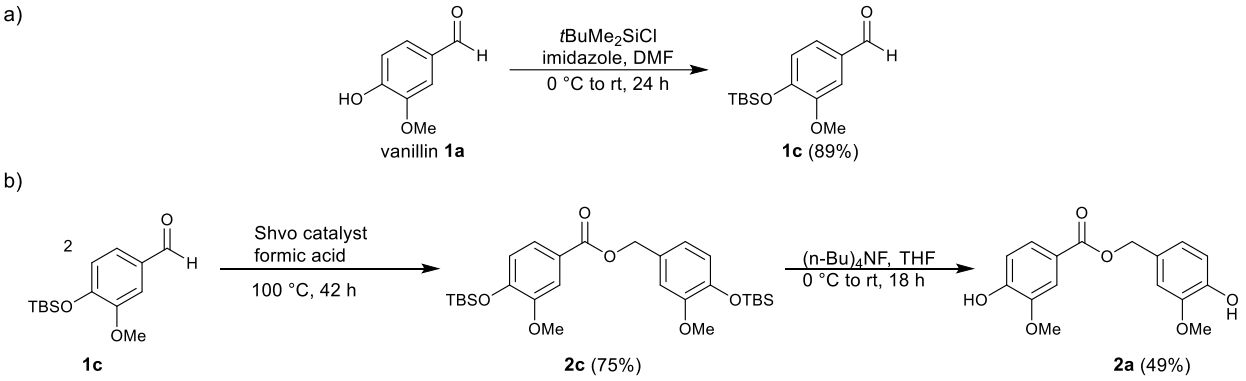

Scheme 18. a) Protection of vanillin with TBSCl; b) route to compound **2a**.

Unfortunately, the subsequent attempts to functionalize vanillin dimer **2a** with the polymerizable handles (either an allyl or epoxy group) were unsuccessful, since the basic conditions required for these transformations promoted ester cleavage instead, as previously mentioned (Scheme 19b). In the case of allylation, ^{1}H nuclear magnetic resonance (NMR) analysis confirmed the cleavage, since the observed products corresponded to allylation of both the carboxylic acid and the alcohol, occurring after breakage of the ester (Scheme 19a). Several modifications of the reaction conditions were explored in an effort to suppress this undesired cleavage. These included using non-nucleophilic bases such as DIPEA or DBU, switching solvents from acetone to THF or DMF, performing the reaction at room temperature and replacing allyl bromide with allyl tosylate. However, none of these strategies prevented ester breakdown, and the desired functionalized dimer could not be obtained.

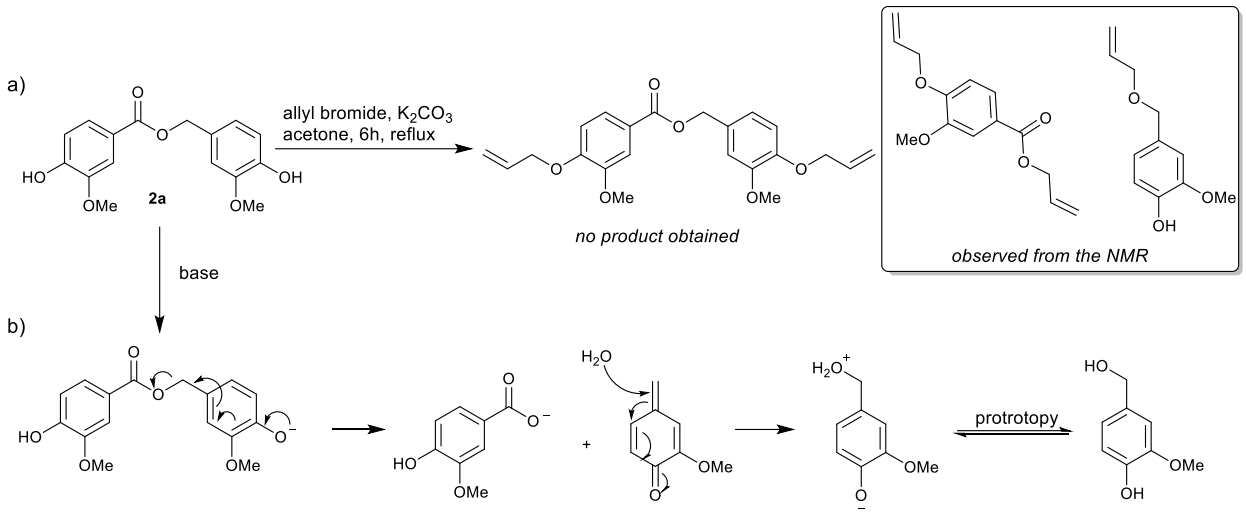

Scheme 19. a) Attempt to allylate vanillin dimer **2a**; b) base promoted degradation of vanillin dimer **2a**.

Since the strategy of introducing polymerizable handles such as an allyl or epoxy groups after dimerization proved unsuccessful, an alternative approach was explored, involving the introduction of a polymerizable functionality directly onto the hydroxyl group of vanillin before the dimerization step.

At first, introduction of an allyl functionality was attempted. The allylation of compound **1a** proceeded to the desired product **1e**, albeit with a moderate yield (Scheme 20a). The subsequent dimerization step of the allylated monomer afforded the formation of the ester but with simultaneous hydrogenation of the allyl double bond (Scheme 20b), making it therefore impossible to use the obtained product for further polymerization. This hydrogenation is not unexpected, as the Shvo catalyst employed in the reaction operates via a hydrogen transfer mechanism, which can reduce C=C bonds under the reaction conditions.

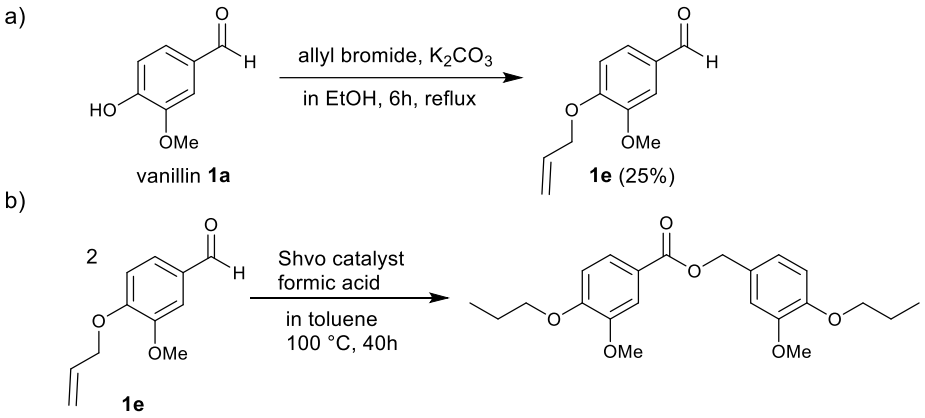

Scheme 20. a) Allylation of vanillin; b) dimerization of **1e**.

Introduction of an epoxide group was then explored. Vanillin was at first successfully functionalized using epichorohydrin (Scheme 21) and monomer **1d** was obtained in 60% yield.

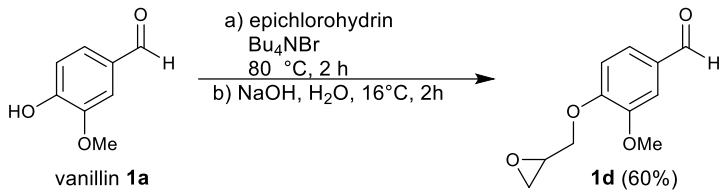

Scheme 21. Synthesis of epoxy-functionalized vanillin **1d** via reaction of vanillin **1a** with epichlorohydrin under basic conditions.

The dimerization reaction of **1d** in the presence of the Shvo catalyst was then attempted. Initially, the reaction was carried out under solventless conditions at 100 °C using 2.5 mol% catalyst which was added in two portions over 48 h. This led to a 70% conversion of the starting material to the product **2d** (Table 1, Entry 1). In order to improve the conversion, an optimization of the reaction conditions was performed. Introducing a small amount of toluene prevented sublimation of the starting material, and improved the yield to 81% (Entry 2) . Further optimization by varying catalyst loading and reaction time showed that adding 3.75 mol% catalyst in three portions over 36 or 72 h gave high and consistent conversions (89% and 88%, Entries 3 and 4). Although increasing the loading to 5 mol% and extending the reaction to 96 h provided a slightly higher conversion of 92% (Entry 5), the conditions with 3.75 mol% catalyst over 36 h represented the best compromise between efficiency and practicality.

The dimerization conditions reported by Simon and Darses,[102] employing $[RuCl_2(p\text{-cym})]_2$ with $CyPPh_2$ to generate the active catalyst *in situ* were also tested. While this method afforded high conversions for aromatic aldehydes in their study, it proved ineffective for the epoxy-functionalized substrate **1d**, which remained unreacted. The lack of reactivity may be attributed to the high oxygen content of **1d**, which could interfere with catalyst performance under these conditions.

Table 1. Optimization table for the dimerization of epoxy vanillin monomer **1d**.

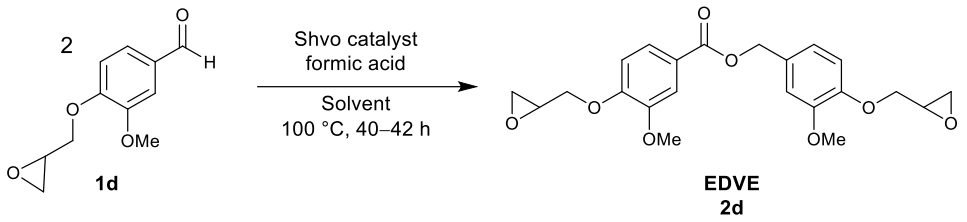

Entry	Shvo Catalyst (mol%)	HCOOH (mol%)	Solvent (mL/mmol vanillin)	Time (h)	Conv. (%)
1	2.5	20	No solvent	48	70
2	2.5	20	Toluene (0.6)	48	81
3	3.75	20	Toluene (0.4)	36	89
4	3.75	20	Toluene (0.4)	72	88
5	5	20	Toluene (0.4)	96	92

Once an efficient conversion to EDVE was established, the main challenge became separating product **2d** from residual starting material **1d**. Conventional flash chromatography on silica proved unsuitable, as EDVE exhibited strong retention on the column, resulting in poor recovery and low yields, despite the isolated material being of high purity. More effective purification was achieved using reverse-phase chromatography on a C18 column with an H_2O–MeOH gradient, which allowed smooth elution of the product. Further optimization of column size and flowrate in the purification system ultimately afforded pure EDVE in an improved isolated yield of up to 65%.

EDVE was characterized using NMR, FTIR, HRMS, and single-crystal X-ray diffraction. X-ray diffraction analysis unequivocally confirmed the molecular structure of the target compound, validating the successful formation of the desired dimer. In the ^{1}H NMR spectrum, the appearance of a benzylic $–CH_2$ signal at 5.27 ppm and two distinct $–OCH_3$ peaks at 3.91 and 3.89 ppm (compared to a single $–OCH_3$ peak at 3.93 ppm in the monomer) provided clear evidence for ester bond formation. Correspondingly, the ^{13}C NMR spectrum supported this conclusion, showing the disappearance of the aldehydic carbonyl resonance at 191 ppm and the emergence of a new ester carbonyl peak at 166 ppm, consistent with the formation of the dimeric structure.

In collaboration with Prof. Mats Johansson and Dr. Iuliana Ribca at KTH, the thermal behaviour of EDVE was investigated. The studies confirmed that EDVE is semi-crystalline

and thermally stable up to around 300 °C, undergoing two main degradation steps associated with cleavage of ether and ester bond.

Upon curing with Jeffamine D-400, EDVE formed a crosslinked epoxy thermoset resin, exhibiting a glass transition temperature around 45–50 °C and mechanical and thermal properties comparable to BPA-based epoxies. FTIR analysis confirmed the consumption of epoxy groups and formation of hydroxyl functionalities during curing.

Overall, these results demonstrate that EDVE can serve as a viable bio-based alternative to Bisphenol A, providing similar performance while offering the potential for improved recyclability through its ester-containing structure.

2.3 Conclusions and Outlook

In this work, a ruthenium-catalyzed strategy was developed to access epoxy divanillin ester (EDVE), a promising biobased alternative to bisphenol A (BPA). The initial objective was to obtain a polymerizable vanillin dimer structurally resembling BPA. Two strategies were explored: the functionalization with a polymerizable handle (allyl or epoxy groups) either before or after the dimerization.

The first approach failed as the basic conditions used in the functionalization caused ester cleavage of the dimer. The introduction of an allyl or epoxy group prior to dimerization was then explored. While the dimerization of the allylated vanillin resulted in hydrogenation of the polymerizable handle, the use of an epoxy functionality was instead successful, affording formation the corresponding epoxy divanillin dimer (EDVE). Optimization of the ruthenium-catalyzed reaction afforded EDVE in up to 89% conversion under solvent-free or toluene-assisted conditions, highlighting the efficiency of this method. Subsequent characterization and studies of the thermal properties of the EDVE dimer indicated the formation of the desired product and demonstrated its potential as a BPA substitute.

Importantly, the incorporation of an ester moiety in the EDVE backbone could facilitate future recycling strategies, such as chemical or enzymatic hydrolysis. Overall, EDVE emerges as a valuable addition to the growing portfolio of biobased building blocks, offering a viable pathway toward safer and more sustainable epoxy materials. For future work, it would be interesting to extend this ruthenium-catalyzed dimerization strategy to other biomass-derived phenolic aldehydes, to explore how structural variations influence reactivity, selectivity, and the physicochemical properties of the resulting dimers. This could broaden the accessible library of renewable bisphenol-type monomers, allowing fine-tuning of thermal and mechanical properties for targeted polymer applications.

3. Ruthenium-Catalyzed Synthesis of Tricyclic 1,5-Fused 1,2,3-Triazole Piperazines

While Chapter 2 focused on the valorization of renewable feedstocks through ruthenium-catalyzed transformations, the following chapter explores how the same metal center can be used for catalysis in building complex heterocyclic frameworks. Chapter 3 thus introduces a sequential Ru-catalyzed strategy for the synthesis of tricyclic 1,5-fused 1,2,3-triazole piperazines.

3.1 Background

Thanks to the advent of click chemistry for (3+2) azide-alkyne cycloadditions, which allows easy and quick access to 1,2,3-triazoles, it has become possible to study and apply these molecules in several different contexts, especially in medicinal chemistry and chemical biology.[103] Due to their ability to interact with biological targets, triazoles have gathered significant interest as potential therapeutic agents for various diseases.[104, 105] The triazole ring has shown to be an important component in a plethora of biologically relevant molecules, such as anticancer,[106] anti-inflammatory,[107] antiHIV,[108] antimicrobial[109] and antiviral[110] compounds (Scheme 22).

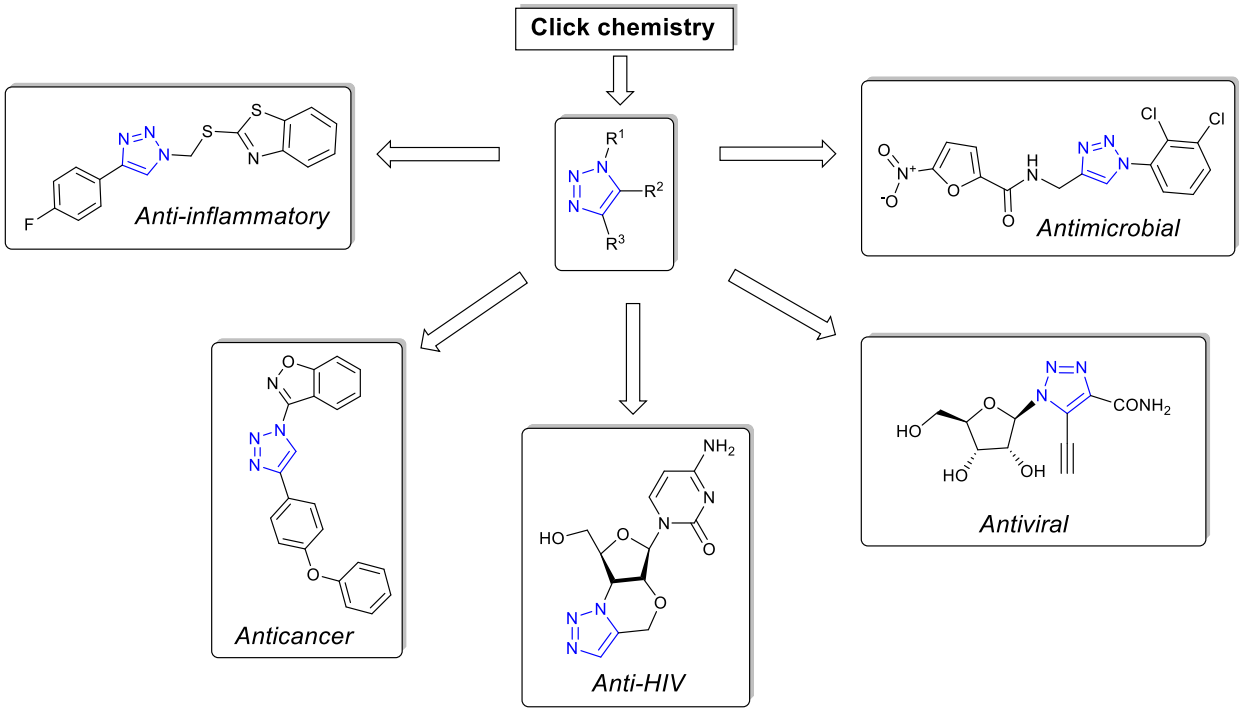

Scheme 22. 1,2,3-Triazoles in biologically active molecules.

Being such appealing structures in drug discovery, several synthetic methods have been recently developed for the preparation of 1,2,3-triazoles, not only to enhance the efficiency of the synthetic pathways for accessing these molecules, but also to produce novel molecules containing a triazole functionality with promising applications.

In particular, piperazine rings fused with 1,2,3-triazoles have shown potential in various applications, such as therapeutics for Alzheimer's disease.[111]

In this project, a synthetic pathway toward tricyclic 1,5-fused 1,2,3-triazole–piperazine compounds (**4**) was established using ruthenium-catalyzed azide–alkyne cycloaddition (RuAAC) and providing a click-chemistry-based approach that has not previously been explored for this class of compounds.[112-117]

The strategy explored involved accessing tricyclic fused triazoles **6** via hydrogen borrowing performed on the 1,4,5-trisubstituted 1,2,3 triazole **5**, obtained via a RuAAC starting from internal alkynes **3** and azide **4** (Scheme 23).

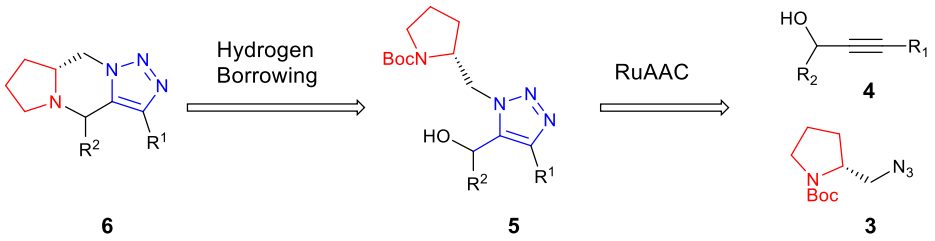

Scheme 23. Proposed retrosynthetic pathway for tricyclic fused triazoles **6**.

3.2 Results and Discussions

At the outset of this work, proline-derived azide **3** (available in both *R* and *S* configurations) was employed directly as a commercial reagent. Its elevated price and limited availability, however, made reliance on the commercial source impractical. For this reason, azide **3** was subsequently prepared in-house from Boc-prolinol, affording the desired product in good yield (Scheme 24, illustrated with the (*R*)-enantiomer).

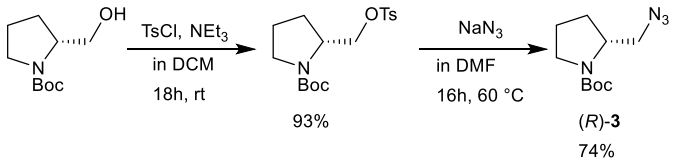

Scheme 24. Synthesis of proline-azide *(R)*-**3**.

As previously mentioned, the RuAAC reaction allows the use of internal alkynes in the azide alkyne cycloaddition reaction. When alkynes such as compounds **4** (Scheme 23) are used as substrates in the reaction with Boc-protected proline-azide, the regioselectivity should

favor the exclusive formation of compound **5**, thanks to the hydrogen bond formation between the chlorine on the catalyst and the -OH group on the substrate. Various conditions for optimizing the reaction between compounds **3** and **4** were explored and the most efficient ones employed [Cp*RuCl(cod)] as the catalyst in toluene at 40 °C. Interestingly, the reaction times changed significantly upon using different catalyst loadings. For instance, employing a 5% catalyst loading of [Ru] resulted in an 85% yield of compound **5a** after 24 hours (Table 2, Entry 1). On the other hand, using a 10% catalyst loading led to a reaction time of approximately 1 hour, yielding 76% of compound **5a** (Entry 2).

Table 2. Optimized conditions for the RuAAC reaction.

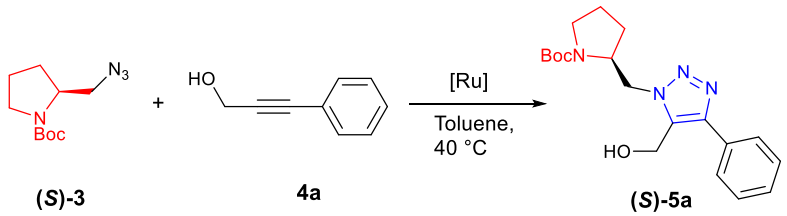

(*S*)-3 **4a** **(*S*)-5a**

Entry	Catalyst	[Ru] (mol%)	t (h)	Yield
1	[Cp*RuClCOD]	5 %	48	85%
2[a]	[Cp*RuClCOD]	10 %	1	76%

[a]Performed on the (*R*)-3 enantiomer.

Once the RuAAC reaction conditions were optimized, the substrate scope was explored under both sets of previously mentioned systems, i.e. 5% catalyst for 24-48 hours reaction time (Method A, Table 2) as well as 10% catalyst with a reaction time of 1 hour (Method B, Table 2).

Method A, compound (*R*)-**5a** was obtained in a robust 85% yield, whereas Method B afforded a slightly lower yield of 76%. Introducing substituents on the aryl group of the alkyne proved facile, resulting in a diverse array of meta- or para-substituted derivatives. These included aryl groups with methyl, methoxy, ester, CF_3, acetyl, dioxole, chloride, and nitrile substitutions, all showing compatibility with the reaction conditions. Interestingly, electron-donating or electron-withdrawing substituents on the 4-aryl group did not notably affect the reaction yield, which remained consistently good for substrates **5b-i** (Scheme 25). However, when employing a more sterically hindered alkyne bearing a methyl substituent in the ortho position on the aryl ring (**5j**), the yield dropped to 64%. Similarly, compound **5k** exhibited a slightly lower yield, likely due to its increased tendency to act as a ligand to ruthenium owing to its *N*-heterocyclic substituent. When the aryl moiety was replaced by an alkyl group (compound **5l**), the yield decreased, whereas substitution with another propargylic alcohol functionality yielded compound **5m** in a 97% yield. Additionally, the use of both alkyn and

aryl secondary alcohols was well tolerated in the reaction, affording compounds **5n** and **5o** in 88% and 95% yield, respectively.

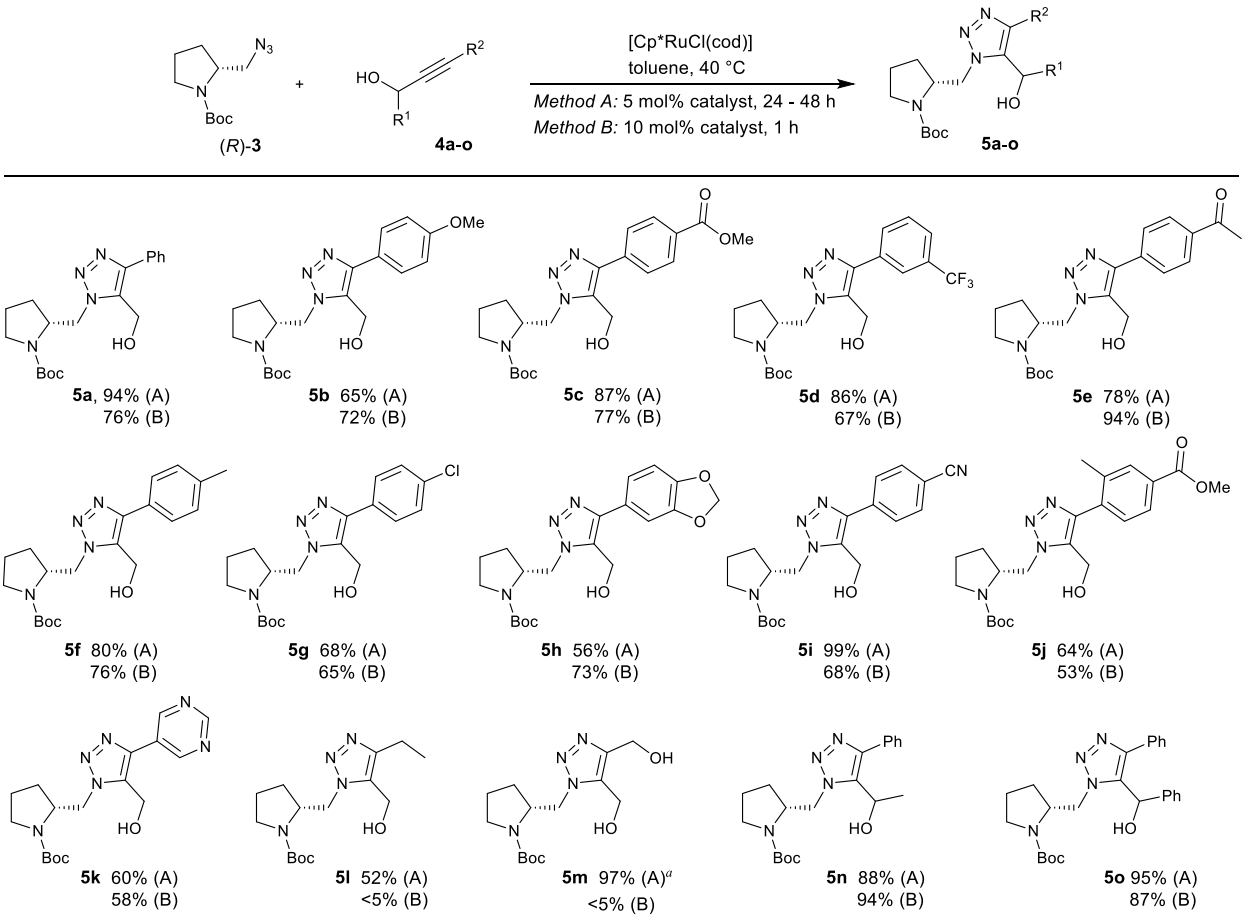

Scheme 25. Substrate scope for the Ru-catalyzed azide–alkyne cycloaddition (RuAAC) between azide **3** and internal alkynes **4** under Method A (5 mol% [Cp*RuCl(cod)], 48 h) and Method B (10 mol%, 1 h), affording 1,4,5-trisubstituted 1,2,3-triazoles **5a–o** in moderate to excellent yields.

The next step of the synthesis involved application of the hydrogen borrowing methodology. To obtain compounds **6** from triazoles **5**, the amine must first be deprotected before the hydrogen borrowing reaction. Initially, a one-pot strategy combining Boc-deprotection and hydrogen borrowing was tested on triazole **5a**. Potassium carbonate (K_2CO_3) was selected as a base, as it has been reported to promote Boc-deprotection[118] and to be employed as a base in hydrogen borrowing reaction.[119] However, the reaction did not afford the desired product (**6a**). This outcome may be attributed to the use of methanol as the solvent, which may have participated in the hydrogen borrowing process. Although the intramolecular pathway leading to a six-membered ring was expected to prevail over the competing

intermolecular processes, solvent participation appears to have prevented the desired transformation.

Given that both RuAAC and hydrogen borrowing can be catalyzed by ruthenium, a one-pot strategy for these two reactions was also explored. The alkyne and the previously Boc-deprotected azide were reacted using [Cp*RuCl(cod)] as the catalyst and triethylamine in toluene at 40°C (Scheme 26). Unfortunately, no sign of the desired product was detected from the crude ^{1}H NMR after stirring for 2 days.

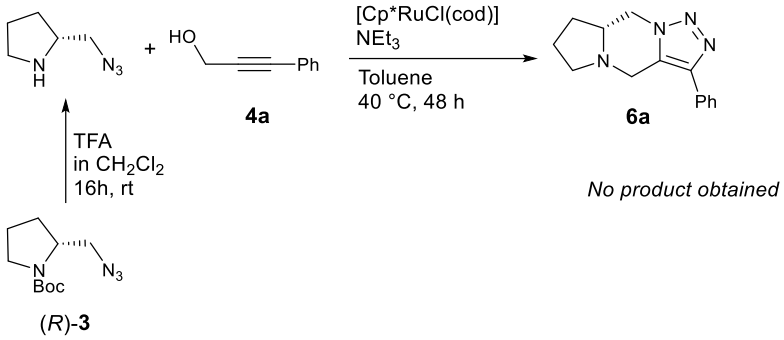

Scheme 26. Attempt to perform a one-pot RuAAC and hydrogen borrowing strategy.

At this stage, different reaction conditions were screened for the hydrogen borrowing step using **5a**-NH as the substrate. As a first approach, the conditions previously reported to be effective for secondary aliphatic amines were applied, employing 4 mol% [Ru(p-cymene)Cl_2]$_2$ in combination with an aminoamide ligand (Scheme 27a).[120] Surprisingly, no formation of the product could be detected via ^{1}H NMR while running the reaction. The Shvo catalyst, which is utilized for the *N*-alkyation of amino acids such as proline with alcohols,[121] was also tried in the reaction, but this attempt did not yield any product either (Scheme 27b). Then, an iridium catalyst, [Cp*$IrCl_2$]$_2$, was briefly screened for the hydrogen borrowing reaction, but unfortunately afforded low yields in the formation of the product.

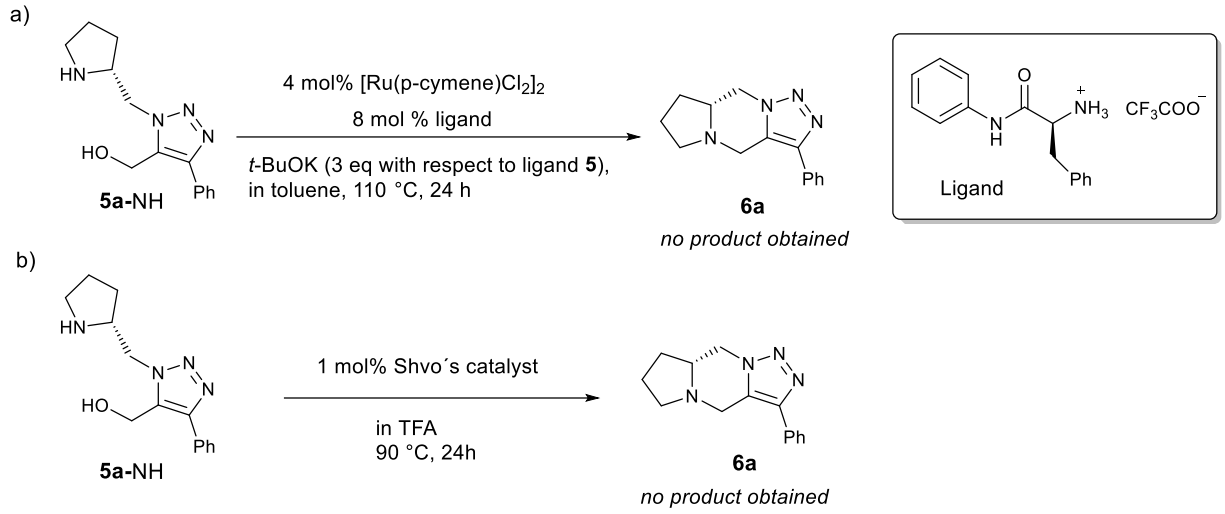

Scheme 27. Hydrogen borrowing conditions with a) ligand **5** and b) Shvo catalyst.

The best conditions among those explores were achieved by employing 5 mol% [Ru(p-cymene)Cl_2]$_2$ as the catalyst with DPEphos as the ligand and triethylamine (NEt_3) as the base, providing the formation of product **6a** with 75% yield. These conditions were subsequently employed for the reaction of the other substrates and the results are shown in Scheme 28.

The reaction showed good tolerance towards functional groups on the aromatic ring such as methoxy and CF_3, and compounds **6b** and **6d** were obtained in 65% and 74% yield, respectively. Cyclization of triazole **5e** to **6e**, which features an acetyl group in the para position of the phenyl ring, was also successful. Although no adverse effects were observed, concurrent transfer hydrogenation of the ketone is a potential side reaction in this case.

Encouragingly, substrate **5g** and **5j** could be cyclized to **6g** and **6j** with moderately good yields. However, compound **6n** was only detected in traces. Unexpectedly, cyclization of the secondary benzylic alcohol **6o** was also unsuccessful. Steric hindrance might be involved in this case, preventing the cyclization from taking place.

The isolation of the final tricyclic compounds proved challenging given their tendency to act as ligands to ruthenium. However, improved yields of separation were achieved by adsorbing the crude product onto an amine-functionalized silica gel samplet before purification with automated flash chromatography.

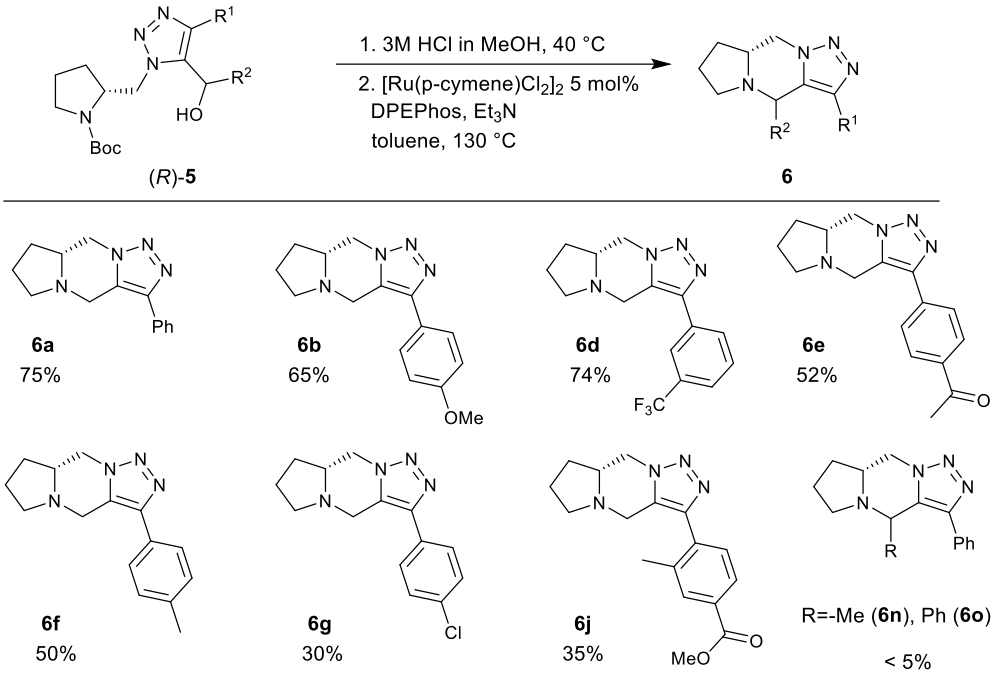

Scheme 28. Substrate scope of the intramolecular Ru-catalyzed hydrogen-borrowing cyclization of triazoles **5** to afford fused triazolo-piperazines **6** under optimized conditions (5 mol% $[Ru(p\text{-cymene})Cl_2]_2$, DPEphos, NEt_3, toluene, 40 °C).

3.3 Conclusions

In this chapter, a novel and efficient methodology has been developed for the synthesis of tricyclic 1,5-fused 1,2,3-triazole piperazines through sequential ruthenium-catalyzed reactions. Initially, Boc-protected prolinol was converted into a proline–azide derivative, which underwent ruthenium-catalyzed azide–alkyne cycloaddition (RuAAC) with a variety of propargylic alcohols under mild conditions, yielding the 1,4,5-trisubstituted 1,2,3-triazoles in up to 99% yield.

Subsequent Boc-deprotection of the amine, followed by an intramolecular ruthenium-catalyzed hydrogen borrowing (HB) reaction afforded fused triazole piperazines in up to 75% yield. One-pot strategies combining RuAAC and HB reactions or deprotection and HB in a single step were explored but proved unsuccessful.

The methodology is highly atom-economical and provides facile access to both trisubstituted triazoles and fused triazole piperazines. Looking ahead, this synthetic strategy could be expanded to include asymmetric variants of the hydrogen borrowing step, enabling access to enantioenriched triazole-fused heterocycles. To further explore the potential of these tricyclic frameworks, future studies could explore their biological activity or their application as chiral ligands.

4.1,4,5-Trisubstituted-1,2,3-Triazole-Appended Prolinol Derivatives as Organocatalysts in Aldol Reactions

Building on the RuAAC methodology developed in Chapter 3, the resulting 1,4,5-trisubstituted 1,2,3-triazoles were explored as potential organocatalysts after Boc-deprotection. This chapter investigates how triazole–pyrrolidine hybrids function as chiral catalysts in aqueous aldol reactions, aiming to link molecular design with catalytic performance.

4.1 Background

Over the years, a wide range of pyrrolidine-based chiral organocatalysts has been developed. Starting from the natural amino acid proline and its derivatives, notable examples include MacMillan's imidazolidinones[122] and Jørgensen and Hayashi's diarylprolinol silyl ethers.[123-125] The structure-reactivity relationship that characterizes these molecules relies on the possibility of tuning four different positions on the scaffold.[126] The corresponding derivatives, constructed around a pyrrolidine ring, can be classified in three main categories: (i) proline-based organocatalysts, including substituted proline and prolinamides, (ii) prolinol-based organocatalysts and, finally, (iii) prolinol-based organocatalysts substituted with diaryl groups (Figure 7).[127]

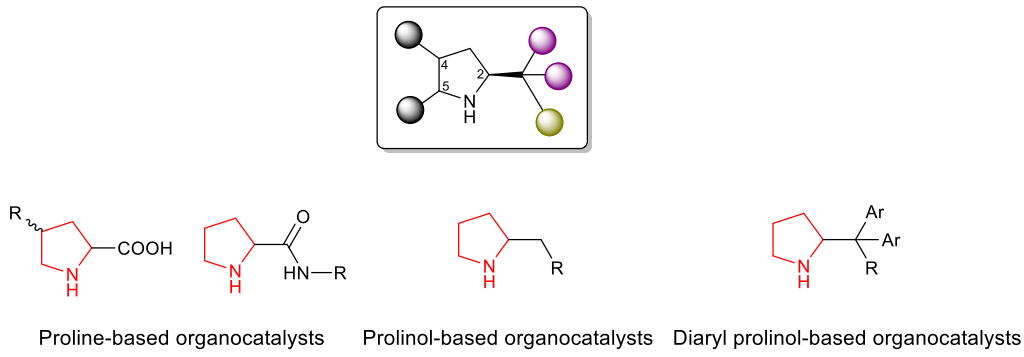

Figure 7. Pyrrolidine-based organocatalysts.

Modifications at different positions of the pyrrolidine ring play distinct roles in tuning catalyst behavior: substituents at the 4- and 5-positions primarily influence stereoelectronic effects, while those at the 2-position impact the stereocontrol of the reactions.[126] Chiral pyrrolidines bearing a hydrogen-bond donor on the C-2 side chain (such as proline, prolinamides or prolinols) typically operate by forming a covalent bond with one substrate while coordinating the second one via hydrogen bonding, directing the stereochemistry. In contrast, chiral

pyrrolidines lacking hydrogen-bond donors at C-2, and instead featuring bulky or rigid substituents, induce stereocontrol by sterically shielding one face of the substrate, thus directing the attack to the opposite side (Scheme 29).[127]

Understanding these distinct activation modes has guided the rational design and structural modification of pyrrolidine-based organocatalysts, aiming to enhance their efficiency and selectivity and to extend their applicability to more challenging and less reactive substrates, as well as towards more sustainable reaction conditions. Consequently, the strong interest in this structural motif has driven significant efforts toward developing novel and efficient asymmetric synthetic routes to substituted chiral pyrrolidines.

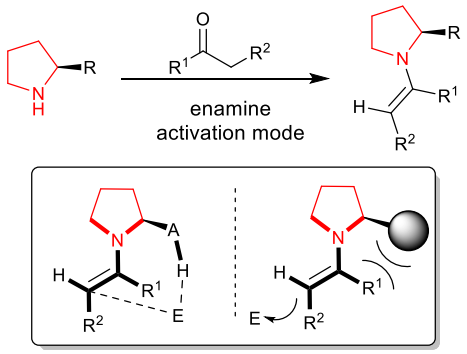

Scheme 29. Pyrrolidine-based stereoselective activation of carbonyl compounds via enamine type catalysis.

The previous chapter described a methodology to access tricyclic 1,5-fused 1,2,3-triazole piperazines. Within this synthetic route, the intermediate triazole-appended prolinol derivatives were envisioned to be promising scaffolds for applications in organocatalysis. In fact, looking at the structure of these compounds, they can be considered as prolinol derivatives, having a pyrrolidine core with a substituent in the C-2 position (Figure 7).

It was hypothesized that the 1,4,5-trisubstituted 1,2,3-triazole substituent on the pyrrolidine ring could help modulate the stereoselectivity of the reaction and enhance catalyst performance in aqueous media, given its known ability to engage in supramolecular interactions like π–π stacking and hydrogen-bonding interactions.[128] These organocatalysts, obtained via RuAAC using internal alkynes, feature three distinct sites on the ring for functionalization (positions 1, 4, and 5 of the triazole), allowing fine-tuning of both the stereoelectronic and steric hindrance of the catalyst structure (Figure 8).

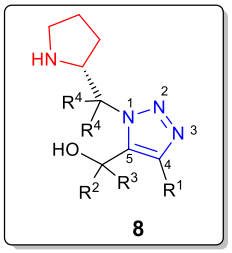

Figure 8. 1,4,5-Trisubstituted-1,2,3-triazole-appended prolinol derivatives

Reports in the literature describe 1,5-substituted 1,2,3-triazoles primarily employed for anchoring organocatalysts to solid-phase,[129-132] with some examples looking at incorporating the 1,2,3-triazole moiety in the organocatalyst and employing it for asymmetric Micheal additions reaction. As an example, Mainkar and co-workers reported a peptidomimetic organocatalyst incorporating a 1,4- or 1,5-disubstituted 1,2,3-triazole unit (Figure 9a). This catalyst enabled Micheal addition reactions with very low catalyst loading (0.5%), no additives, and excellent diastereo- and enantioselectivities.[133] Juaristi and co-workers subsequently developed a pyrrolidine–triazole hybrid catalyst (Figure 9b) that promoted the Michael addition between isobutyraldehyde and β-nitrostyrene in an isopropanol–water (3:1) mixture, using benzoic acid as an additive, achieving good enantioselectivities.[134] In another study, Liang and co-workers synthesized a series of prolinol–triazole-based organocatalysts (Figure 9c) that proved highly efficient under sustainable conditions, catalyzing Micheal additions in water with excellent enantio- and diastereoselectivity.[135]

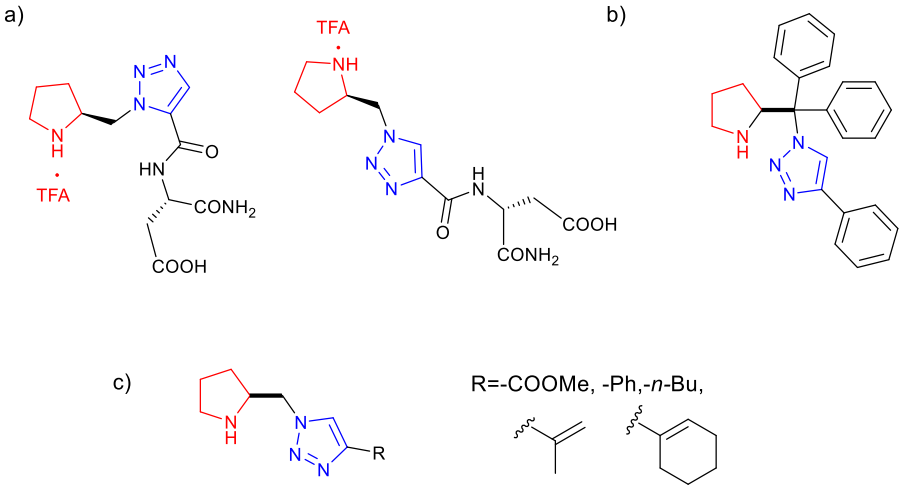

Figure 9. Examples of 1,2,3-triazole–appended prolinol derivatives.

In this chapter, a series of prolinol derivatives featuring 1,4,5-trisubstituted 1,2,3-triazoles were synthesized, employing the procedures previously reported in chapter 3, and evaluated as organocatalysts in a sample aldol reaction (Scheme 30). The goal was to achieve a

diastereo- and enantioselective synthesis of the aldol condensation product while simultaneously screening sustainable reaction conditions.

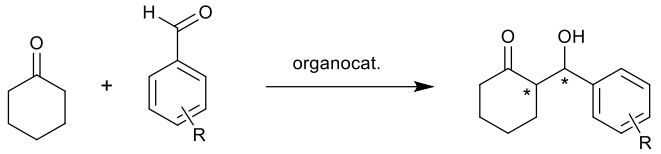

Scheme 30. Sample aldol reaction used to test the triazole-based organocatalysts.

4.2 Results and discussion

The idea was to rationally design the catalysts by changing the substituents on the internal alkynes **7** by making them react with the previously synthesized (*R*)-proline azide (Scheme 24) via a ruthenium-catalyzed azide alkyne cycloaddition reaction. Employing the same conditions of Method B, described in Chapter 3 (Scheme 25) the boc-protected organocatalysts **8a-f** were obtained in good yields. Compounds **8a**, **8b**, and **8c** provide a way of studying how the electronic effects of the substituents on the aryl group and the absence of any substituent in the α-position relative to the hydroxyl group influences the catalysis. In compound **8d**, the presence of a phenyl group in the α-position to the hydroxyl not only increases steric hindrance compared to **8a–c**, but also introduces an additional chiral center. This creates the possibility of forming two diastereomers (*anti* and *syn*) both of which can be evaluated as organocatalysts. These diastereomers are separated in the subsequent boc-deprotection step. Similarly, catalyst **8e** was designed to further enhance steric hindrance at the α-position by incorporating a *tert*-butyl group, allowing investigation of how aromatic versus alkyl substitution in this position affects catalytic behavior. In contrast, compound **8f**, featuring two phenyl groups in the α-position, closely resembles the well-known diaryl prolinol-based organocatalysts, combining increased steric bulk with potential electronic effects that may influence catalytic performance and selectivity.

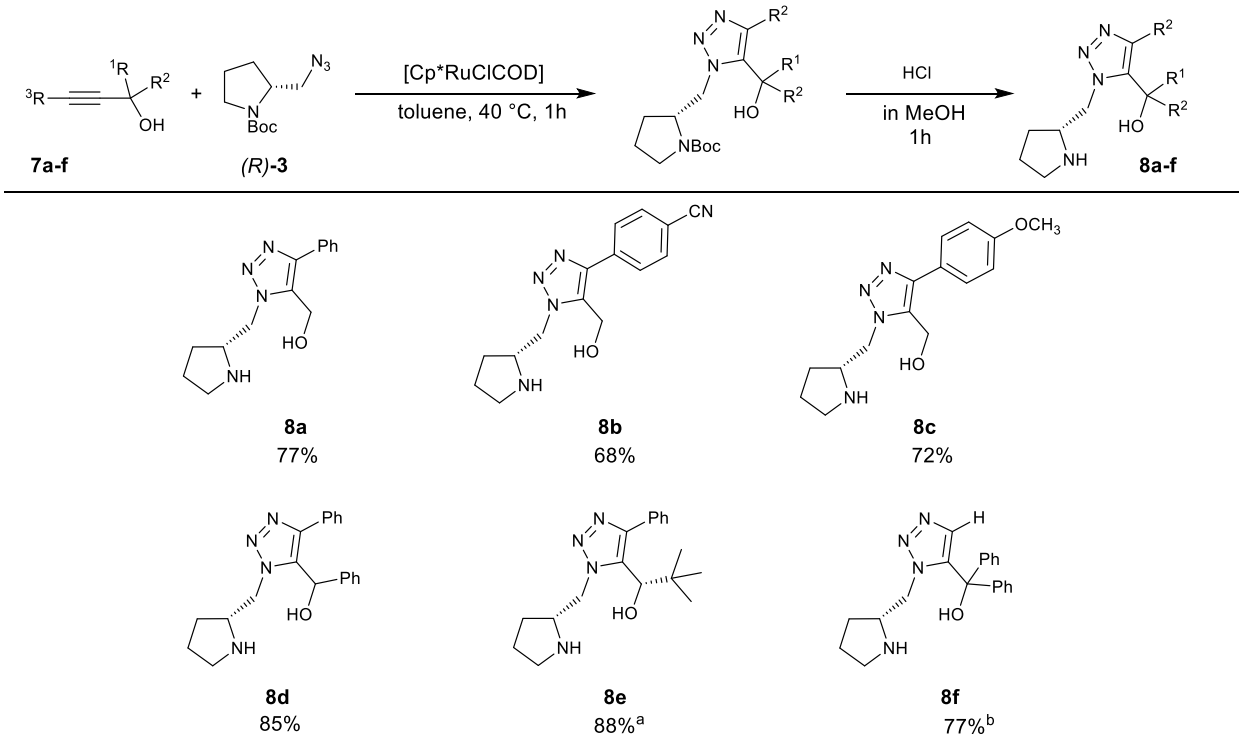

Scheme 31. Synthesis of 1,4,5-trisubstituted-1,2,3-triazole-appended prolinol derivatives **8a–f** via RuAAC reaction of (*R*)-proline azide **3** with substituted alkynes **7**, followed by Boc-deprotection to afford the corresponding free amines. [a]RuAAC reaction performed overnight [b]RuAAC reaction performed overnight, at room temperature with [Cp*RuCl(PPh_3)$_2$] (0.5 mol%) as the catalyst.

The organocatalysts were initially screened in the aldol reaction in water. Classical base-catalyzed aldolization conditions were first tested using Na_2CO_3 and NaOH as bases. When Na_2CO_3 was employed, the reaction between cyclohexanone and *p*-nitrobenzaldehyde afforded good conversion and diastereoselectivity (Table 3, Entry 1). Using NaOH with the same aldehyde increased both yield (68%) and diastereoselectivity (Entry 2). In contrast, when *m*-nitrobenzaldehyde was used as substrate, no product formation was observed with Na_2CO_3 (Entry 3), while a low yield but good diastereomeric ratio was obtained when NaOH was employed (Entry 4). As expected, no enantioselectivity was detected in these base-catalyzed reactions due to the absence of a chiral catalyst. Based on these results, *p*-nitrobenzaldehyde was selected as the substrate for subsequent experiments.

Remaining reactions were performed in the presence of an organocatalyst. The use of (*R*)-proline did not yield any product (Entry 5). This is probably due to the fact that to perform reactions in water efficiently, proline usually needs to be functionalized with hydrophobic groups. In aqueous organocatalysis, reactions generally occur at the interface of a biphasic system, where the organic reagents form a separate phase from water. Catalysts with surfactant-like properties facilitate the formation of emulsions, enhancing contact between the two phases and enabling the transfer of water-soluble reagents to the reactive

interphase.[136, 137] On the other hand, when the less polar prolinol was used as a catalyst in water, the reaction afforded a very good yield and excellent diastereoselectivity. A modest enantiomeric excess of 24% was observed for the *syn* product, while the *anti* diastereomer showed no detectable enantioselectivity (Entry 6).

Given the encouraging performance of (*R*)-prolinol, some of the previously synthesized prolinol-derived organocatalysts were subsequently screened in water to evaluate whether the presence of the 1,2,3-triazole ring and its substituents could further enhance the enantioselectivity. Catalyst **8a** provided an excellent conversion of 91% and slightly lower diastereoselectivity compared to prolinol, although the enantiomeric excesses for both *syn* and *anti* products were not significantly improved (Table 3, Entry 7). In contrast, catalyst **8b** afforded a better diastereomeric ratio between the two isomers but with a lower yield (52%) and reduced *ee* for the *syn* product (Entry 8). When using catalysts **8d** (both *syn* and *anti* isomers), no product formation was observed even after 96 hours of reaction time or upon addition of TFA as an additive (Entries 9 and 10). The use of TFA with catalyst **8a** did not improve enantioselectivity and, conversely, completely suppressed product formation probably by forming a salt with the pyrrolidine amine (Entry 11).

Table 3. Screening of reaction conditions for the organocatalyzed aldol condensation in water.

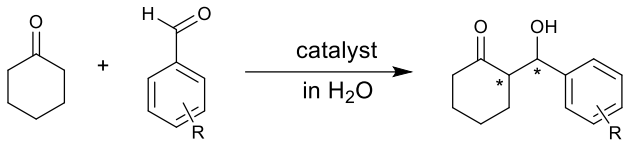

Entry[a]	R	Catalyst/additive	Yield[b] (%)	Anti/syn *(dr)*	ee anti (%)	ee syn (%)
1	4-NO_2	Na_2CO_3	67	73/27	-	-
2	4-NO_2	NaOH	68	88/12	-	-
3	3-NO_2	Na_2CO_3	-	-	-	-
4	3-NO_2	NaOH	18	68/42	-	-
5	4-NO_2	(*R*)-Proline	-	-	-	-
6	4-NO_2	(*R*)-Prolinol	83	72/28	-	24
7	4-NO_2	**8a**	91	60/40	9	27
8	4-NO_2	**8b**	52	80/20	8	20
9[c]	4-NO_2	*syn/anti*-**8d**	-	-	-	-
10[d]	4-NO_2	*syn*-**8d**/ TFA	-	-	-	-
11[d]	4-NO_2	**8a** / TFA	-	-	-	-

[a]Reaction conditions: 1 eq aldehyde, 1.05 eq cyclohexanone, 25% catalyst/additive, 15 mL of water, reaction times of 48h; [b]Isolated yield; [c]Both the *anti* and *syn*-**8d** catalysts were tried in this reaction; [d] Reaction time of 96 h.

Solventless conditions, performing the reaction with an excess of cyclohexanone, were also screened and the results are summarized in Table 4. When **8a** was employed in a 1:1 mixture

of water and cyclohexanone, the reaction afforded a 95% conversion and moderate diastereoselectivity (*dr* = 62:38) with improved enantioselectivities compared to when only water was used as solvent (Table 4, Entry 1). Performing the reaction in neat cyclohexanone led to a similar conversion (93%) and a slightly lower diastereomeric ratio (59:41), though the enantioselectivity improved to 30% *ee* (*syn*) and 58% *ee* (*anti*) (Entry 2).

Since the results were promising, we screened the rest of the catalysts under these solventless conditions. Catalysts **8b** and **8c** gave a lower yield (53% and 60%) but comparable enantioselectivity, showing that the substituent on the aromatic ring at the 4 position of the triazole does not seem to affect the yield or the selectivity of the reaction.

Table 4. Screening of reaction conditions for the organocatalyzed aldol condensation in cyclohexanone.

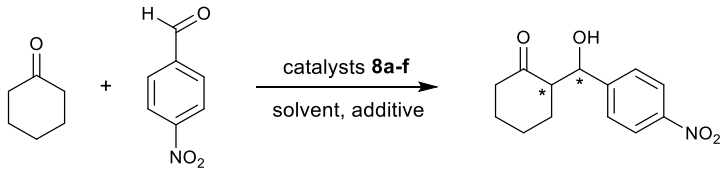

Entry[a]	Catalyst (25 mol%)	Solvent	Time(h)	Yield[b] (%)	anti:syn (*dr*)	*ee* anti	*ee* syn
1	**8a**	H_2O:cyclohexanone (1:1)	48	95	62:38	13	51
2	**8a**	-	48	93	59:41	30	58
3	**8b**	-	48	53	60:40	36	58
4	**8c**	-	48	60	50:50	34	58
5	*syn*-**8d**	-	24	96	60:40	**72**	55
6	*anti*-**8d**	-	24	73	70:30	29	55
7	*syn*-**8e**	-	48	92	59:41	38	56
8	**8f**	-	24	94	69:31	27	58

[a]Reaction conditions: 0.1 mmols of aldehyde, 0.5 mL cyclohexanone , 25% catalyst, 15 mL of water, reaction times of 48h; [b] Isolated yields.

Interestingly, both diastereomeric forms of **8d** (*syn* and *anti*) were catalytically active, giving high conversions (96% and 73%) and improved diastereoselectivities (60:40 and 70:30, respectively, Entries 5 and 6). The *syn*-**8d** catalyst also provided the highest enantioselectivity (72% *ee* for *anti* product) among the tested systems, suggesting a favorable steric and electronic environment for asymmetric induction.

Unfortunately, catalyst *syn*-**8e,** despite guaranteeing excellent conversion, did not improve the *dr* or *ee* of the reaction (Table 4, Entry 7). Similarly, the bulkier **8f** derivative maintained high conversion with slightly improved diastereoselectivity but only moderate enantiocontrol (Entry 8).

4.3 Conclusions

A new class of triazole appended-prolinol compounds has been designed and synthesized to be evaluated as organocatalysts in the aldol reaction between *p*-nitrobenzaldehyde and cyclohexanone. When the screening of reaction conditions was performed, the obtained results show that the aldol reaction in water did not provide a high enantioselectivity. On the other hand, when the reaction was conducted under solventless conditions or using an excess of cyclohexanone as the solvent, the catalytic performance increased and an appreciable *ee* was observed. Catalyst *syn*-**8d** afforded the highest *ee* for the *syn* product (72%), in a very good yield and with an acceptable diastereomeric ratio. The other catalysts gave more or less similar results under these reaction conditions. Even if promising results were obtained, a more thorough screening of reaction conditions is necessary in order to improve the diastereomeric ratio and the enantiomeric excess for the catalysis with *syn*-**8d**.

Future plans involve trying to improve the diastereoselectivity by conducting the reaction at lower temperatures (around 0 °C), trying additives in the reaction to see how they influence the selectivity, and modifying the quantities of cyclohexanone and catalyst. In terms of screening other catalysts than those investigated above, it would be interesting to synthesize catalyst **8g** where the two additional phenyl groups increase the steric hindrance on the C-2 carbon of the pyrrolidine ring (Figure 10, **9**). Furthermore, the evaluation of the effects of the hydroxyl group in the reaction could be carried out by protecting it as a silyl ether (Figure 10, **8h**) or by replacing it with other functional groups. Expanding the substrate scope by screening a broader range of aldehydes and ketones would also provide a more comprehensive understanding of the catalyst's performance.

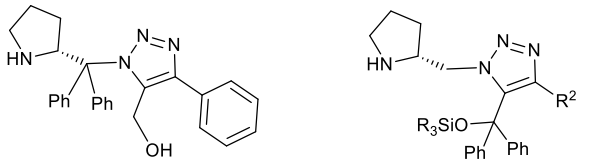

9 **8h**

Figure 10. Structures of planned organocatalysts for future studies.

5. 1,4,5-Trisubstituted 1,2,3-triazole based oligomers for sensing applications

In the final part of this work, the modular triazole framework is leveraged for supramolecular recognition. While Chapter 4 focused on catalysis, Chapter 5 explores the same structural motif for molecular sensing, demonstrating the versatility of triazole-based architectures.

5.1 Context and Background of the Project

This project is part of a multidisciplinary collaboration bridging organic chemistry, nanotechnology, and biochemistry, with the overarching goal of developing a chemosensor capable of specifically detecting biomarkers derived from antibiotic-resistant bacteria. A chemosensor is defined as a device capable of transforming chemical inputs arising from interactions between a synthetic receptor and the analyte, into analytically valuable signals via a transducer.[138] The initiative, funded by the European Union (MSCA ITN - PEST BIN), arose in response to the growing global threat of antibiotic resistance—an issue that jeopardizes the achievements of modern medicine. The lack of effective surveillance systems, underreporting, as well as limited data sharing and coordination continue to hinder the implementation of control strategies, leading to low awareness and accelerated spread of antibiotic resistance. Rapid and accurate detection of resistant bacterial strains is therefore essential for effective infection control. In this context, the development of an inexpensive, easy-to-use sensing platform could have a major impact on monitoring resistant pathogens, strengthening surveillance efforts, and guiding appropriate treatment decisions.

The project was carried out collaboratively, involving one PhD student specializing in biochemistry/biology responsible for isolating the biomarkers (analyte) from antibiotic-resistant *S. pneumoniae*, another PhD student (myself) synthesizing the receptor molecules and attaching them to graphene using a linker, and a third PhD student focusing on the fabrication of graphene-based transducers to generate an electrical signal upon receptor–biomarker binding (Figure 11).

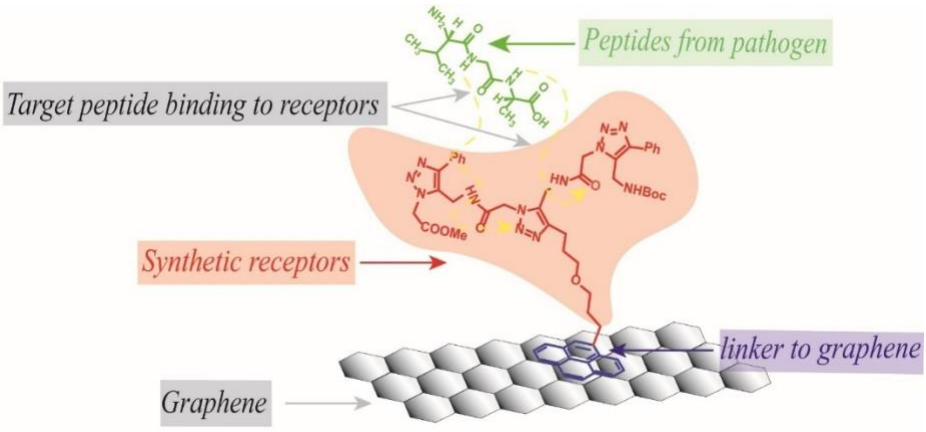

Figure 11. Visual representation of the final envisioned biosensor platform.

The work presented in this chapter focuses specifically on the design and preparation of a synthetic receptor for sensing applications. As discussed in Section 1.4, synthetic receptors offer several advantages over biological ones, which, although highly selective, often suffer from instability, high production costs, and limited functionalization flexibility. In contrast, synthetic receptors can be readily prepared and modified in the laboratory, allowing precise structural tuning through controlled functionalization and choice of the synthetic pathways that would grant efficiency and reproducibility.

To combine these advantages, the receptor design centered on 1,4,5-trisubstituted 1,2,3-triazoles as modular building blocks, which, connected through peptide coupling, can afford linear and/or cyclic oligomeric structures. This approach relies on two well-established and reliable synthetic transformations, i.e. ruthenium-catalyzed azide–alkyne cycloaddition (RuAAC) for the preparation and diversification of triazole monomers together with amide coupling for their assembly into peptidomimetic oligomers. These specific oligomeric structures have not yet been reported for sensing purposes, but 1,2,3-triazoles have been studied both in peptidomimetics and sensing.

The unique structure and electronic properties of 1,2,3-triazoles make them highly versatile molecules capable of engaging in multiple types of intermolecular interactions, which is why they have attracted significant attention for sensing applications.[128] These heterocycles are aromatic systems containing 6 π-electrons, enabling π–π stacking interactions with other aromatic species. Additionally, the strong dipole moment, almost aligned with the C–H bond, governs their acid–base behavior: the C–H proton at position 5 exhibits remarkably high acidity, while the nitrogen at position 1 acts as a basic site (Figure 12). This dual character renders 1,2,3-triazoles effective as both hydrogen-bond donors and acceptors, allowing them to interact with anions through the acidic C–H site and with metal centers or hydrogen-bond donors (–YH) through the N1 atom. Notably, this behavior closely resembles that of the amide bond, which explains the frequent use of triazoles as amide bioisosteres

(Figure 12). These mentioned features of 1,2,3-triazoles make them ideal candidates to prepare chemosensor platform for ions or ion pair recognition.

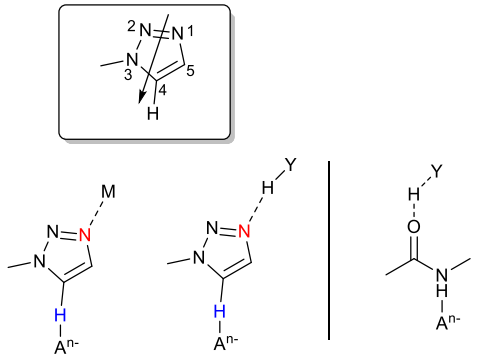

Figure 12. Dipole moment of triazoles, its effect on ion coordination and comparison with the amidic bond.

1,4-Disubstituted 1,2,3-triazoles prepared via CuAAC have been widely explored in ion recognition, offering not only a simple synthesis and mild reaction conditions, but also high sensitivity, rapid response time, and in some cases allowing on-site analysis.[139]

As an example, Kim and co-workers reported a triazole-based receptor incorporating pyrene units, which was found to selectively recognize Zn^{2+} and Cd^{2+} ions in acetonitrile. Coordination of these metal ions to the triazole moieties induced a conformational change in the receptor, leading to quenching of the excimer emission and a corresponding turn-on of the monomer fluorescence (Scheme 32a).[140] In a work reported by Beer and coworkers, a triazole-containing ion-pair receptor was shown to cooperatively bind halide and monovalent cation pairs in aqueous media. Spectroscopic and crystallographic analyses revealed that the triazole units play a dual role, coordinating simultaneously to both the cation and anion guests, thereby enhancing the overall binding strength and selectivity of the receptor (Scheme 32b).[141] A neutral halogen bonding macrocyclic anion receptor based on a pseudocyclopeptide with three 5-iodo-1,2,3-triazole subunits was developed by Kubik and coworkers, and has shown affinity for chloride ion (Scheme 32c).[142]

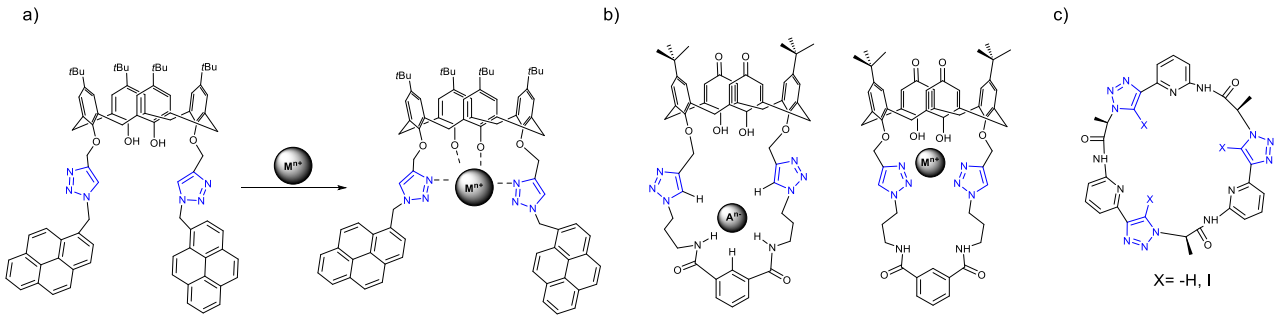

Scheme 32. Examples of triazole contining chemsensors for a) metal detection; b) ion pair detection; c) anion detection.

As briefly mentioned earlier, 1,4 and 1,5 disubstituted 1,2,3-triazoles are well known bioisosteres with potential applications in peptidomimetic thanks to the electronic similarities between their structures and the *cis* or *trans* amide bond (Figure 13).[143]

This led to the incorporation of these motifs in peptidic structures to form peptidotriazolamers. In these structures, every second peptide bond is replaced by a triazole unit. These hybrid foldamers combine features of peptides and triazoles, offering structural stability and biological relevance. They are considered promising candidates to bridge the gap between small-molecule drugs and protein-based therapeutics.[144]

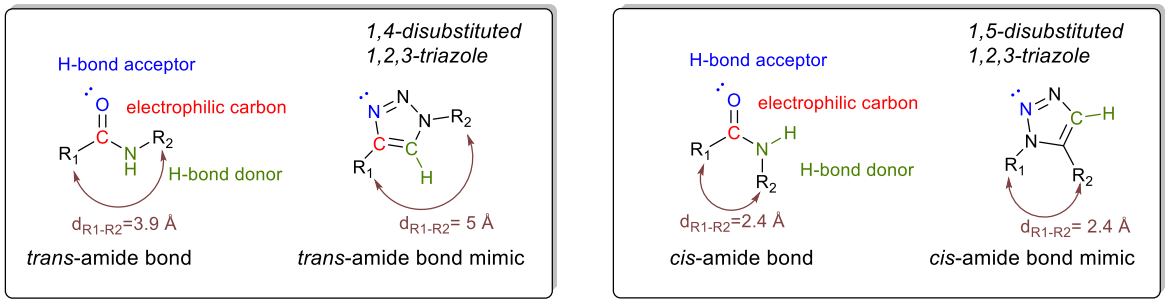

Figure 13. 1,4 and 1,5- disubstituted 1,2,3-triazoles as isosteres for cis and trans amide bonds.

Previous efforts of the Kann group focused on the preparation of peptidotriazolamers based on triazoles prepared via RuAAC. Initially, achiral δ-peptide–inspired trimers and tetramers containing 1,5-disubstituted 1,2,3-triazoles (Figure 14a) were synthesized and their conformational analysis and quantum chemical calculations showed the concurrence of various conformers with comparable stabilities.[145] At a later stage, introduction of lateral chains led to the synthesis of a chiral 1,5-disubstituted 1,2,3-triazole trimer (Figure 14b).[146]

Cyclization of peptidotriazolamers based on 1,4-disubstituted 1,2,3-triazoles prepared with CuAAC to form azamacrocycles was achieved by Izzo and coworkers in 2022. Interestingly, they carried out an head-to-tail cyclization of both a dimeric and trimeric linear oligoamides previously assembled via solid phase synthesis(Figure 14c).[147]

While these studies primarily focused on the conformational and structural properties of triazole-based foldamers, they did not explore their potential as receptors or sensors, however.

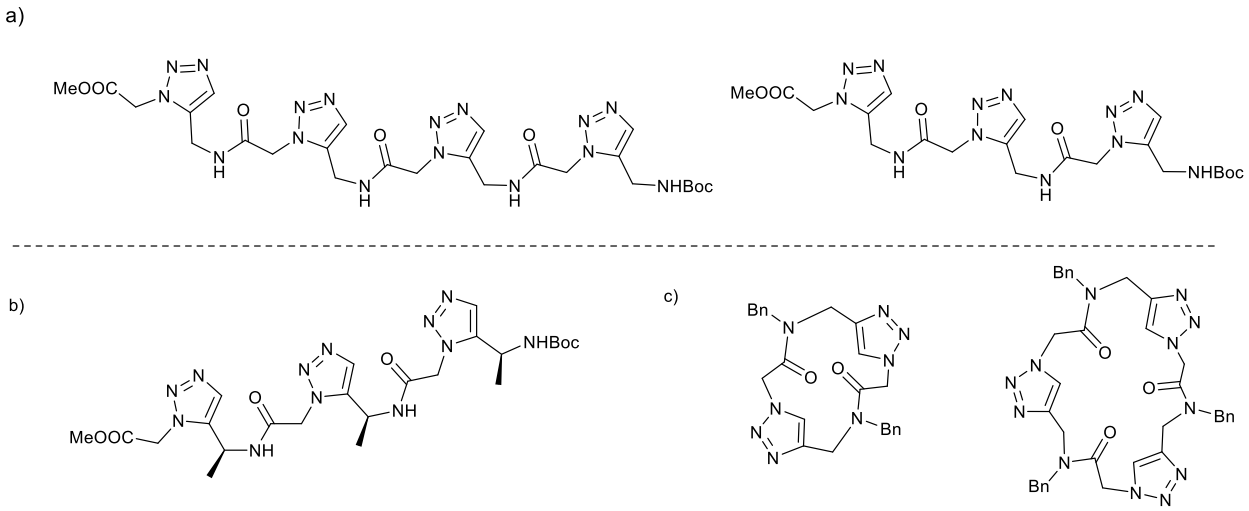

Figure 14. Peptidotriazolamers oligomers a) achiral, formed via RuAAC; b) chiral formed via RuAAC; c) cyclic, formed via CuAAC.

In this chapter, differently substituted 1,4,5-trisubstituted 1,2,3-triazoles synthesized using RuAAC were used as building blocks to prepare linear peptidotriazolamers and their corresponding macrocycles, and were then applied for sensing purposes. The possibility of three substitution sites allowed the synthesis of diffferent building blocks that can be mixed and matched to form different oligomers, with the potential for either a 1,4- or a 1,5-connectivity between the monomer units (Figure 15). This gives rise to oligomers with different spatial orientations, a feature that critically affects their folding behavior and interaction with analytes.

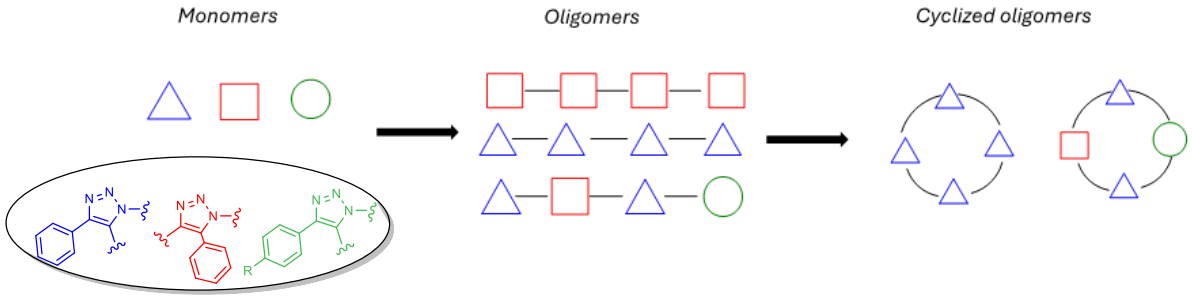

Figure 15. Design of linear and cyclic peptidotriazolamers composed of 1,2,3-triazole units linked through 1,4- or 1,5-connectivity.

5.2 Synthesis of the Triazolamers

To synthesize the 1,2,3-triazole monomers needed to construct triazolamers, an initial Sonogashira coupling was performed between *N*-Boc-propargylamine and a series of iodoarenes (Scheme 33). The yields obtained and the spectral data for these compounds were in line with previously reported data for compounds **10a-e**.

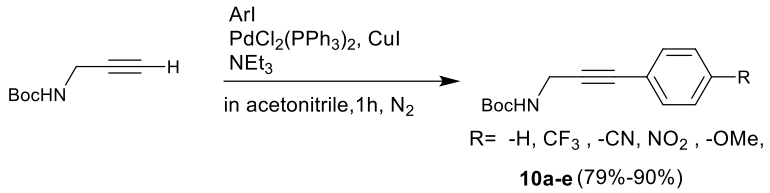

Scheme 33. Sonogashira coupling for the synthesis of alkynes **10a-e**.

Subsequently, the obtained internal alkynes **10a-e** were employed in the RuAAC reaction with methyl 2-azidoacetate, using [Cp*RuCl(cod)] as the catalyst in dichloromethane. When alkyne **10a**, lacking substituents on the aromatic ring, was tested the reaction proceeded smoothly, consuming the starting materials within just 30 minutes. This reaction yielded both isomers (**11a**, **11f**) in a 4:1 ratio, achieving a quantitative yield. Expanding the investigation to the other internal alkynes **10b-e** revealed a similar trend, but in these cases, even if small amounts of the minor isomer were observed, only the major isomer was isolated, i.e., compounds **11b-e** (Scheme 34).

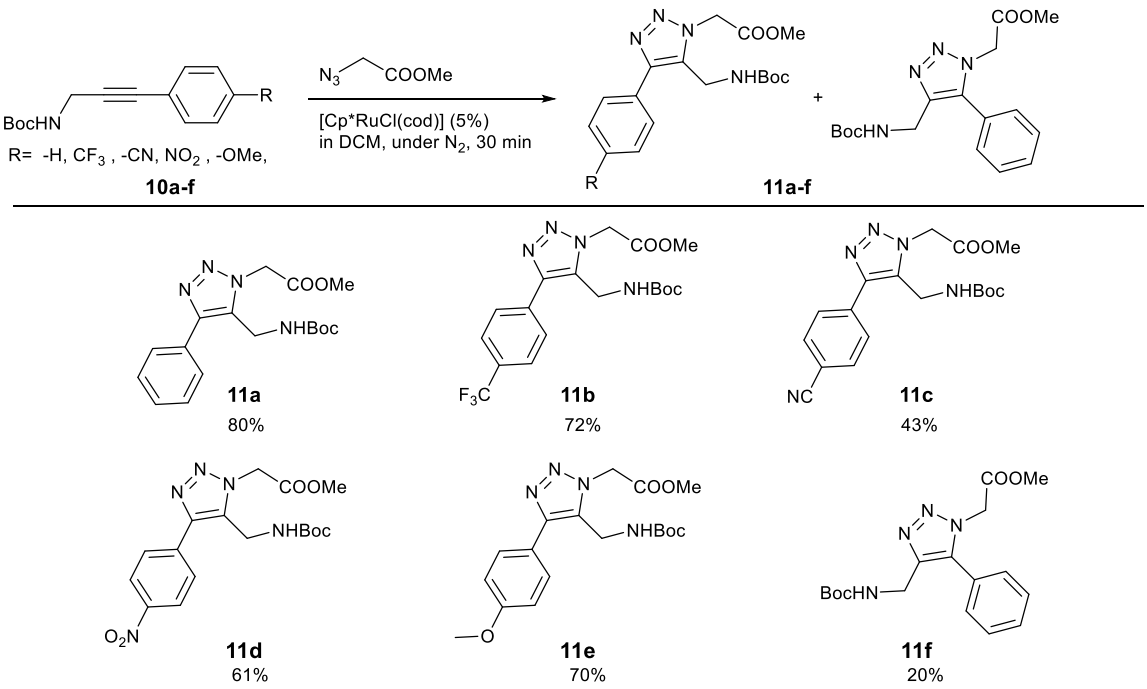

Scheme 34. Synthesis of 1,4,5-trisubstituted-1,2,3-triazole monomers.

At this stage, compound **11a** was connected to the other monomers via amide bond formation, affording dimers **12a–f** (Scheme 35). The procedure involved Boc-deprotection of compound **11a** and ester hydrolysis of the corresponding partner monomers (**11b–f**), followed by HATU-mediated coupling of the two units. The desired dimers were successfully obtained in yields ranging from 24% to 84%.

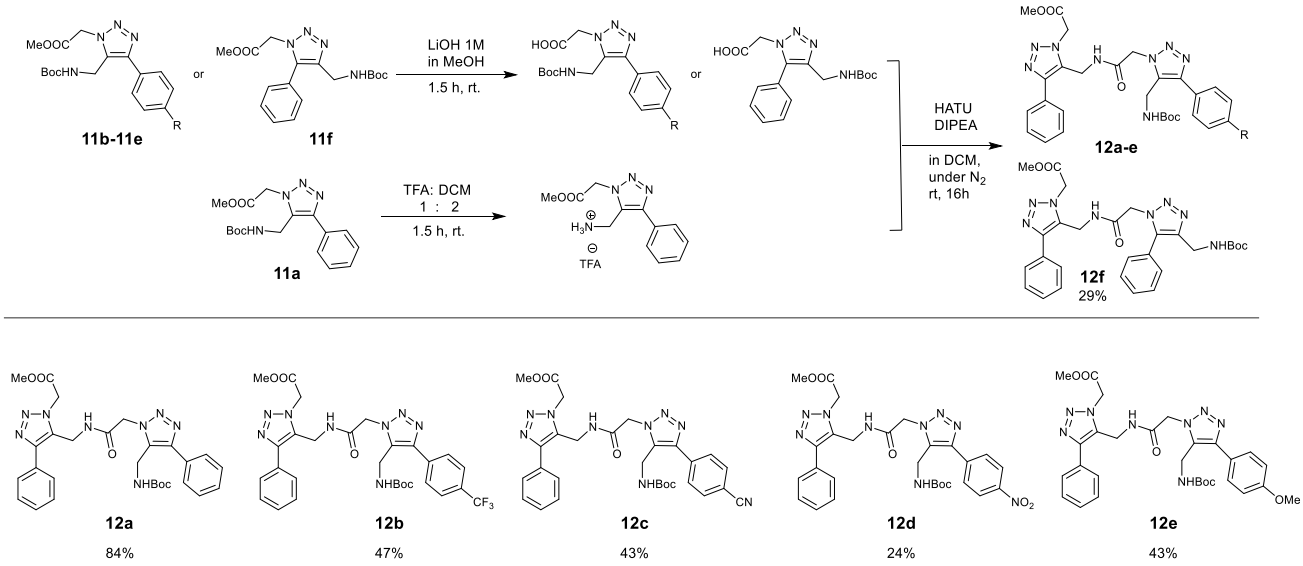

Scheme 35. Synthesis of triazole-based dimers **12a-f.**

It is important to mention that the use of the amine salt with TFA is crucial in order to avoid formation of the corresponding 1,2,3-triazole fused δ-lactam shown below (Figure 16), which was isolated when the salt was quenched through performing a basic workup at the end of the deprotection.

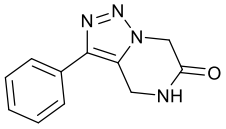

Figure 16. Undesired cyclization product.

Once the dimers were obtained, preparation of tetramers was attempted by coupling dimer **12a** with itself or with **12f** but, unfortunately, the desired product was not isolated. The ^{1}H NMR of the crude product was complex and no clear conclusions concerning the outcome of the reaction could be made. As the tetramers proved challenging to obtain, the corresponding trimeric structures were targeted instead by reacting dimers **12a-f** with monomers **11a**, affording trimers **13a-f** (Scheme 36).

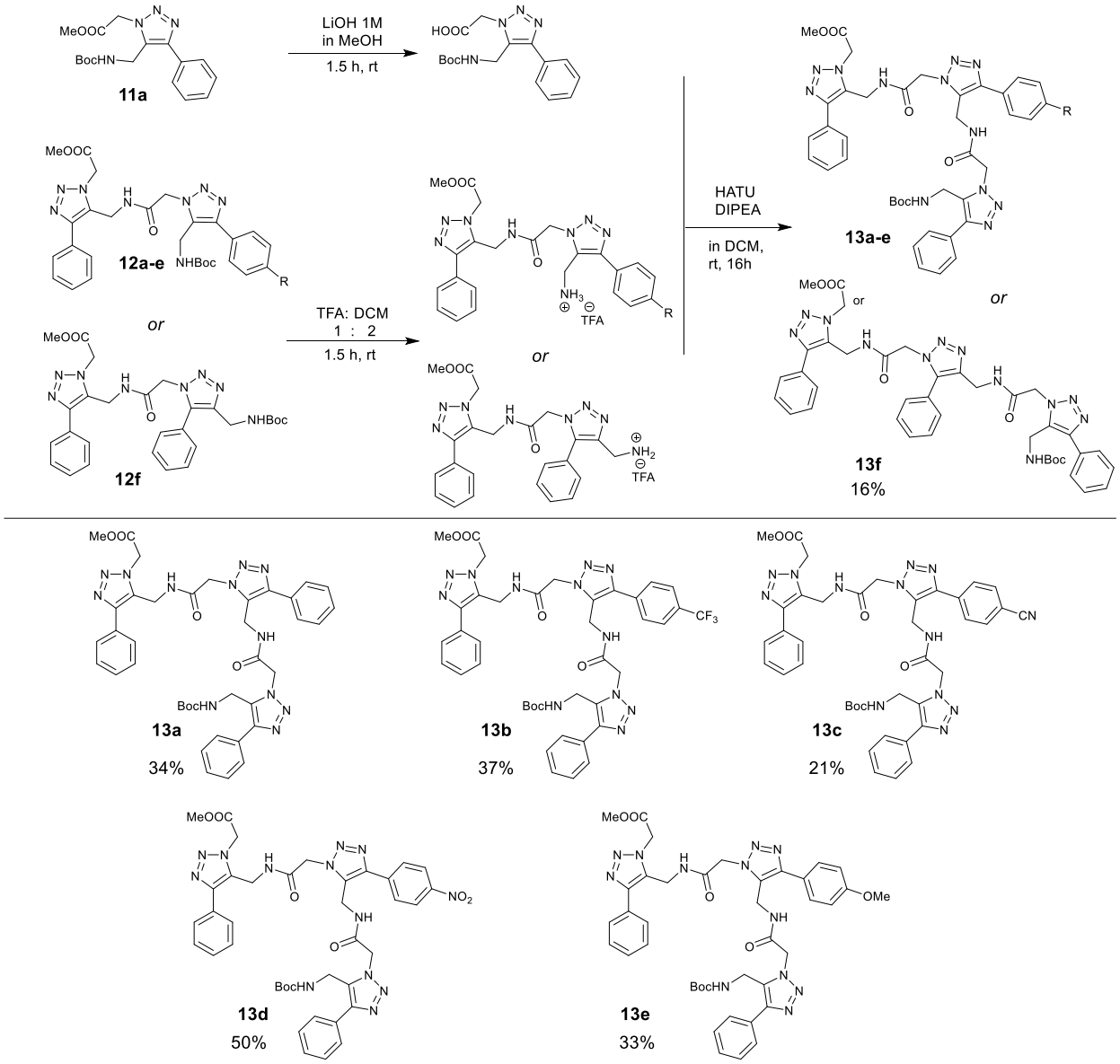

Scheme 36. Synthesis of triazole-based trimers **13a-e**.

After obtaining the linear oligomers, dimers **12a** and **12f** together with trimer **13a** were selected for cyclization. The oligomeric structures were hydrolyzed to the corresponding carboxylic acid and subsequently treated with TFA to remove the Boc-group. The resulting intermediate, deprotected at both ends, was subjected to the amide coupling conditions (DIPEA/HATU), but using DMF as the solvent. Small amounts of compounds *cyclo*-**12a**, *cyclo*-**12f** and *cyclo*-**13a** were obtained (Figure17).

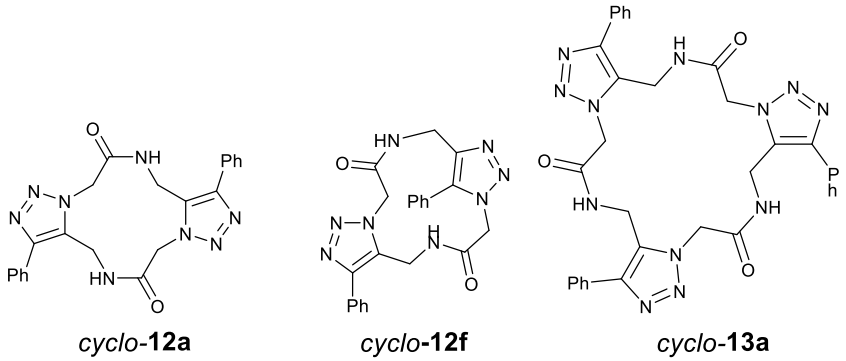

Figure 17. Macrocyclic triazolamers obtained after intramolecular cyclization.

As previously discussed, the synthesized oligomeric structures were designed for sensing applications, to be evaluated through UV/Vis spectroscopy in solution and by monitoring changes in the electrical conductivity or resistance of graphene-based devices upon receptor–analyte interactions on the surface. To enhance both the UV/Vis and fluorescence responses, and to further investigate the interaction of these systems with graphene, a trimer appended to a polyaromatic unit was conceived as an additional receptor candidate. The pyrene moiety was chosen due to its well-known ability to exhibit changes in fluorescence properties upon binding to fluorescent amino acids or to metal ions, thus providing a binding indication.[148] Moreover, pyrene can interact strongly with graphene through π–π stacking,[149] allowing the detection of the analyte via electron density changes in an eventual final graphene-based sensor. To access such receptor architectures, the functionalization of commercially available 1-(bromomethyl)pyrene and 1-(bromopropyl) pyrene with trimer **13g** was planned, leading to the target compounds **15a** and **15b** (n = 1, 3) (Scheme 37).

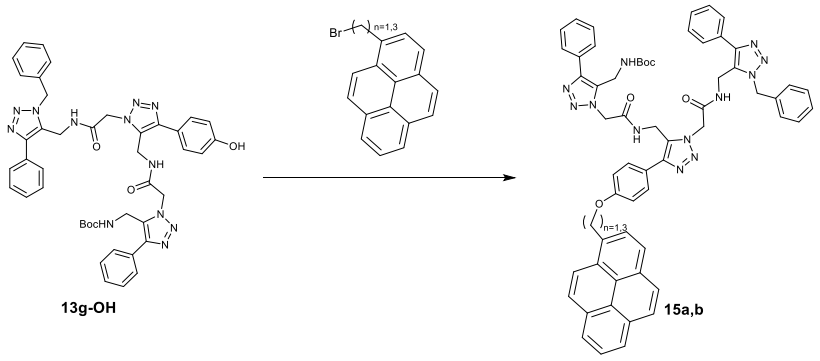

Scheme 37. Functionalization of bromomethyl/bromopropyl pyrene with triazole based trimer.

In order to obtain trimer **13g,** the synthesis of three different monomers was required. Monomer **11a** was synthesized according to the procedure in Scheme 33. The synthesis of monomers **11g** and **11h** are shown in Schemes 38 and 40, respectively. Desired internal alkyne **10g** was obtained after TIPS-protection of 1-iodo phenol and a

subsequent Sonogashira coupling. It was then utilized in the RuAAC reaction, that yielded triazole **11g** in a 60% yield (Scheme 38).

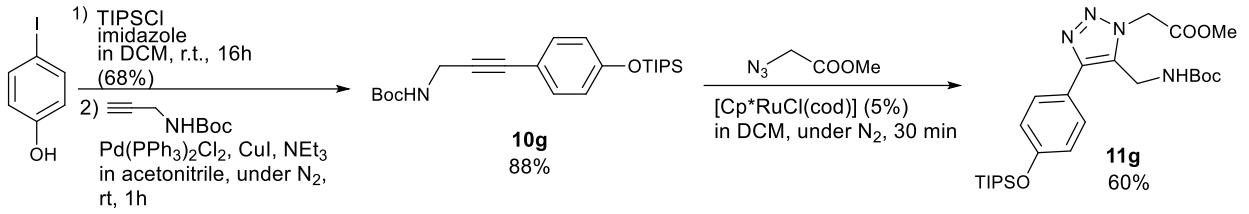

Scheme 38. Synthesis of triazole monomer **11g**.

After obtaining triazole **11g**, coupling with 1-(bromomethyl)pyrene was attempted both to evaluate the feasibility of the reaction and to explore the fluorescence properties of the resulting molecule, providing insight into the expected behavior upon subsequent trimer attachment to the pyrene unit. The phenol group was deprotected using TBAF, followed by a Williamson etherification with 1-(bromomethyl)pyrene, affording compound **14** in 10% yield (Scheme 39).

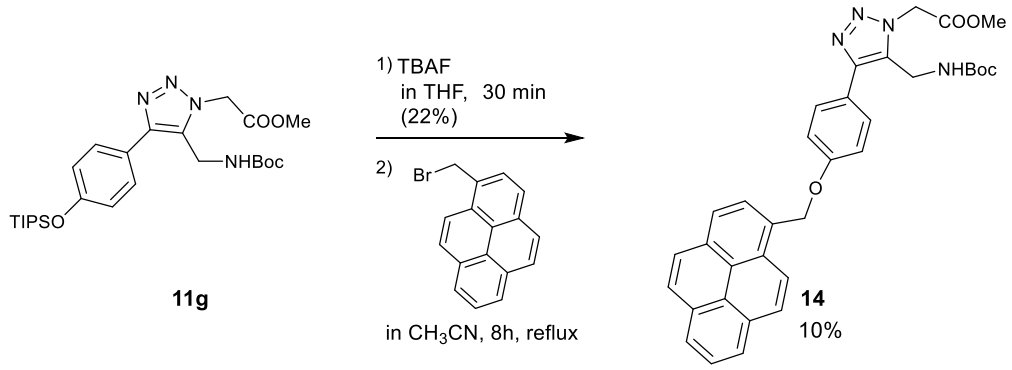

Scheme 39. Coupling of triazole **11g** with 1-(bromomethyl)-pyrene.

The low yields obtained in both the deprotection step (22%) and the etherification (10%) prompted further investigation. The modest yield of the etherification reaction was attributed to the fact that it was performed only once and on a very small scale. In contrast, the unexpectedly low yield of the TIPS deprotection with TBAF raised greater concern, as this transformation is generally known to proceed smoothly and with near-quantitative efficiency.[150] Detailed NMR analysis of the crude product suggested that TBAF not only promoted TIPS removal but also induced hydrolysis of the methyl ester substituent on the triazole ring. Although uncommon, a precedent for this behavior exists in the literature, where TBAF was reported to catalyze deacylation of cellulose esters.[151] Mechanistic studies proposed that fluoride ions released from TBAF can deprotonate the acyl group, generating a ketene intermediate that subsequently reacts with water to form the corresponding acid—the water originating either from residual solvent moisture or from TBAF hydration.[152] For this

reason, although the initial strategy involved using only two different monomers for the trimer synthesis (two units of **11a** and one unit of **11g**), it became necessary to replace the –COOMe-terminated triazole with one lacking this functional group. Consequently, compound **11h**, bearing a phenyl substituent instead of the methyl ester, was employed in its place.

After obtaining alkyne **10a**, in accordance with the procedure reported in Scheme 33, it was subsequently used in the RuAAC reaction with benzyl azide, affording the final triazole **11h** in 68% yield (Scheme 40).

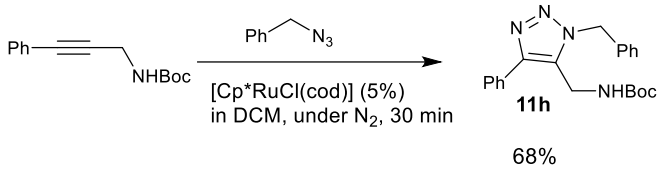

Scheme 40. Synthesis of triazole **11h**.

With all the required building blocks available, the corresponding trimer was synthesized. The methyl ester of monomer **11g** was first hydrolyzed, and the amine of monomer **11h** was deprotected, enabling the amide coupling to afford dimer **12g** (Scheme 41). Despite the modest yield obtained, the use of a sufficiently large quantity of starting materials allowed the synthesis to proceed to the trimer formation step.

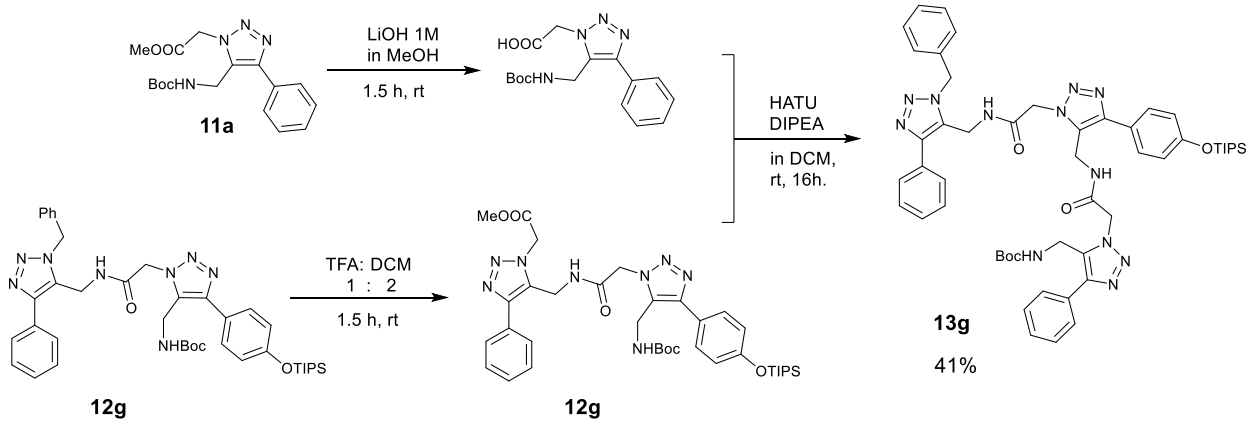

Scheme 41. Synthesis of dimer **12g**.

The next step in our synthesis involves the coupling of dimer **12g** and monomer **11a**, which yielded the corresponding trimer in 41% yield (Scheme 42).

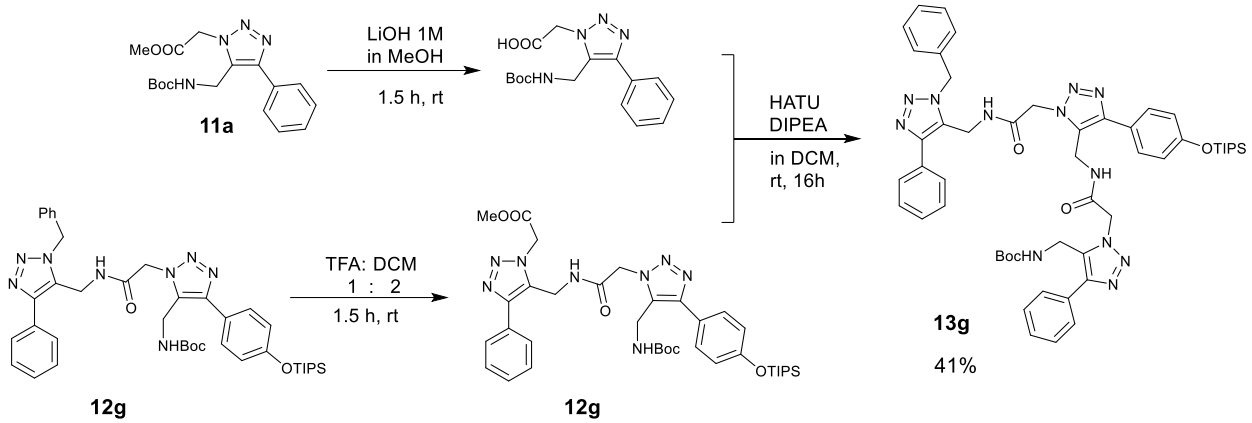

Scheme 42. Synthesis of trimer **13g**.

The same conditions employed in scheme **39** were used for deprotection and functionalization with the pyrene moiety, but unfortunately no conversion to the desired product **15** was observed (Scheme 43). When the solvent was changed from acetonitrile to dimethyl formamide (DMF) and the reaction performed at 80 °C, ^{1}H NMR of one of the fractions isolated after column chromatography indicated possible formation of the product. The difficulties in isolating **15a** could be due to π–π stacking effects, which can result in very low solubility. The optimization of this reaction is ongoing. and once in place, the interaction of 15a with graphene will be studied in collaboration with the Yurgens group at the Dept. of Microtechnology and Nanoscience at Chalmers.

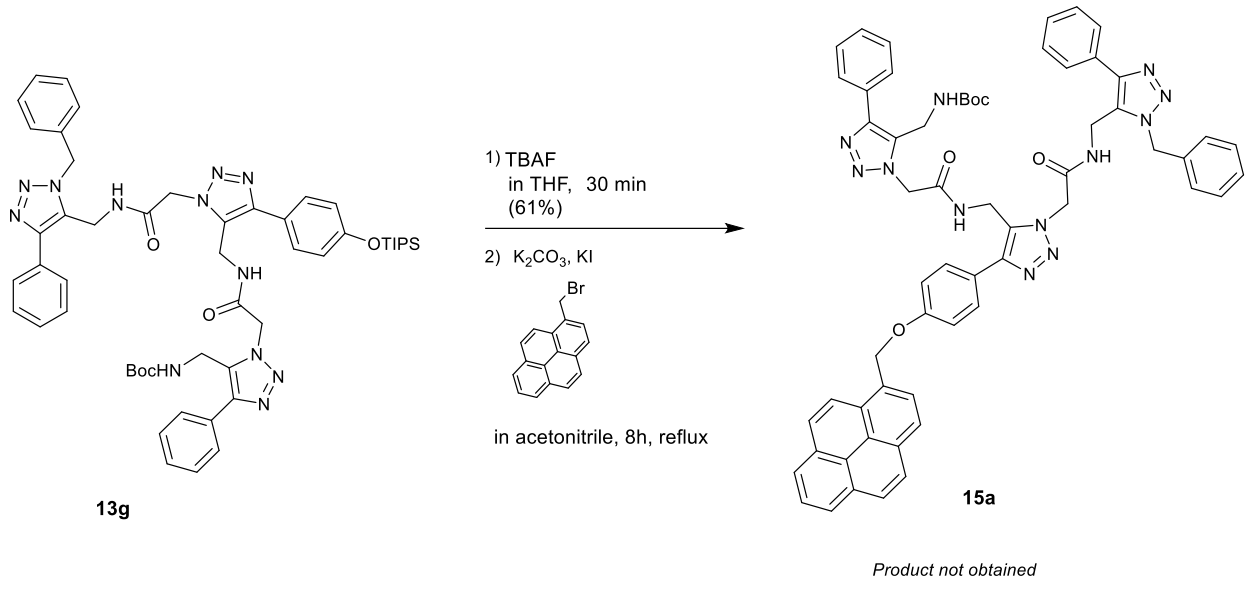

Scheme 43. Attempt at pyrene functionalization with trimer **13g** to form **15a**.

5.3 Ion Sensing

To evaluate the halide-binding ability of the synthesized oligomers, their interactions with different tetrabutylammonium (TBA) halide salts were examined using ^{1}H NMR spectroscopy. 5 mM solutions of the compounds in DMSO-d_6 (dimer **12a**, trimers **13a-f** and *cyclo*-**12a**, *cyclo*-**12f** and *cyclo*-**13a**) were treated with five equivalents of the respective halide salt, and the resulting mixtures were analyzed by ^{1}H NMR.

In the case of **12a**, the addition of TBAF caused partial degradation of the dimer, while TBAI induced no observable spectral changes. A slight downfield shift of the amide N–H signal was detected upon addition of TBABr, and a more pronounced shift was observed with TBACl, suggesting a tentative binding affinity trend of $Cl^- > Br^- > I^-$ (Figure 18a) with fluoride ion excluded due to side reactions. As an open-chain receptor, **12a** can adopt flexible conformations to interact with different anions, implying that electronic effects and hydrogen-bonding strength, rather than ion size, govern the observed binding behavior.

The cyclized analogue (*cyclo*-**12a**) was also tested with TBACl. Its N–H resonance showed a smaller downfield shift upon chloride addition compared to the linear dimer **12a**, consistent with weaker binding (Figure 18b). This difference is attributed to the increased rigidity and smaller cavity of the macrocyclic structure, which likely enforces a side-on interaction with the chloride rather than full encapsulation.

a)

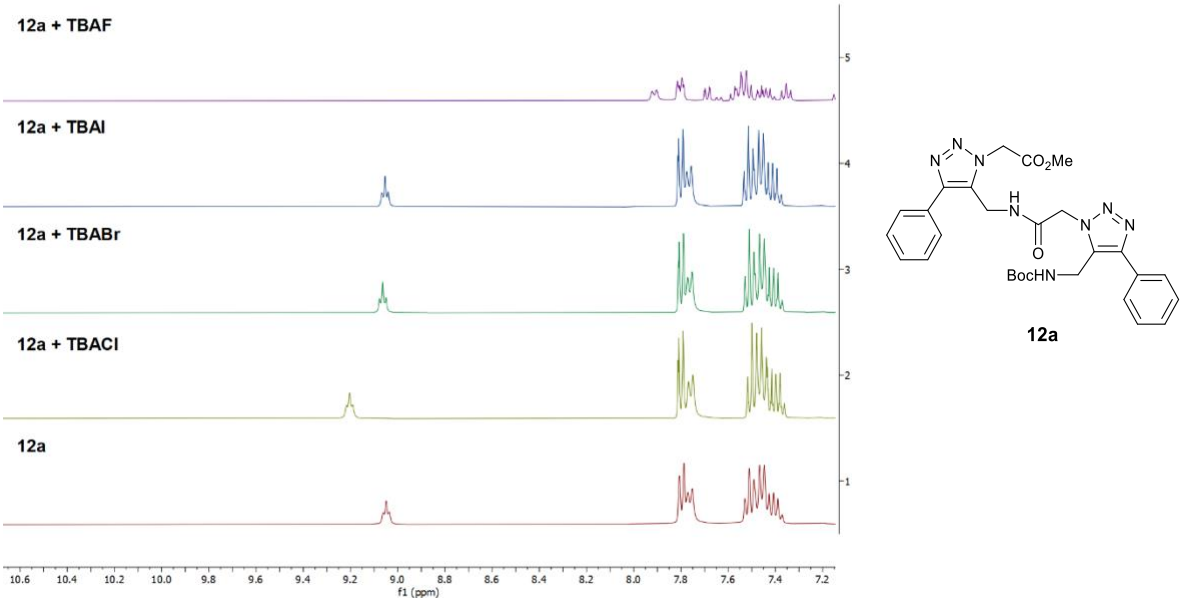

b)

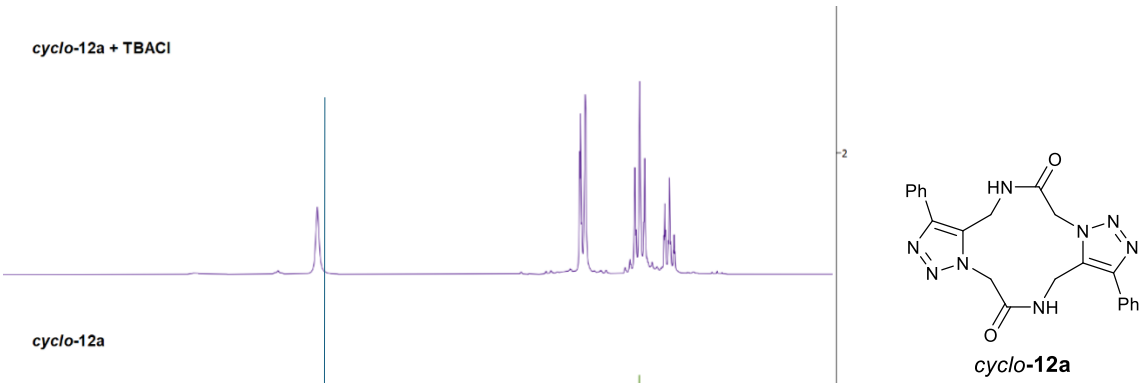

Figure 18. Halide ion sensing properties of a) dimer **12a**; b) dimer *cyclo*-**12a**.

Further binding studies were conducted using trimers **13a–f** to assess their ability to interact with halide ions. These trimers contain two central N–H bonds, both of which exhibited a downfield chemical shift upon addition of TBACl. A slight downfield shift was also detected for one of the methylene singlets adjacent to the carbonyl, suggesting that chloride coordination influences the local electronic environment of nearby groups.

a)

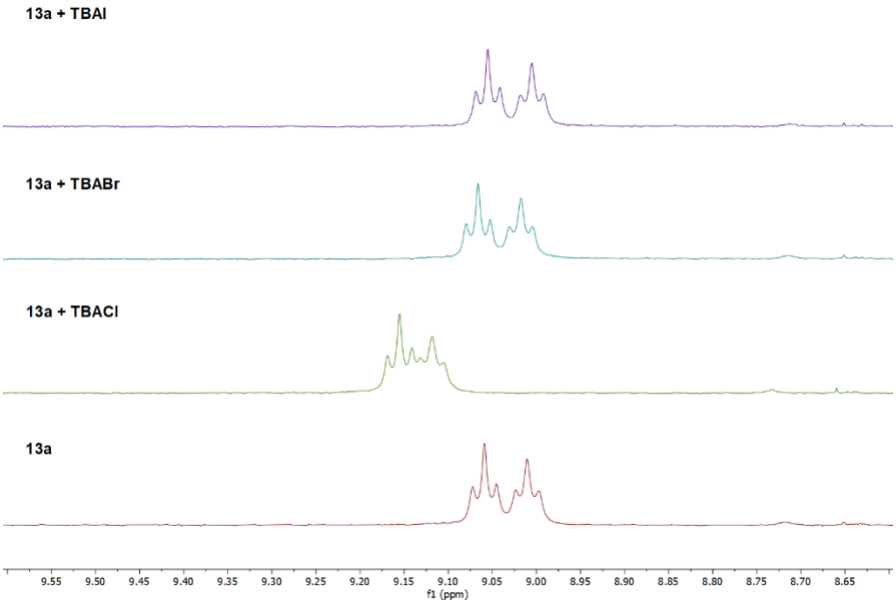

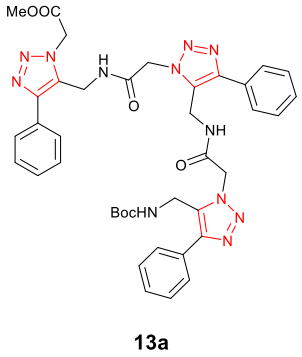

b)

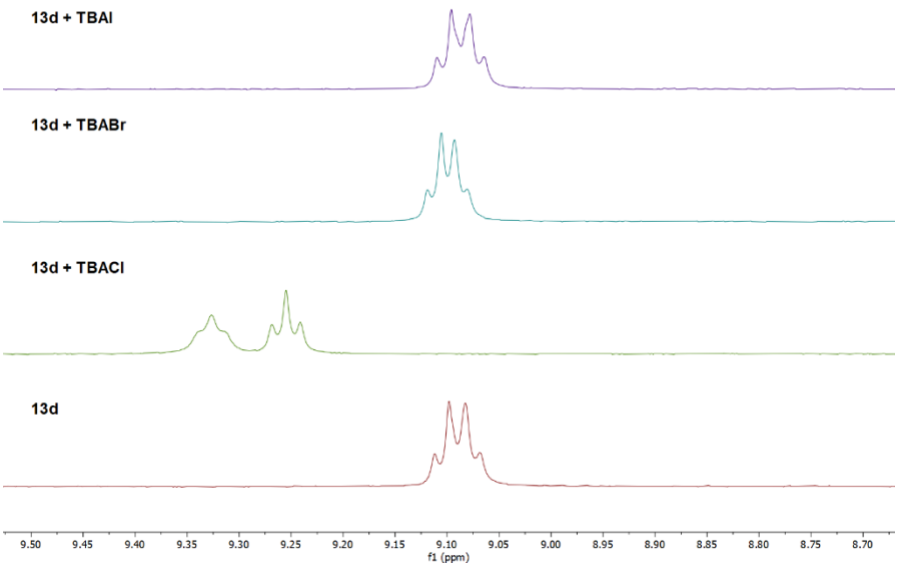

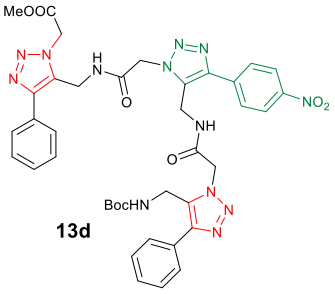

Figure 19. ^{1}H NMR spectra illustrating halide ion sensing responses of a) trimer **13a** and b) trimer **13d**.

Similar behavior was observed across the series (**13a–f**) upon treatment with TBAX (X = I, Br, Cl), with the magnitude of the shift increasing along the halide series. ^{1}H NMR shifts for trimer **9a** are reported in Figure 19a. Notably, trimer **13d** displayed the most pronounced response toward chloride ions, where the apparent N–H quartet at 9.10 ppm split into two

distinct triplets at 9.25 and 9.33 ppm, consistent with specific chloride binding (Figure 19b). Further NMR studies also confirmed these interactions. In particular ^{1}H–^{1}H NOESY experiments of **13d** revealed clear spectral differences between the free and chloride-bound forms, particularly in the N–H region, indicating conformational changes of the trimer structure upon anion coordination.

In addition to halide-binding studies, the interaction of dimer **12a** with various metal ions was examined using UV–Vis spectroscopy to evaluate its potential as a metal-ion sensor. Absorption spectra were recorded in the 200–800 nm range for solutions containing 0.5 mM of different metal salts in methanol, including Ba^{2+}, Ca^{2+}, Co^{2+}, Cu^{2+}, Mg^{2+}, Mn^{2+}, Ni^{2+}, and Zn^{2+}. Among these, only the addition of Cu^{2+} ions produced significant spectral changes, indicating a strong and selective interaction between the dimer and copper ions (Figure 20a).

To further investigate this behavior, a copper titration experiment was performed by incrementally adding 3 µL portions of a 0.1 mM $CuCl_2$ solution to 3 mL of a 2 µM solution of **12a** in MeOH, while continuously monitoring the spectral response by UV–Vis spectroscopy. A clear evolution of the absorption bands was observed upon increasing Cu^{2+} concentration, confirming specific coordination and sensitivity of **12a** toward copper(II) ions (Figure 20b).

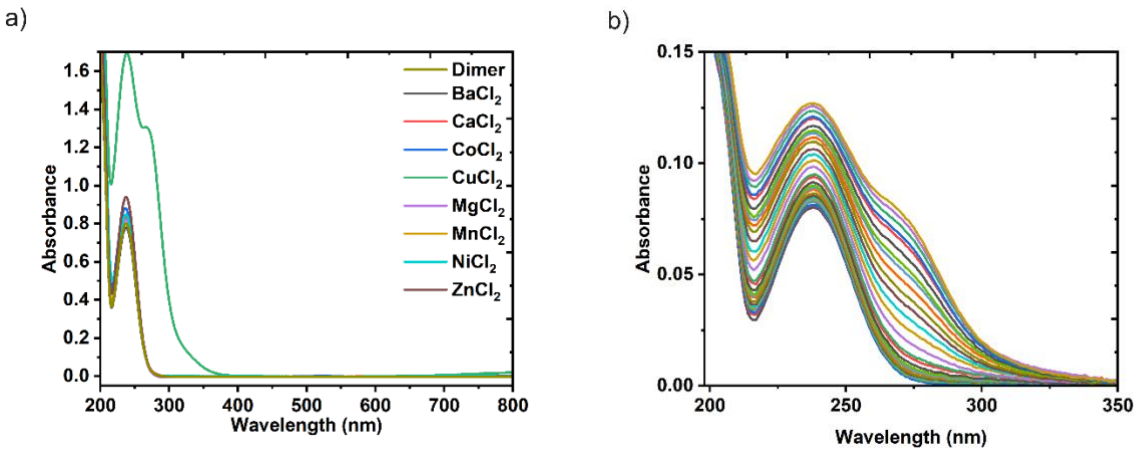

Figure 20. UV–Vis absorption spectra of dimer 12a: a) screening against various divalent metal ions (M^{2+}); b) titration with Cu^{2+} ions.

Further studies are planned to expand the investigation of metal–ion interactions and to better understand their binding behavior. Complementary computational analyses and crystallographic studies are currently ongoing to elucidate the structural nature of the triazolamer-ion complexes and to determine the specific binding sites within the triazolamer framework.

5.4 Conclusions and Outlook

To conclude, a new class of 1,4,5-trisubstituted 1,2,3-triazole-based oligomers was successfully designed and developed as synthetic receptors for potential sensing applications. Their synthesis relied on robust and well-established methodologies, namely click chemistry (RuAAC) and peptide coupling, allowing modular and versatile access to a range of differently substituted dimers and trimers. These compounds were characterized by NMR, HRMS, and XRD, and their sensing properties were evaluated toward both anions and metal ions.

NMR anion-binding studies revealed consistent trends across the oligomeric series, showing selective recognition of chloride ions over other halides (with fluoride excluded due to receptor degradation). UV/Vis spectroscopic studies demonstrated that dimer **12a** exhibited selective binding toward Cu^{2+} ions, a finding further supported by titration experiments confirming its high sensitivity and specificity. Current ongoing computational studies could help gaining more information about the folding of these structures and their interaction with ions.

Building on these results, further investigations are underway to expand the scope of these receptors toward biomolecule recognition and alternative detection methods, such as fluorescence- or graphene-based sensing. For this purpose, efforts are focused on the functionalization of pyrene with trimer **13g**, which could enhance optical properties and enable π–π stacking immobilization on graphene surfaces. Optimization of this step may benefit from improved purification techniques (e.g., HPLC or recrystallization) or by employing pyrene derivatives with extended linkers to reduce steric hindrance. Additionally, synthesizing a cyclized analogue (*cyclo*-**13g**) could provide valuable insights into how structural rigidity affects recognition behavior.

If successful, these developments would represent a significant step toward the realization of the initially planned graphene-based chemosensing platform, capable of detecting ions and small peptides with high selectivity and sensitivity—bridging molecular design with practical sensing applications.

6. Concluding Remarks

The work presented in this thesis demonstrates how ruthenium catalysis and click chemistry can enable the design of functional molecules through efficient synthetic routes, with potential applications in catalysis, materials science, and molecular recognition. The overarching goal has been to explore how the modularity and selectivity of ruthenium-catalyzed transformations can be harnessed to construct increasingly complex molecular architectures from simple and renewable precursors.

From the valorization of biomass-derived vanillin to the design of 1,2,3-triazole-fused tricyclic structures and triazole-based organocatalysts and synthetic receptors, these studies collectively highlight the importance of molecular design as a driving force in advancing synthetic innovation and in addressing sustainability challanges.

Starting from the valorization of biomass-derived compounds, the ruthenium-catalyzed dimerization of a vanillin derivative was employed for the synthesis of epoxy divanillin ester (EDVE), which could be used as a biobased alternative to bisphenol A (BPA), highlighting the potential of Ru catalysis for developing recyclable and sustainable polymer precursors starting from sustainable biomass derived sources. Expanding this strategy to more aromatic aldehydes and adding other polymerizable functionalities could lead to a broader family of biobased thermosets and recyclable materials.

A sequential RuAAC-hydrogen borrowing methodology was then developed to access tricyclic 1,2,3-triazole-fused piperazine scaffolds. The molecular design of the internal alkynes used as substrates for the RuAAC step allowed control over regioselectivity and, consequently, over functionalization of the triazole intermediates. This ensured the substituents to be organized in the right positions for the subsequent intramolecular hydrogen borrowing reaction. Future studies could explore the catalytic and biological potential of these tricyclic frameworks, particularly as chiral ligands or bioactive compounds.

The potential of the prolinol-derived 1,4,5-trisubstituted 1,2,3-triazoles, obtained as intermediates in the previous synthetic route, was further explored in stereoselective aldol reactions. Obtained as products of the RuAAC, the 1,2,3-triazoles structures, integrated in the prolinol derived scaffold, offer a modular platform in which substituents can be varied systematically, which enables systematic tuning of both the electronic and steric properties. The study aimed at assessing how these modifications of the triazole scaffold can influence catalytic activity and selectivity of these organocatalysts in aqueous and solvent-free conditions. Promising preliminary results were obtained and further optimization, expansion

of the substrate scope, or application to other transformations, such as Michael additions, could help establish these systems as viable, sustainable tools for asymmetric synthesis.

The RuAAC methodology was then further extended to the design and synthesis of 1,4,5-trisubstituted 1,2,3-triazole-based oligomers, assembled through amide coupling to yield both linear and cyclic peptidotriazolamers, intended as synthetic receptors for sensing purposes. In this case, the RuAAC reaction enabled precise control over connectivity (1,4- or 1,5-linkages) and substituent patterns of the monomer units, allowing systematic modulation of the geometry and binding environment of the resulting receptors. Preliminary sensing studies demonstrated the ability of these peptidotriazlamers to interact selectively with the Cl^- anion and Cu^{2+} metal ion, highlighting their potential as synthetic receptors. Future outlook include applying these receptors for biomolecule recognition and integrating them into graphene-based chemosensing platforms.

Altogether, the methodologies developed in this work exemplify how rational molecular design, guided by ruthenium catalysis, can generate versatile and sustainable synthetic tools. By combining renewable chemistry, catalytic efficiency, and molecular functionality, this research contributes to advancing the development of greener materials, asymmetric transformations, and next-generation sensing platforms.

7. Acknowledgments

This project has received funding from the European Union's Horizon 2020 research and innovation program under the Marie Skłodowska-Curie grant agreement No. 955626. as well as from the Area of Advance Nano (Chalmers) and the Swedish Research Council (grant no. 2023-04342).

I would like to express my gratitude and thank the people who made it possible:

First of all, my Supervisor Nina Kann for her valuable help with my thesis and for giving me the opportunity to join her group as a PhD student to collaborate on this challenging project. I am grateful for finding in her a good and understanding supervisor, always ready to help me and keep me on track.

My cosupervisor Morten Grøtli, for the help and guidance on the project during these years.

Jerker Mårtensson, my examiner, for always being available to discuss chemistry and for his valuable insights.

Naicons industry, in Milan, for hosting me for one month and Thomas Vernay for introducing me to the microbiology field and teaching me how to work in a biology lab.

The Madsen´s group, in DTU, Copenhagen, for hosting me for two months as an exchange PhD student, especially Oliver Rafn Dan for guiding me through the photocatalysis techniques.

The work package for the PEST-BIN project, especially Munis Khan and Leonarda Acha Alarcon for the collaborations in the biosensor part of my thesis.

Past and present members of the Kann Group, especially Dr. Maitrayee Trivedi, for all the help on the sensor project and for all the support and motivation she infused me with, Dr. Lorenzo Celio for all the fun we had in the lab during his stay and our attempted collaboration on a total synthesis project (until we got scooped), Agnes Ingvarsson, for all the discussions and good time we had Alva Seljee and Mees Martein Hendrikx for the synthetic help and nice discussions.

All the master and bachelor students I supervised during my doctoral studies: Yixu Wang, Annaelle Roy, Mélina Detournay, Alexandra Marty, Kevin Van Zitteren, Marilou Bagge, Abdinasir Farhan Ahmed, for their precious help on the projects.

The other ESRs of the PEST-BIN Project, Lydia, Thomás, José, Margot, Sara P., Ghalib, Mukil, Sara R., Ema, Anja for the awesome time we spent together in each summer school, I feel honored to have shared these experiences with all of you.

Past and present members of the department, which made this PhD experience so full and unforgivable and with whom I had the best time in Gothenburg: Angela Gutierrez Leighton, Arkecia Damascena Santana, Dr. August Runemark, Dr. Chandrakanth Patlolla, Dr. Cheng Peng, Dr. Danbo Wang, Ebba Matic, Dr. Francoise Amombo-Noa, Hassan Mourad, Ishan Sarkar (also for creating the cover image, which beautifully represents the essence of this work), Jelka Feldhusen, Dr. Mangmang Shi, Dr. Maureen Gumbo, Dr. Salah Ghellab, Dr. Shima Ghasemi, Dr. Valentina Maruzzo, Vanessa Chivere, Yao Yuge and Dr. Zenghua Wu.

All the researchers from the MedChem Seminars, for the insightful and useful discussions about the projects.

To the friends I made here in Gothenburg during this PhD journey, in and outside of the university. Giuli, grazie per tutto il supporto e il sostegno che mi hai dato in questi anni, sono contenta di poter chiamare amica una persona come te. Mari, my favorite Greek person, thanks for being an amazing friend and for all the shared craziness and southern European vibes during these years, being friends with you made the cloudy and gloomy Sweden seem way more fun and livable. Leo, thank you for being such an inspiring person and for always being able to make me see the bright side in every situation, your strength is contagious and inspiring. Munis and Henghzi, thank you for all the shared moments and friendship built during these years.

Ai miei amici in Italia, per non avermi mai fatto sentire sola ed esserci sempre stati: Ali, Guendi, Vale, Valentina, Mono.

Last but not least, my family:

My mother and my father, Giovanna e Giovanni. Non sarei qui se non fosse stato per voi, tutto ció che sono e che diventeró lo devo a voi. My grandma Maria, my aunts Daniela, Patrizia, Iolanda and my cousin Rossella. Grazie per tutto l´amore incondizionato che mi avete sempre dato, vi voglio bene.

8. References

(1) Nicolau, K. C. *Proc. R. Soc. A.* **2014**, *470*, 20130690.
(2) Anslyn, E. V.; Dougherty, D. A. In *Modern Physical Organic Chemistry*, University Science Books, 2006; pp 490-494.
(3) Kato, M.; Zhang, J. Z.; Paul, N.; Reisner, E. *Chem. Soc. Rev.* **2014**, *43*, 6485-6497.
(4) Kojima, T. Overview of the Catalytic Chemistry of Metal Complexes. In *Redox-based Catalytic Chemistry of Transition Metal Complexes*, Kojima, T. Ed.; Vol. 2; Royal Society of Chemistry, 2024; pp 1-7.
(5) List, B. *Chem. Rev.* **2007**, *107*, 5413-5415.
(6) Hegedus, L. S. Transition Metals in the Synthesis of Complex Organic Molecules. University Science Books, 1999; pp 1-4.
(7) Srinivas, N. R.; Barbhaiya, R. H.; Midha, K. K. *J. Pharm. Sci.* **2001**, *90*, 1205-1215.
(8) Lohray, B. B. *Curr. Sci.* **2001**, *81*, 1519-1525.
(9) Basset, J. M. *Actu. Chim.* **2005**, 6-8.
(10) López, M. D. A. *An. Real Acad. Farm.* **2010**, *76*, 541-571.
(11) Zaia, J. *Anal. Bioanal. Chem* **2023**, *415*, 527-532.
(12) Noyori, R.; Ohkuma, T.; Kitamura, M.; Takaya, H.; Sayo, N.; Kumobayashi, H.; Akutagawa, S. *J. Am. Chem. Soc.* **1987**, *109*, 5856-5858.
(13) Rodríguez, S.; Kayser, M. M.; Stewart, J. D. *J. Am. Chem. Soc.* **2001**, *123*, 1547-1555.
(14) Littke, A. F.; Fu, G. C. *J. Org. Chem.* **1999**, *64*, 10-11.
(15) Hajos, Z. G.; Parrish, D. R. *J. Org. Chem.* **1974**, *39*, 1615-1621.
(16) Eder, U.; Sauer, G.; Weichert, R. *Angew. Chem., Int. Ed.* **1971**, *10*, 496-497.
(17) Dondoni, A.; Massi, A. *Angew. Chem. Int. Ed.* **2008**, *47*, 4638-4660.
(18) Pierre, J. L. *Chem. Soc. Rev.* **2000**, *29*, 251-257.
(19) Boerner, L. K. *Chem. Eng. News* **2021**, *99*, 5.
(20) Dalko, P. I.; Moisan, L. *Angew. Chem., Int. Ed.* **2001**, *40*, 3726-3748.
(21) Dalko, P. I.; Moisan, L. *Angew. Chem., Int. Ed.* **2004**, *43*, 5138-5175.
(22) List, B.; Lerner, R. A.; Barbas, C. F. *J. Am. Chem. Soc.* **2000**, *122*, 2395-2396.
(23) List, B. *Synlett* **2001**, 1675-1686.
(24) Kristofíková, D.; Modrocká, V.; Meciarová, M.; Sebesta, R. *ChemSusChem* **2020**, *13*, 2828-2858.
(25) Zu, L. S.; Wang, J.; Li, H.; Wang, W. *Org. Lett.* **2006**, *8*, 3077-3079.
(26) Radi, M.; Bernardo, V.; Bechi, B.; Castagnolo, D.; Pagano, M.; Botta, M. *Tetrahedron Lett.* **2009**, *50*, 6572-6575.
(27) Kolb, H. C.; Finn, M. G.; Sharpless, K. B. *Angew. Chem. Int. Ed.* **2001**, *40*, 2004-2021.
(28) Devaraj, N. K.; Finn, M. G. *Chem. Rev.* **2021**, *121*, 6697-6698.
(29) Hein, C. D.; Liu, X. M.; Wang, D. *Pharm. Res.* **2008**, *25*, 2216-2230.
(30) Luu, T.; Gristwood, K.; Knight, J. C.; Jörg, M. *Bioconjugate Chem.* **2024**, *35*, 715-731.
(31) Dheer, D.; Singh, V.; Shankar, R. *Bioorg. Chem.* **2017**, *71*, 30-54.
(32) Thirumurugan, P.; Matosiuk, D.; Jozwiak, K. *Chem. Rev.* **2013**, *113*, 4905-4979.
(33) Kolb, H. C.; Sharpless, K. B. *Drug Discov. Today* **2003**, *8*, 1128-1137.
(34) Zurro, M.; Mancheño, O. G. *Chem. Rec.* **2017**, *17*, 485-498.
(35) Bhatnagar, A.; Pakhariya, R. P.; Pemawat, G. *Top. Curr. Chem.* **2025**, *383*.

(36) Huisgen, R. *Angew. Chem. Int. Ed.* **1963**, *75*, 742-754.
(37) Huisgen, R. *Angew. Chem. Int. Ed.* **1963**, *75*, 604-637.
(38) Beutick, S. E.; Vermeeren, P.; Hamlin, T. A. *Chem. Asian J.* **2022**, *17*, e202200553.
(39) Tornoe, C. W.; Christensen, C.; Meldal, M. *J. Org. Chem.* **2002**, *67*, 3057-3064.
(40) Rostovtsev, V. V.; Green, L. G.; Fokin, V. V.; Sharpless, K. B. *Angew. Chem., Int. Ed.* **2002**, *41*, 2596-2599.
(41) Himo, F.; Lovell, T.; Hilgraf, R.; Rostovtsev, V. V.; Noodleman, L.; Sharpless, K. B.; Fokin, V. V. *J. Am. Chem. Soc.* **2005**, *127*, 210-216.
(42) Worrell, B. T.; Malik, J. A.; Fokin, V. V. *Science* **2013**, *340*, 457-460.
(43) Neumann, S.; Biewend, M.; Rana, S.; Binder, W. H. *Macromol. Rapid Commun.* **2020**, *41*, 1900359.
(44) Rani, A.; Singh, G.; Singh, A.; Maqbool, U.; Kaur, G.; Singh, J. *RSC Adv.* **2020**, *10*, 5610-5635.
(45) Oh, K.; Guan, Z. B. *Chem. Commun.* **2006**, 3069-3071.
(46) Xu, C. Y.; Huang, M. Z. *Chin. Chem. Lett.* **2006**, *17*, 883-886.
(47) Zhang, L.; Chen, X. G.; Xue, P.; Sun, H. H. Y.; Williams, I. D.; Sharpless, K. B.; Fokin, V. V.; Jia, G. C. *J. Am. Chem. Soc.* **2005**, *127*, 15998-15999.
(48) Majireck, M. M.; Weinreb, S. M. *J. Org. Chem.* **2006**, *71*, 8680-8683.
(49) Boren, B. C.; Narayan, S.; Rasmussen, L. K.; Zhang, L.; Zhao, H. T.; Lin, Z. Y.; Jia, G. C.; Fokin, V. V. *J. Am. Chem. Soc.* **2008**, *130*, 8923-8930.
(50) Ferrara, F.; Beke-Somfai, T.; Kann, N. *Eur. J. Org. Chem.* **2024**, *27*, e202400113.
(51) Johansson, J. R.; Beke-Somfai, T.; Stålsmeden, A. S.; Kann, N. *Chem. Rev.* **2016**, *116*, 14726-14768.
(52) Grob, N. M.; Schibli, R.; Béhé, M.; Valverde, I. E.; Mindt, T. L. *ACS Med. Chem. Lett.* **2021**, *12*, 585-592.
(53) Pacifico, S.; Kerckhoffs, A.; Fallow, A. J.; Foreman, R. E.; Guerrini, R.; McDonald, J.; Lambert, D. G.; Jamieson, A. G. *Org. Biomol. Chem.* **2017**, *15*, 4704-4710.
(54) Bouchet, F.; Barnier, J. P.; Sayah, I.; Bagdad, Y.; Miteva, M. A.; Arthur, M.; Etheve-Quelquejeu, M.; Iannazzo, L. *ChemMedChem* **2023**, *18*, e202300077.
(55) Agard, N. J.; Prescher, J. A.; Bertozzi, C. R. *J. Am. Chem. Soc.* **2005**, *127*, 11196-11196.
(56) Wang, D.; Astruc, D. *Chem. Rev.* **2015**, *115*, 6621-6686.
(57) Brieger, G.; Nestrick, T. J. *Chem. Rev.* **1974**, *74*, 567-580.
(58) Johnstone, R. A. W.; Wilby, A. H.; Entwistle, I. D. *Chem. Rev.* **1985**, *85*, 129-170.
(59) Zassinovich, G.; Mestroni, G.; Gladiali, S. *Chem. Rev.* **1992**, *92*, 1051-1069.
(60) Braude, E. A.; Linstead, R. P. *J. Chem. Soc.* **1954**, 3544-3547.
(61) Smith, M. B.; March, J. In *March's Advanced Organic Chemistry: Reactions, Mechanisms and Structure*, 6th ed.; John Wiley: Hoboken, NJ, 2007; pp 1863-1865.
(62) Sharifi, S.; Sharifi, H.; Koza, D.; Aminkhani, A. *Monatsh. Chem.* **2021**, *152*, 803-808.
(63) Blum, Y.; Shvo, Y. *Isr. J. Chem.* **1984**, *24*, 144-148.
(64) Blum, Y.; Czarkie, D.; Rahamim, Y.; Shvo, Y. *Organometallics* **1985**, *4*, 1459-1461.
(65) Shvo, Y.; Czarkie, D.; Rahamim, Y.; Chodosh, D. F. *J. Am. Chem. Soc.* **1986**, *108*, 7400-7402.

(66) Warner;, M. C.; Casey;, C. P.; Bäckvall;, J.-E. Shvo's Catalyst in Hydrogen Transfer Reactions. In *Bifunctional Molecular Catalysis*, Topics in Organometallic Chemistry, Vol. 37; Springer: Berlin, 2011; pp 85-125.
(67) Corma, A.; Navas, J.; Sabater, M. J. *Chem. Rev.* **2018**, *118*, 1410-1459.
(68) Reed-Berendt, B. G.; Latham, D. E.; Dambatta, M. B.; Morrill, L. C. *ACS Cent. Sci.* **2021**, *7*, 570-585.
(69) Salvatore, R. N.; Yoon, C. H.; Jung, K. W. *Tetrahedron* **2001**, *57*, 7785-7811.
(70) Nugent, T. C.; El-Shazly, M. *Adv. Synth. Catal.* **2010**, *352*, 753-819.
(71) Forero-Cortés, P. A.; Haydl, A. M. *Org. Process Res. Dev.* **2019**, *23*, 1478-1483.
(72) Müller;, T. E.; Hultzsch;, K. C.; Yus;, M.; Foubelo;, F.; Tada;, M. *Chem. Rev.* **2008**, *108*, 3795–3892.
(73) Ortiz, E.; Shezaf, J. Z.; Shen, W. J.; Krische, M. J. *Chem. Sci.* **2022**, *13*, 12625-12633.
(74) Fujita, K.; Li, Z. Z.; Ozeki, N.; Yamaguchi, R. *Tetrahedron Lett.* **2003**, *44*, 2687-2690.
(75) Martínez-Asencio, A.; Yus, M.; Ramón, D. J. *Synthesis* **2011**, 3730-3740.
(76) Elangovan, S.; Neumann, J.; Sortais, J. B.; Junge, K.; Darcel, C.; Beller, M. *Nat. Commun.* **2016**, *7*, 12641.
(77) Rawlings, A. J.; Diorazio, L. J.; Wills, M. *Org. Lett.* **2015**, *17*, 1086-1089.
(78) Rösler, S.; Ertl, M.; Irrgang, T.; Kempe, R. *Angew. Chem., Int. Ed.* **2015**, *54*, 15046-15050.
(79) Bertoli, M.; Choualeb, A.; Lough, A. J.; Moore, B.; Spasyuk, D.; Gusev, D. G. *Organometallics* **2011**, *30*, 3479-3482.
(80) Xu, Z. J.; Wang, D. S.; Yu, X. L.; Yang, Y. C.; Wang, D. W. *Adv. Synth. Catal.* **2017**, *359*, 3332-3340.
(81) Kallmeier, F.; Fertig, R.; Irrgang, T.; Kempe, R. *Angew. Chem., Int. Ed.* **2020**, *59*, 11789-11793.
(82) Podyacheva, E.; Afanasyev, O.; Vasilyev, D. V.; Chusov, D. *ACS Catal.* **2022**, *12*, 7142-7198.
(83) Nalikezhathu, A.; Williams, T. J. *Synthesis* **2025**, *57*, 2893-2908.
(84) Fujita, K. I.; Fujii, T.; Yamaguchi, R. *Org. Lett.* **2004**, *6*, 3525-3528.
(85) Miao, L.; DiMaggio, S. C.; Shu, H.; Trudell, M. L. *Org. Lett.* **2009**, *11*, 1579-1582.
(86) Rocchitta, G.; Spanu, A.; Babudieri, S.; Latte, G.; Madeddu, G.; Galleri, G.; Nuvoli, S.; Bagella, P.; Demartis, M. I.; Fiore, V.; et al. *Sensors* **2016**, *16*, 780.
(87) M.Peck;, E.; Smith, B. D. Applications of Synthetic Receptors for Biomolecules. In *Synthetic Receptors for Biomolecules: Design Principles and Applications.*, Monographs in Supramolecular Chemistry, Royal Society of Chemistry, 2015; pp 1-30.
(88) Douteau-Guével, N.; Coleman, A. W.; Morel, J. P.; Morel-Desrosiers, N. *J. Chem. Soc., Perkin Trans.* **1999**, 629-633.
(89) Aslam, S.; Kousar, I.; Rani, S.; Altaf, W.; Bristy, S.; Skouta, R. *Molecules* **2025**, *30*, 1450.
(90) Valeur, B.; Leray, I. *Coord. Chem. Rev.* **2000**, *205*, 3-40.
(91) Mahajan, P. G.; Dige, N. C.; Vanjare, B. D.; Kamaraj, E.; Seo, S. Y.; Lee, K. H. *J. Photochem. Photobiol., A* **2019**, *385*, 112089.
(92) Kashyap, S.; Singh, R.; Singh, U. P. *Coord. Chem. Rev.* **2020**, *417*, 213369.
(93) Müller, L. K.; Duznovic, I.; Tietze, D.; Weber, W.; Ali, M.; Stein, V.; Ensinger, W.; Tietze, A. A. *Chem. Eur. J.* **2020**, *26*, 8511-8517.

(94) Wang, Y.; Xiang, J. F.; Jiang, H. *Chem. Eur. J.* **2011**, *17*, 613-619.
(95) Yang, L.; Wang, X. C.; Dai, M.; Chen, B.; Qiao, Y. B.; Deng, H. J.; Zhang, D. F.; Zhang, Y. Z.; de Almeida, C.; Chiu, A. S. F.; et al. *Energy* **2021**, *228*, 120533.
(96) Claudio-Quiroga, G.; Poza, C. *Sustain. Dev.* **2024**, *32*, 4707-4725.
(97) Blasi, A.; Verardi, A.; Lopresto, C. G.; Siciliano, S.; Sangiorgio, P. *Recycling* **2023**, *8*, 61.
(98) Cazier, E. A.; Pham, T. N.; Cossus, L.; Abla, M.; Ilc, T.; Lawrence, P. *Waste Manage.* **2024**, *188*, 11-38.
(99) Sun, Z. H.; Fridrich, B.; de Santi, A.; Elangovan, S.; Barta, K. *Chem. Rev.* **2018**, *118*, 614-678.
(100) Liguori, F.; Moreno-Marrodan, C.; Barbaro, P. *Chem. Soc. Rev.* **2020**, *49*, 6329-6363.
(101) Ren, T. H.; Chen, Q.; Zhao, C. B.; Zheng, Q.; Xie, H. B.; North, M. *Green Chem.* **2020**, *22*, 1542-1547.
(102) Simon, M. O.; Darses, S. *Adv. Synth. Catal.* **2010**, *352*, 305-308.
(103) Johansson, J. R.; Beke-Somfai, T.; Stålsmeden, A. S.; Kann, N. *Chem. Rev.* **2016**, *116*, 14726-14768.
(104) Nehra, N.; Tittal, R. K.; Ghule, V. D. *ACS Omega* **2021**, *6*, 27089-27100.
(105) Kumar, S.; Khokra, S. L.; Yadav, A. *Future J. Pharm. Sci.* **2021**, *7*, 106.
(106) Ashwini, N.; Garg, M.; Mohan, C. D.; Fuchs, J. E.; Rangappa, S.; Anusha, S.; Swaroop, T. R.; Rakesh, K. S.; Kanojia, D.; Madan, V.; et al. *Biorg. Med. Chem.* **2015**, *23*, 6157-6165.
(107) Shafi, S.; Alam, M. M.; Mulakayala, N.; Mulakayala, C.; Vanaja, G.; Kalle, A. M.; Pallu, R.; Alam, M. S. *Eur. J. Med. Chem.* **2012**, *49*, 324-333.
(108) Rahul, P.; Thomas, J.; Dehaen, W.; John, J. *Mol.* **2023**, *28*, 308.
(109) Kamal, A.; Hussaini, S. M. A.; Sucharitha, M. L.; Poornachandra, Y.; Sultana, F.; Kumar, C. G. *Org. Biomol. Chem.* **2015**, *13*, 9388-9397.
(110) Ostrowski, T.; Januszczyk, P.; Cieslak, M.; Kazmierczak-Baranska, J.; Nawrot, B.; Bartoszak-Adamska, E.; Zeidler, J. *Biorg. Med. Chem.* **2011**, *19*, 4386-4398.
(111) Oehlrich, D.; Peschiulli, A.; Tresadern, G.; Van Gool, M.; Vega, J. A.; De Lucas, A. I.; de Diego, S. A. A.; Prokopcova, H.; Austin, N.; Van Brandt, S.; et al. *ACS Med. Chem.* **2019**, *10*, 1159-1165.
(112) Mohapatra, D. K.; Maity, P. K.; Gonnade, R. G.; Chorghade, M. S.; Gurjar, M. K. *Synlett* **2007**, 1893-1896.
(113) Dhondge, A. P.; Afraj, S. N.; Nuzlia, C.; Chen, C. P.; Lee, G. H. *Eur. J. Org. Chem.* **2013**, *2013*, 4119-4130.
(114) Afraj, S. N.; Chen, C. P.; Lee, G. H. *RSC Adv.* **2014**, *4*, 26301-26308.
(115) Afraj, S. N.; Chen, C. P. *Asian J. Org. Chem.* **2016**, *5*, 257-263.
(116) Cao, J.; Xu, G.; Li, P. Y.; Tao, M. L.; Zhang, W. Q. *ACS Sustain. Chem. Eng* **2017**, *5*, 3438-3447.
(117) Chen, Y.; He, Y. M.; Zhang, S. S.; Miao, T. T.; Fan, Q. H. *Angew. Chem. Int. Ed.* **2019**, *58*, 3809-3813.
(118) Dandepally, S. R.; Williams, A. L. *Tetrahedron Lett.* **2009**, *50*, 1071-1074.
(119) Podyacheva, E.; Afanasyev, O. I.; Vasilyev, D. V.; Chusov, D. *ACS Catal.* **2022**, *12*, 7142-7198.
(120) Enyong, A. B.; Moasser, B. *J. Org. Chem.* **2014**, *79*, 7553-7563.
(121) Yan, T.; Feringa, B. L.; Barta, K. *Sci. Adv.* **2017**, *3*, eaao6494.

(122) Ahrendt, K. A.; Borths, C. J.; MacMillan, D. W. C. *J. Am. Chem. Soc.* **2000**, *122*, 4243-4244.
(123) Jensen, K. L.; Dickmeiss, G.; Jiang, H.; Albrecht, L.; Jorgensen, K. A. *Acc. Chem. Res.* **2012**, *45*, 248-264.
(124) Klier, L.; Tur, F.; Poulsen, P. H.; Jorgensen, K. A. *Chem. Soc. Rev.* **2017**, *46*, 1080-1102.
(125) Hayashi, Y.; Gotoh, H.; Hayashi, T.; Shoji, M. *Angew. Chem., Int. Ed.* **2005**, *44*, 4212-4215.
(126) Vega-Peñaloza, A.; Paria, S.; Bonchio, M.; Dell'Amico, L.; Companyó, X. *ACS Catal.* **2019**, *9*, 6058-6072.
(127) Quintavalla, A.; Carboni, D.; Lombardo, M. *Molecules* **2023**, *28*, 2234.
(128) Schulze, B.; Schubert, U. S. *Chem. Soc. Rev.* **2014**, *43*, 2522-2571.
(129) Cambeiro, X. C.; Martín-Rapún, R.; Miranda, P. O.; Sayalero, S.; Alza, E.; Llanes, P.; Pericàs, M. A. *Beilstein J. Org. Chem.* **2011**, *7*, 1486-1493.
(130) Font, D.; Bastero, A.; Sayalero, S.; Jimeno, C.; Pericàs, M. A. *Org. Lett.* **2007**, *9*, 1943-1946.
(131) Riente, P.; Yadav, J.; Pericàs, M. A. *Org. Lett.* **2012**, *14*, 3668-3671.
(132) Porta, R.; Benaglia, M.; Puglisi, A.; Mandoli, A.; Gualandi, A.; Cozzi, P. G. *ChemSusChem* **2014**, *7*, 3534-3540.
(133) Chandrasekhar, S.; Kumar, C. P.; Kumar, T. P.; Haribabu, K.; Jagadeesh, B.; Lakshmi, J. K.; Mainkar, P. S. *RSC Adv.* **2014**, *4*, 30325-30331.
(134) Reyes-Rangel, G.; Vargas-Caporali, J.; Juaristi, E. *Tetrahedron* **2016**, *72*, 379-391.
(135) Yan, Z. Y.; Niu, Y. N.; Wei, H. L.; Wu, L. Y.; Zhao, Y. B.; Liang, Y. M. *Tetrahedron-Asymmetry* **2006**, *17*, 3288-3293.
(136) Liu, J.; Wang, L. *Synthesis* **2017**, *49*, 960-972.
(137) Vachan, B. S.; Karuppasamy, M.; Vinoth, P.; Kumar, S. V.; Perumal, S.; Sridharan, V.; Menéndez, J. C. *Adv. Synth. Catal.* **2020**, *362*, 87-110.
(138) Hulanicki, A.; Glab, S.; Ingman, F. *Pure Appl. Chem.* **1991**, *63*, 1247-1250.
(139) Singh, G.; George, N.; Singh, R.; Singh, G.; Sushma; Kaur, G.; Singh, H.; Singh, J. *Appl. Organomet. Chem.* **2023**, *37*, e6897.
(140) Park, S. Y.; Yoon, J. H.; Hong, C. S.; Souane, R.; Kim, J. S.; Matthews, S. E.; Vicens, J. *J. Org. Chem.* **2008**, *73*, 8212-8218.
(141) Picot, S. C.; Mullaney, B. R.; Beer, P. D. *Chem. Eur. J.* **2012**, *18*, 6230-6237.
(142) Mungalpara, D.; Stegmüller, S.; Kubik, S. *Chem. Commun.* **2017**, *53*, 5095-5098.
(143) Schröder, D. C.; Kracker, O.; Fröhr, T.; Góra, J.; Jewginski, M.; Niess, A.; Antes, I.; Latajka, R.; Marion, A.; Sewald, N. *Front. Chem.* **2019**, *7*.
(144) Tonali, N.; Hericks, L.; Schröder, D. C.; Kracker, O.; Krzemieniecki, R.; Kaffy, J.; Le Joncour, V.; Laakkonen, P.; Marion, A.; Ongeri, S.; et al. *ChemPlusChem* **2021**, *86*, 840-851.
(145) Johansson, J. R.; Hermansson, E.; Nordén, B.; Kann, N.; Beke-Somfai, T. *Eur. J. Org. Chem.* **2014**, *2014*, 2703-2713.
(146) Stålsmeden, A. S.; Paterson, A. J.; Szigyártó, I. C.; Thunberg, L.; Johansson, J. R.; Beke-Somfai, T.; Kann, N. *Org. Biomol. Chem.* **2020**, *18*, 1957-1967.
(147) Araszczuk, A. M.; D'Amato, A.; Schettini, R.; Costabile, C.; Della Sala, G.; Pierri, G.; Tedesco, C.; De Riccardis, F.; Izzo, I. *Org. Lett.* **2022**, *24*, 7752-7756.

(148) Rhee, H. W.; Lee, C. R.; Cho, S. H.; Song, M. R.; Cashel, M.; Choy, H. E.; Seok, Y. J.; Hong, J. I. *J. Am. Chem. Soc.* **2008**, *130*, 784-785.
(149) Cao, M. M.; Fu, A. P.; Wang, Z. H.; Liu, J. Q.; Kong, N.; Zong, X. D.; Liu, H. H.; Gooding, J. J. *J. Phys. Chem.* **2014**, *118*, 2650-2659.
(150) Avery, M. A.; Muraleedharan, K. M.; Desai, P. V.; Bandyopadhyaya, A. K.; Furtado, M. M.; Tekwani, B. L. *J. Med. Chem.* **2003**, *46*, 4244-4258.
(151) Xu, D. G.; Edgar, K. J. *Biomacromolecules* **2012**, *13*, 299-303.
(152) Zheng, X. Y.; Gandour, R. D.; Edgar, K. J. *Biomacromolecules* **2013**, *14*, 1388-1394.